UNIVERSIDADE DE TAUBATÉ
PROGRAMA DE PÓS-GRADUAÇÃO EM CIÊNCIAS AMBIENTAIS
Revista Ambiente & Água
An Interdisciplinary Journal of Applied Science

COD removal (%)

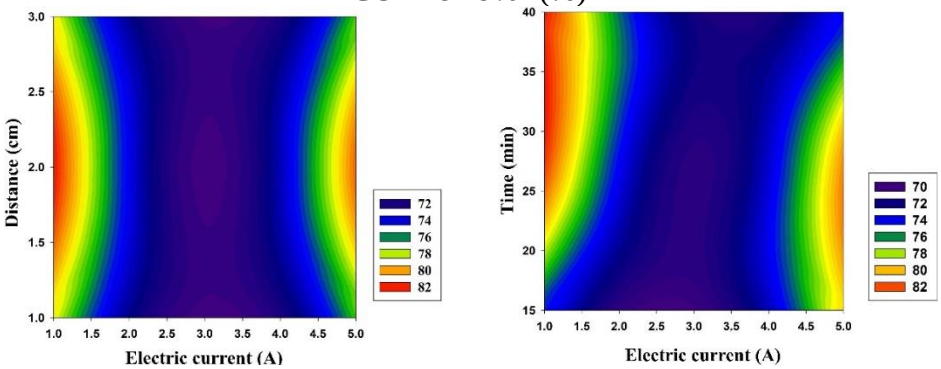

Turbidity removal (%)

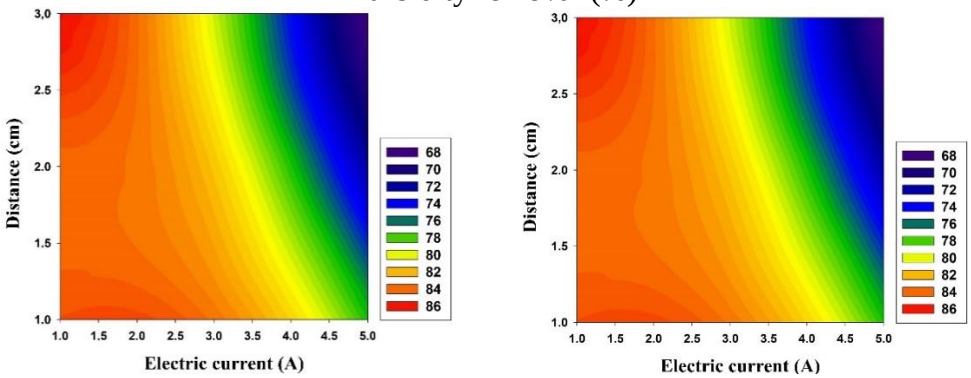

Color removal (%)

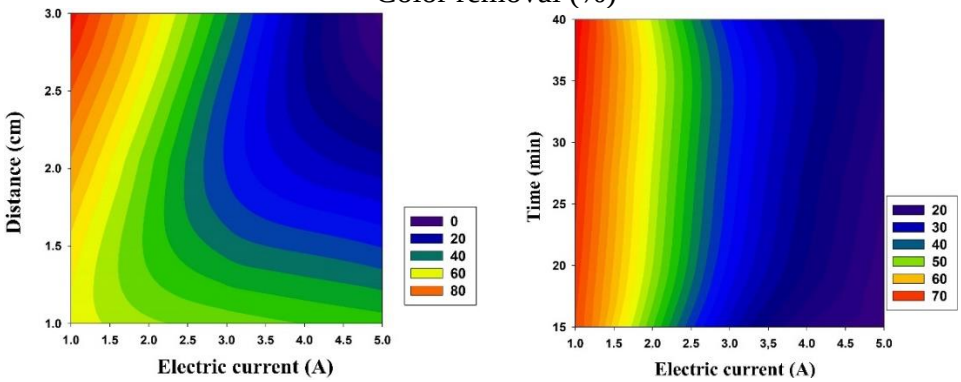

ISSN = 1980-993X (Online)
http://www.ambi-agua.net

Library catalog entry by Liliane Castro CRB/8-6748

Revista Ambiente & Água - An Interdisciplinary Journal of Applied Science / Instituto de Pesquisas Ambientais em Bacias Hidrográficas. Taubaté. v. 17, n.5 (2006) - Taubaté: IPABHi, 2022.
Quadrimestral (2006 – 2013), Trimestral (2014 – 2016), Bimestral (2017), Publicação Contínua a partir de Janeiro de 2018.

Resumo em português e inglês.
ISSN 1980-993X

1. Ciências ambientais. 2. Recursos hídricos. I. Instituto de Pesquisas Ambientais em Bacias Hidrográficas.

CDD - 333.705
CDU - (03)556.18

TABLE OF CONTENTS

COVER:

Results from research designed to investigate the efficiency of electrocoagulation in removing COD, turbidity, and apparent color from healthcare waste (HCW), these graphs show the percent removal of these parameters as a function of electric current, electrode distance, and hydraulic retention time. One of the conclusions associated with these results is that the high removal of turbidity, COD, and apparent color showed that electrocoagulation was effective for treating gas scrubber effluents. Source: SANTOS, M.A. dos. *et al*. Optimization of effluent treatment from healthcare waste incineration by electrocoagulation with iron electrodes. **Rev. Ambient. Água, Taubaté, vol. 17 n. 5, p. 1-12, 2022.** ***doi:10.4136/ambi-agua.2834***

ARTICLES

Ambiente & Água - An Interdisciplinary Journal of Applied Science
ISSN 1980-993X – doi:10.4136/1980-993X
www.ambi-agua.net
E-mail: ambi.agua@gmail.com

Influence of land use and occupation on the chemical and physical fractions of organic matter in cultivated and native areas in the Atlantic Forest biome

ARTICLES doi:10.4136/ambi-agua.2814

Received: 10 Nov. 2021; Accepted: 20 May 2022

Giovana Tetsuya Lopes[1]; Jean Sérgio Rosset[2]; Jefferson Matheus Barros Ozório[3*]; Ozielly Maiane Mendes da Silva[2]; Wesley Vieira dos Santos[1]; José Victor Hugo dos Santos[2]; Andrea dos Santos Gonçalves[2]; Eloi Panachuki[1]

[1]Departamento de Solos. Universidade Estadual de Mato Grosso do Sul (UEMS), Unidade Universitária de Aquidauana, Rodovia Graziela Maciel Barroso, Km 12, Zona Rural, CEP: 79200-000, Aquidauana, MS, Brazil. E-mail: giovana_tetsuya@hotmail.com, wesley.vsanto070@gmail.com, eloip@uems.br
[2]Departamento de Solos. Universidade Estadual de Mato Grosso do Sul (UEMS), Unidade Universitária de Mundo Novo, BR 163, Km 20,2, CEP: 79980-000, Mundo Novo, MS, Brazil. E-mail: rosset@uems.br, oziellymaiane@gmail.com, jvictorhugo@outlook.com, aerdna133@gmail.com
[3]Departamento de Solos. Universidade Estadual de Mato Grosso do Sul (UEMS), Unidade Universitária de Dourados, Cidade Universitária de Dourados, s/n, CEP: 79804-97, Dourados, MS, Brazil.
[*]Corresponding author. E-mail: ozorio.jmb@outlook.com

ABSTRACT

This study quantified the C content of the chemical and physical fractions of SOM in different management systems in an Argisoil of sandy texture. The study was carried out in a reference area of Native Forest (NF), and in three managed areas: Permanent Pasture (PP), No-Tillage System (NTS) and an area of Private Natural Heritage Reserve (PNHR) in the process of natural regeneration. Soil samples were collected in the layers 0.0-0.05, 0.05-0.10 and 0.10-0.20 m. We assessed the soil density (Sd), total organic carbon (TOC) content, chemical fractionation of SOM with determination of the C contents of the fulvic acids (FA), humic acids (HA) and humin (HUM), with subsequent calculations of the HA/FA ratios, AE/HUM, stock (StockC), physical granulometric fractionation and determination of C contents of particulate organic matter (C-POM) and carbon management index (CMI). Higher TOC contents were observed for the NF area. The C-HA and C-HUM contents were higher in the NF and NTS. NF showed higher C-POM levels in all layers evaluated. For the C-MOM, the NTS area was superior to the other managed areas. The managed areas had lower StockPOM values than the NF. The managed areas had lower CMI values in relation to NF. The NTS area showed that, even in crop succession, it contributes to the improvement of the soil organic fraction over the adoption time. On the other hand, the areas of PP and PNHR showed that inadequate management favors the reduction of edaphic quality.

Keywords: carbon in soil, carbon management index, chemical fractionation, physical fractionation.

Influência do uso e ocupação do solo sob as frações químicas e físicas da matéria orgânica em áreas cultivadas e nativa no bioma Mata Atlântica

RESUMO

O objetivo deste trabalho foi quantificar os teores de C das frações químicas e físicas da MOS em diferentes sistemas de manejo em um Argissolo textura arenosa. O estudo foi realizado em uma área de referência de Mata Nativa (MN) e três áreas manejadas: pastagem permanente (PP), sistema plantio direto (SPD) e área de Reserva Particular de Patrimônio Natural em processo de regeneração natural (RPPN). Foram coletadas amostras de solos das camadas de 0-0,05, 0,05-0,10 e 0,10-0,20 m. Foi determinado a densidade do solo (Ds) os teores de carbono orgânico total (COT) o fracionamento químico da MOS com determinação dos teores de C dos ácidos fúlvicos (AF), ácidos húmicos (AH) e humina (HUM), com posteriores cálculos das relações AH/AF, EA/HUM, estoque (EstC), fracionamento físico-granulométrico e determinação dos teores de C da matéria orgânica particulada (C-MOP) e índice de manejo de carbono (IMC). Observou-se maiores teores de COT para a área de MN, especialmente nas camadas de 0-0,05 e 0,05-0,10 m. Os teores de C-HUM predominam em relação aos teores de C-AH e C-AF. Os teores de C-AH e de C-HUM foram superiores em MN e SPD. A MN apresentou maiores teores de C-MOP em todas as camadas avaliadas. Para o C-MOM a área de SPD foi superior as demais áreas manejadas. As áreas manejadas apresentaram valores de EstMOP inferiores à MN. Nas duas primeiras camadas, a área de MN apresentou maiores EstMOM. As áreas manejadas apresentaram valores inferiores de IMC em relação a MN. A área de SPD demonstrou que, mesmo em sucessão, contribui para melhoria da fração orgânica do solo ao longo do tempo de adoção, se aproximando às condições da MN. Já as áreas de PP e RPPN evidenciaram que o manejo inadequado favorece na diminuição da qualidade edáfica.

Palavras-chave: carbono do solo, fracionamento físico, fracionamento químico, índice de manejo de carbono.

1. INTRODUCTION

Soil quality (SQ) is complex and is based on its ability to support ecosystem services, balancing physical, chemical and biological quality. It is totally dependent on the management system adopted and on the relationship between the ecosystem and the environment (Doran and Parkin, 1994). Studies on SQ have been improved by several authors, who have developed methods and quality indices which allow different applications for different types of soils and regions. The indicators applied must be sensitive to the management and use of the edaphic environment, being efficient and accurate in identifying changes in soil attributes also in a short evaluation period (Aziz *et al.*, 2013; Marques *et al.*, 2015; Magalhães *et al.*, 2016; Lal, 2018).

Soil organic matter (MOS), by determining the organic carbon content (C), is one of the most sensitive indicators to assess changes in the quality of the edaphic environment (Borges *et al.*, 2015). In addition, in natural environments the stock of C is in balance between the rates of entry and exit, and when they present some type of disturbance that influences litter deposition (Barros and Fearnside, 2016), it ends up modifying the dynamics of C stock in these areas (Rosset *et al.*, 2014; Loss *et al.*, 2015; Koven *et al.*, 2017). However, in many cases, only the quantification of C is not enough to identify possible changes in the quality of the edaphic environment (Diniz *et al.*, 2020).

SOM fractionation techniques are important for evaluation because they are able to express changes in the quality of the soil organic fraction (Rosset *et al.*, 2014; 2016), even in a short period of time (Loss *et al.*, 2015). This happens because most fractions of SOM are located in

different compartments and differ in cycling time, rates of microbial and biochemical degradation, accessibility of microorganisms and interactions with the mineral part of the soil (Kunde *et al.*, 2016).

Chemically, SOM is divided into two parts, one composed of the unhumified fraction, composed of little decayed plant and animal remains and organic compounds with biochemical categories of proteins, sugars, waxes, greases and resins; and the other of humic substances (HS). HS are separated into three fractions: fulvic acids (FA), humic acids (HA) and humin (HUM); and are differentiated according to their molecular weight, increasingly FA>HA>HUM; they are soluble in different pH ranges, among other characteristics. FA are soluble in alkaline or acid pH, HA are soluble in alkaline pH and HUM is insoluble in any pH range (Benites *et al.*, 2003; Gazolla *et al.*, 2015; Olk *et al.*, 2019).

The HUM fraction is responsible for the aggregation of mineral particles and, in most tropical soils, represents much of the humified C. The HA represent the intermediate fraction, between the organic compounds of higher chemical stability (HUM) and the occurrence of free oxidized organic acids in the soil solution (FA). The FA have higher solubility, being mainly responsible for cation transport mechanisms in the soil, and being the most unstable fraction of the humification process (Baldotto and Baldotto, 2014; Lehmann and Kleber, 2015).

The physical-granulometric fractionation divides the SOM into two organic fractions: particulate organic matter (POM), with fractions of more than 53 μm in size and mineral organic matter (MOM), with fractions of less than 53 μm in size (Cambardella and Elliott, 1992), with subsequent determinations and calculations of their respective C contents (C-POM and C-MOM). C-POM is sensitive in identifying changes in land use, even within a short period of time (Loss *et al.*, 2015; Rosset *et al.*, 2019), whereas C-MOM is less altered by changes in land use due to longer cycling time (Bayer *et al.*, 2004).

Considering the physical fractionation of SOM, the carbon management index (CMI) is calculated, which is a relative measure of the impacts of soil management, and combines quantitative and qualitative characteristics to analyze the quality of the areas (Blair *et al.*, 1995). This method makes it possible to infer whether current management practices are harmful to the maintenance of SOM and, consequently, of soil quality over the years of cultivation (Conceição *et al.*, 2014; Nanzer *et al.*, 2019).

Therefore, in addition to the quantification of C, it is important to characterize the quality of C stored underground as a consequence of the adoption of different management systems under different soil conditions and regional climate. This study therefore evaluated soil quality by chemical and physical fractionation of soil organic matter in areas with sandy soil and different management systems.

2. MATERIAL AND METHODS

2.1. Location, Climate, Soil and History of Study Areas

Soil samples were collected in different management systems with known history, located in the district of Porto Morumbi, municipality of Eldorado, Cone-sul region of Mato Grosso do Sul, Brazil (Figure 1). The study areas are located at coordinates 23º48' latitude S and 54º06' longitude W, with an average altitude of 272 meters, and located within the Environmental Preservation Area (APA) of the Islands and Floodplains of the Paraná River (Ilhas e Várzeas do Rio Paraná) (ICMBio, 2019). The climate of the region is subtropical – Cfa, according to Koppen classification (Peel *et al.*, 2007) with average temperature of the coldest month between 14 and 15ºC and rainfall ranging from 1,400 to 1,700 mm per year (Mato Grosso do Sul, 2015).

Three managed areas and an adjacent reference area (Native Forest - NF - Atlantic Forest Vegetation with phyto physiognomy of Semidecidual Seasonal Forest) without anthropic action were evaluated. The three managed areas are: permanent pasture with the species *Brachiaria brizantha* (PP), no-tillage system in succession of soybean (summer) and corn crops (second

harvest) (NTS), as well as a Private Natural Heritage Reserve in process of natural regeneration with secondary vegetation (PNHR) (Table 1).

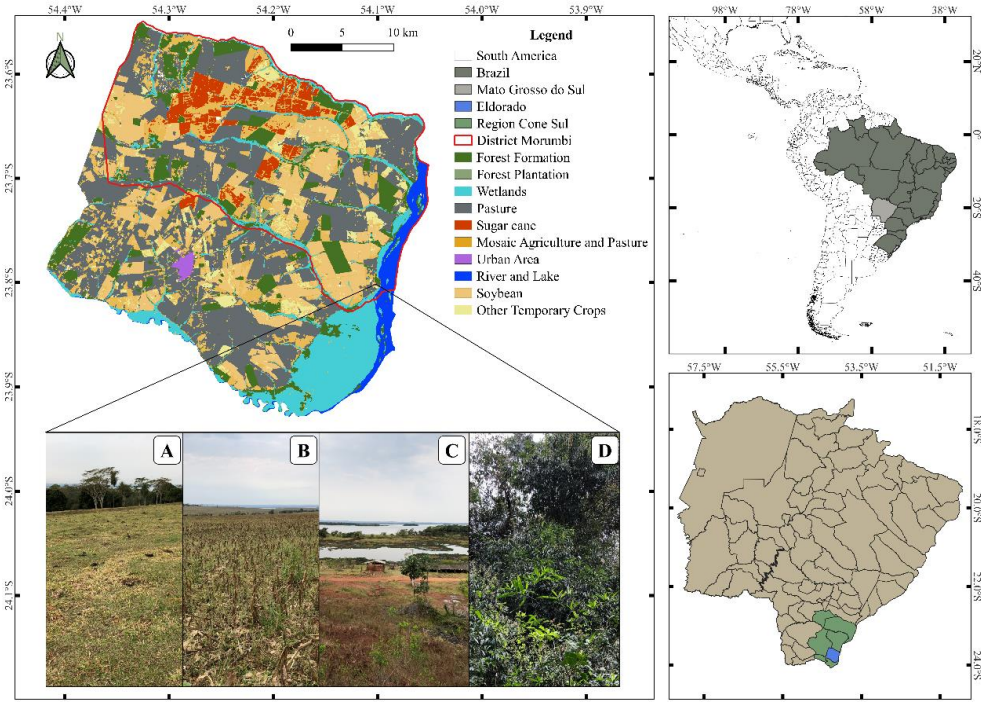

Figure 1. Experimental location map, with land use and occupation data for the city of Eldorado - MS, Brazil. Data
Source: MapBiomas project (2021). Qgis Development Team (2021).

Table 1. History and description of the changes in management systems of the different study áreas.

Area	Management history
PP	Area of 5 hectares, cultivated with the species *Brachiaria brizantha* Hochst Stapf cv. MG4 permanently for 10 years. Area used for grazing cattle with a capacity of 1.2 animal unit (AU) ha^{-1} with visible signs of degradation.
NTS	Area of 50 hectares, cultivated under a no-tillage system in succession of soybean (summer) and corn (second harvest) crops, and this type of system has been employed in the area for the last 10 years.
PNHR	Area of 15 hectares. Private Natural Heritage Reserve - Forest remnant of the Atlantic Forest biome, degraded area and in process of natural regeneration for 2 years.
NF	Area of 20 hectares. Native vegetation of Atlantic Forest - Semidecidual Seasonal Forest. Represented in the study as the original condition of the soil, without anthropic action.

PP: Permanent Pasture, NTS: No-Tillage System, PNHR: Private Natural Heritage Reserve, NF: Native Forest.

All four areas studied are on soil classified as Typical Dystrophic Red Argiole (Santos *et al.*, 2018), equivalent Acrisols (IUSS Working Group Wrb, 2015) and Ultisols (NRCS, 2014) of sandy texture (Santos *et al.*, 2018), making up four different systems, analyzed in a completely randomized design. The use and management of the present study areas are displayed in Table 1, and are described according to the chronology of use in Figure 2.

In each of the four study areas, disturbed soil samples from the 0-0.2 m layer were collected for soil physical and chemical characterization analyses (Table 2).

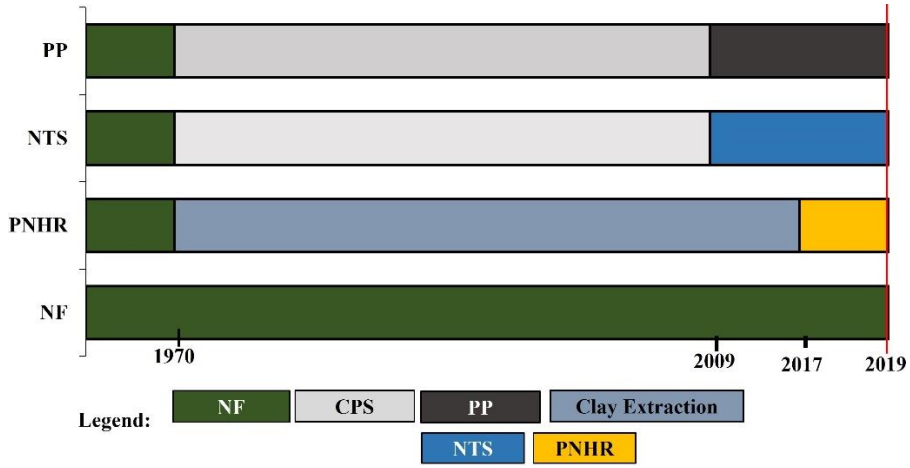

Figure 2. History of uses and changes in use of areas, with the respective implementation dates of each management system: NF: Native Forest; CPS: Conventional Preparation System; NTS: No-tillage System; PP: Permanent Pasture; PNHR: Private Natural Heritage Reserve.

Table 2. Physical and chemical attributes of the soil in the 0-0.2 m layer of the four areas studied in the district of Porto Morumbi, Eldorado, MS.

MS	Sand	Silt	Argila	pH	OM	P	K	Ca	Mg	Al	H+Al	SB	CEC	V
		g kg^{-1}		$CaCl_2$	g dm^{-3}	mg dm^{-3}				cmol$_c$dm^{-3}				%
PP	860	43	97	4.59	14.76	6.79	0.04	0.80	0.60	0.13	1.40	1.44	2.84	50.70
NTS	794	59	147	4.07	20.77	13.88	0.17	1.10	0.80	0.39	2.80	2.07	4.87	42.50
PNHR	894	26	80	4.13	13.39	10.44	0.05	0.60	0.30	0.30	1.80	0.95	2.75	34.50
NF	832	44	124	4.69	26.78	12.01	0.15	3.00	1.10	0.10	2.40	4.25	6.65	63.90

MS: Management system; PP: permanent pasture; NTS: no-tillage system; PNHR: Private Natural Heritage Reserve; NF: native forest. Physical characterization – Granulometry: pipette method. Chemical characterization – Mehlich (P and K); KCl 1N (Ca, Mg and Al); Calcium Chloride (pH); Calcium Acetate pH 7 (H + Al); CEC: Cationic exchange capacity; OM: Organic matter; V: Base Saturation; SB: Sum of bases.

For each of the four study areas, composite disturbed soil samples were collected in five replicates in the layers of 0.00-0.05, 0.05-0.10 and 0.10-0.20 m, each composite sample being represented by five simple samples. In all areas and layers, undisturbed samples were also collected with the aid of a volumetric ring with five replicates.

After collection, a procedure was performed to obtain air-dried fine earth (TADS). The Sd was determined by the methodology described by Claessen (1997). The total organic carbon (TOC) was obtained through the method of (Yeomans and Bremner, 1988).

The chemical fractionation of soil organic matter (SOM) was determined following the differential solubility method established by the International Society of Humic Substances (Swift, 1996), according to the adaptation of Benites *et al.* (2003), based on the characteristics of differential solubility by differentiating the fractions of fulvic acid (FA), humic acid (HA) and humin (HUM), with subsequent determinations of the C-FA, C-HA and C-HUM contents.

From the analyses of C of FA, HA and HUM, the values of alkaline extract (AE) (AE = HA+FA) and the ratios of HA/FA and AE/HUM were calculated to verify the humification processes of the SOM. In addition, the C stocks of the humic fractions were calculated according to the equivalent mass method (Reis *et al.*, 2018; Ozório *et al.*, 2020). The physical-granulometric fractions of the MOS were determined according to the method of Cambardella and Elliott (1992), obtaining the particulate organic matter (POM) and mineral organic matter (C-MOM). Subsequently, C stocks of particulate organic matter (StockC-POM) and mineral organic matter (StockC-MOM) were calculated following the equivalent mass method (Reis *et al.*, 2018; Ozório *et al.*, 2020). Then, the following indices were calculated to evaluate the quality of the soil organic fraction: carbon stock index (CSI), lability of SOM (L), lability index (LI) and carbon management index (CMI) according to Blair *et al.* (1995).

After the laboratory analyses were performed, the results were assessed in a completely randomized design, submitted to variance analysis employing the F-test, and the mean values were compared by the Tukey test at 5% probability with the aid of the R Core Team program (2021). All tests were performed using ExpDes.pt (Ferreira *et al.*, 2018). A complementary analysis was also performed using the multivariate technique of principal component analysis – PCA, to assess the interrelationships involving all variables and explain these variables in terms of their inherent dimensions (Silva *et al.*, 2020). In order to identify the correlation between the variables, a correction matrix was performed using Pearson's correlation method (Bravo *et al.*, 2020).

3. RESULTS AND DISCUSSION

3.1. Chemical fractions of soil organic matter

The areas of PP, NTS and PNHR had similar soil density values (Sd) ($p<0.05$) in all layers evaluated. In the 0.00-0.05 m layer, the values ranged from 1.37 Mg m^{-3} to 1.52 Mg m^{-3}. In the layer 0.05-0.10 m there was variation from 1.39 Mg m^{-3} to 1.44 Mg m^{-3}. The NTS area showed ($p<0.05$) higher Sd in relation to NF in the layers of 0.00-0.05 and 0.05-0.10 m. In the 0.10-0.20 m layer the Sd values were similar in all the areas evaluated (Table 3).

The higher Sd in the NTS area may be a consequence of the short management time without soil revolving and the succession of crops, requiring more time for positive changes in the soil's physical attributes (Anghinoni, 2007), as well as the frequent traffic of machinery that favor this result. The results corroborated the studies of Rosset *et al.* (2014), Corrêa *et al.* (2016) and Falcão *et al.* (2020) also in areas of soybean/corn succession.

Table 3. Carbon contents of fulvic acid (C-FA), humic acid (C-HA) and humin (C-HUM), HA/FA ratio, alkaline extract (EA)/HUM and carbon stock of fulvic acid fractions (Stock- FA), humic acid (Stock-HA) and humin (Stock-HUM) in different areas evaluated.

MS	Sd	TOC	C-FA	C-HA	C-HUM	HA/FA	AE/HUM	Stock-FA	Stock-HA	Stock-HUM
		g kg^{-1}				-	-		Mg ha^{-1}	
						0-00.05 m				
PP	1.44ab	7.28c	2.22a	1.03c	3.72c	0.48b	0.88b	2.83a	1.31c	4.74c
NTS	1.52a	11.46b	2.48a	1.83b	5.46b	0.76b	0.81b	3.16a	2.34b	6.96b
PNHR	1.37ab	7.61c	2.41a	1.31c	2.82c	0.55b	1.33a	3.07a	1.67c	3.59c
NF	1.27b	16.42a	2.30a	2.95a	7.25a	1.31a	0.74b	2.93a	3.76a	9.23a
CV (%)	12.43	15.17	19.61	14.12	18.21	21.65	20.15	19.61	14.12	18.21
						0.05-0.10 m				
PP	1.39ab	6.79b	1.92a	0.75c	3.39b	0.41c	0.79b	2.39a	0.94c	4.21b
NTS	1.54a	10.19b	2.01a	1.80b	5.69a	0.92ab	0.68b	2.50a	2.25b	7.08a
PNHR	1.44ab	5.75d	2.11a	1.43b	2.36b	0.68bc	1.52a	2.63a	1.79b	2.94b
NF	1.25b	10.21a	2.22a	2.30a	6.39a	1.18a	0.76b	2.77a	3.23a	7.95a
CV (%)	17.15	13.75	16.37	15.20	13.14	23.49	20.09	16.37	15.2	13.14
						0.10-0.20 m				
PP	1.45a	7.04c	2.22a	1.23c	2.94b	0.55b	1.17b	2.83a	1.58c	3.75b
NTS	1.45a	10.67b	2.20a	2.17ab	4.88a	1.07b	0.93b	2.81a	2.77ab	6.22a
PNHR	1.37a	6.56c	1.94ab	1.80bc	1.92b	0.93b	2.05a	2.48ab	2.30bc	2.46b
NF	1.29a	13.41a	1.39b	2.57a	5.30a	1.92a	0.74b	1.77b	3.28a	6.77a
CV (%)	16.43	17.22	20.71	17.61	16.90	28.71	22.45	20.71	17.61	16.90

Means followed by the same lowercase letter in the column for each system and layer do not differ statistically by the Tukey test (5%). MS: Management system; PP: permanent pasture; NTS: no-tillage system; PNHR: Private Natural Heritage Reserve; NF: native forest. CV(%): coefficient of variation.

The NF area had the highest TOC contents, especially in the 0.00-0.05 and 0.05-0.10 m layers, with contents of 16.41 and 13.59 g kg^{-1}, respectively. In the 0.10-0.20 m layer, the areas of NTS and NF were similar ($p<0.05$) (Table 3). The highest content of TOC in the area of NF may be related to the continuous deposition of litter along with the absence of anthropic actions, especially soil revolving, favoring the increase of TOC contents (Loss *et al.*, 2015; Nanzer *et al.*, 2019). Also comparing NF areas of the Atlantic Forest biome, Rosset *et al.* (2016; 2019), Martins *et al.* (2020), Troian *et al.* (2020) and Ozório *et al.* (2019) found higher contents of TOC in NF in relation to areas of PP and NTS.

The different TOC contents are the result of alteration, production and decomposition of organic residues and depend directly on natural factors associated with pedogenetic processes, but are mainly altered by anthropic actions in soil management (Lal, 2018; Falcão *et al.*, 2020; Santos *et al.*, 2021). The highest TOC contents in the NTS area in relation to the areas of PP and PNHR may be associated with the absence of soil revolving due to the cultivation of corn/soybean in succession in the area. In addition, the low levels of TOC in the areas of PP and PNHR are due to their advanced stage of degradation, with animal overcrowding in PP and the history of soil exploration/extraction of raw material destined to the region's potteries for several decades in the PNHR area.

In all areas studied, C-HUM contents predominated in relation to C-HA and C-FA contents (Table 3). This fact is related to the greater recalcitrance of this fraction compared to the FA and HA fractions (Han *et al.*, 2016). Similar results were found by Rosset *et al.* (2016) and Rosa *et al.* (2017) under different soil conditions, climate and management systems.

The C-FA contents ranged from 1.39 to 2.48 g kg^{-1}, but there were no differences ($p<0.05$) between the studied areas, except for the 0.10-0.20 m layer, with lower content in the NF and higher content in the areas of PP and NTS (Table 3). The FA have a lower nitrogen carbon (C/N) ratio compared to the other fractions, facilitating their decomposition by soil microorganisms (Dobbss *et al.*, 2009). Moreover, this fraction is responsible for the process of transporting cations in the soil, being also fundamental for the cycling of C and nutrients. However, this fraction is highly sensitive to changes in management and can be easily lost due to inadequate management in certain areas (Baldotto and Baldotto, 2014).

The C-HA contents ranged from 0.75 to 2.95 g kg^{-1}, with higher levels observed in the NF area in all evaluated layers, similar ($p<0.05$) to the NTS area in the 0.10-0.20 m layer. In general, the areas of PP and PNHR had lower levels of C-HA ($p<0.05$) in relation to the other areas (Table 3). This may be related to soil management used in these areas over the last few years, which do not advance the SOM humification process, with consequent lower C levels of the chemically more stable fractions of C (Guimarães *et al.*, 2013).

The C-HUM contents ranged from 1.92 to 7.25 g kg^{-1}, as did those of C-HA; the C-HUM contents were higher in the NF area in all layers evaluated, being similar ($p<0.05$) only in relation to the NTS area in the 0.10-0.20 m layer. These results of C-HUM contents are related to TOC contents (Table 3), mainly because the HUM fraction represents the majority of the soil TOC. It is noteworthy that the C-HUM contents in the NTS area were higher ($p<0.05$) than the other two anthropized areas in all evaluated layers (Table 1). Due to the lower soil disturbance due to non-revolving, over the years of cultivation the NTS provides greater stability of C (Guimarães *et al.*, 2013) with predominance of the HUM fraction (Rosset *et al.*, 2016). On the other hand, the lowest levels of C-HUM in the areas of PP and PNHR (Table 3) are associated with non-conservationist management of these areas over the last years, as also evidenced in the lower TOC contents of these areas.

With the exception of the NF area in all layers, and the NTS area in the 0.10-0.20 m layer, the values of the HA/FA ratio were below 1.00 (Table 3). The HA/FA ratio is useful, mainly to reflect the quality of humus, in which the higher the ratio, the higher the condition of SOM humification and the better the quality and stability of the soil organic fraction (Pfleger *et al.*,

2017, Diniz *et al.*, 2020).

Considering the results, it can be affirmed that the areas of PP and PNHR have lower stabilization of the SOM, with consequent lower quality of the soil organic fraction, with a higher proportion of FA in relation to HA, with damage to other edaphic attributes, such as soil structural stability.

However, it is important to highlight that in soils under tropical climate conditions, along with the presence of soils with more sandy texture, the HA/FA ratio is usually lower due to the high rate of decomposition of plant residues under the soil. For the AE/HUM ratio, the PNHR area had higher values in all evaluated layers, ranging from 1.33 to 2.05, differing ($p<0.05$) from all other areas (Table 3). Higher values of this relationship indicate greater presence of less stable fractions of C (FA and HA), in relation to the fraction of greater chemical stability (HUM).

The StockC-FA ranged from 1.77 to 3.16 Mg ha^{-1}, but did not differ ($p<0.05$) between the management systems evaluated in the layers 0.00-0.05 m and 0.05-0.10 m. In the 0.10-0.20 m layer, the NF area had lower StockC-FA in relation to the PP and NTS areas (Table 3). Among the soil humic substances, the FA fraction is the first to undergo quantitative changes, as it reflects the first stage for the stabilization of the SOM (Rosa *et al.*, 2017).

The NF area had the highest StockC-HA in the first two layers, 3.76 Mg ha^{-1} and 3.23 Mg ha^{-1}, respectively, similar ($p<0.05$) to the NTS area in the 0.10-0.20 m layer. The PP area stood out negatively, with lower values of StockC-HA in all layers, similar to PNHR in the layers of 0-0.05 and 0.10-0.20 m, and with lower stock (0.94 Mg ha^{-1}) in the 0.05-0.10 m layer (Table 3).

The highest StockC-HUM in the 0.00-0.05 m layer was observed in NF with a value of 9.23 Mg ha^{-1}, differing ($p<0.05$) from the other areas. In the layers 0.05-0.10 m and 0.10-0.20 m, the StockC-HUM was similar ($p<0.05$) between the NTS and NF areas, different from that observed in the PNHR and PP areas, which had the lowest StockC-HUM (Table 3). These results corroborate the C contents of the SOM fractions and also the TOC contents, mainly because the HUM fraction represents the majority of the soil TOC.

It is important to highlight that, among the managed areas, the NTS, even in soybean/corn succession implemented since 2009, had higher levels and C stock of the most stable fractions of the SOM, being similar to NF in the most superficial layer (Table 3). Rosset *et al.* (2016) report that the accumulation of C in the most recalcitrant fractions of SOM tends to increase as a function of the time of adoption of the NTS.

Through the quantitative results of C contents, with qualitative inferences in relation to the chemical fractions of the SOM (Table 3), it is possible to observe that the PNHR area, due to the anthropic actions of soil exploration for clay extraction, had low C stocks of the most stable fractions of the SOM (HA and HUM) in addition to the lowest HA/FA ratio and highest AE/HUM ratio (Table 3). The same thing happened in the PP area, because this area is in an advanced stage of degradation, impairing the processes of humification of the SOM, with consequent lower chemical stabilization.

3.2. Physical Fractions of Soil Organic Matter

In all layers evaluated, the NF area had higher ($p<0.05$) carbon content of particulate organic matter (C-POM) when compared to the three managed systems, reaching 4.04 g kg^{-1} in the 0.00-0.05 m layer (Table 4). These higher levels of C-POM in the surface layer coincide with the pattern of the highest TOC contents observed in this area (Table 3). Similar data were found by Kunde *et al.* (2016); Rosset *et al.* (2019); Bieluczyk *et al.* (2020); Ferreira *et al.* (2020) and Santos *et al.* (2021), comparing different types of native vegetation with managed areas.

Comparing only the managed areas, it was observed that the NTS area showed higher C-POM ($p<0.05$) than PP in the 0.00-0.05 m layer and PNHR in all layers, with values of 2.19 g kg^{-1}, 1.85 g kg^{-1} and 1.68 g kg^{-1}, respectively, for the layers 0.00-0.05, 0.05-0.10 and 0.10-0.20

m (Table 4). These higher levels observed in NTS are due to the minimal soil disturbance of this area, added to the accumulation of plant residues over the years of cultivation, as also observed by Melo *et al.* (2016) and Rosset *et al.* (2019) in NTS areas in succession of soybean/corn crops. In general, the highest levels of C-POM observed in the soil surface layer occur due to the higher intake of plant residues in this layer, together with the absence of anthropic actions that impair the accumulation of particulate C (Rosset *et al.*, 2014; Kunde *et al.*, 2016; Nanzer *et al.*, 2019).

Table 4. Carbon contents of particulate organic matter (C-POM), mineral organic matter (C-MOM), POM carbon stock (Stock POM) and MOM (Stock MOM), carbon stock index (CSI), lability (L), lability index (LI) and carbon management index (CMI) of the different areas evaluated in the district of Porto Morumbi, municipality of Eldorado, Mato Grosso do Sul.

MS	C-POM	C-MOM	Stock MOP	Stock MOM	CSI	L	LI	CMI
	g kg^{-1}		Mg ha^{-1}					
			0.00-0.05 m					
PP	1.70c	5.56c	2.17c	7.08c	0.44c	0.31a	0.95a	42.13b
NTS	2.19b	9.26b	2.80b	11.79b	0.69b	0.23b	0.73b	50.95b
PNHR	1.74c	5.85c	2.22c	7.45c	0.46c	0.30ab	0.92ab	42.61b
MN	4.04a	12.37a	5.14a	15.75a	1.00a	0.32a	1.00a	100.00a
CV (%)	8.06	5.89	8.06	5.89	4.70	12.34	12.85	9.55
			0.05-0.10 m					
PP	1.78b	5.25c	2.21b	6.54c	0.51c	0.34a	1.27a	65.51b
NTS	1.85b	8.51b	2.31b	10.58b	0.76b	0.21b	0.80b	61.67b
PNHR	1.35c	4.95c	1.68c	6.16c	0.46d	0.27b	1.01ab	47.07c
MN	2.89a	10.70a	3.60a	13.31a	1.00a	0.27b	1.00a	100.00a
CV (%)	7.54	4.53	7.54	4.53	3.22	13.01	15.14	10.27
			0.10-0.20 m					
PP	1.45b	5.33b	1.85b	6.80b	0.66b	0.27ab	0.89a	59.04bc
NTS	1.68b	8.49a	2.15b	10.84a	1.00a	0.19b	0.64b	64.21b
PNHR	1.11c	4.63b	1.42c	5.91b	0.56c	0.24ab	0.77ab	44.46c
MN	2.41a	7.79a	3.08a	9.95a	1.00a	0.31a	1.00a	100.00a
CV (%)	10.24	7.00	10.24	7.00	6.27	16.91	15.63	13.49

Means followed by equal letters in the column, in each layer, do not differ from each other by Tukey's test (5%). MS: management system; PP: permanent pasture; NTS: no-tillage system; PNHR: Private Natural Heritage Reserve and NF: native forest; CV= Coefficient of variation.

It is also important to highlight the lowest levels of C-POM in the PNHR area, ranging from 1.11 to 1.35 g kg^{-1}, demonstrating low potential for labile C accumulation in this area. The differences ($p<0.05$) in C-POM contents in the studied areas reinforce the potential of this fraction to be used as an indicator of soil quality due to the sensitivity to demonstrate changes in a short period of time, resulting from the use of the edaphic environment (Conceição *et al.*, 2013; Briedis *et al.*, 2018; Bongiorno *et al.*, 2019; Rosset *et al.*, 2019). Higher C-POM levels are related to the aggregation process, where these labile fractions are slowly occluded in soil aggregates, leading to physical protection of SOM (Tobiasová, 2011). However, through the change in land use and cultivation, the labile fractions are constantly exposed to microbial activity and subject to mineralization, hindering the occlusion process and, consequently, promoting the reduction of SOM levels (La Scala *et al.*, 2008) as reported by Gmach *et al.* (2018).

The NF area also had the highest levels of C-MOM in all layers, being similar ($p<0.05$) to

the NTS in the layer of 0.10-0.20 m, with contents ranging from 7.79 g kg^{-1} to 12.37 g kg^{-1} (Table 4). The NTS area had intermediate levels in the layers of 0.00-0.05 m and 0.05-0.10 m, with 9.26 g kg^{-1} and 8.51 g kg^{-1}, respectively. The highest levels of C-MOM (Table 4) are mainly related to the higher levels of TOC in these areas (Table 3), added to non-revolving, and to the contribution of POM stabilization over time, where the labile fraction of C becomes the most recalcitrant fraction, with consequent stabilization of the SOM over time (Ozório *et al.*, 2020).

Relating to the low TOC contents (Table 3), as well as low C-POM contents, the PP and PNHR areas had the lowest C-MOM levels in all three layers evaluated (Table 4). Since C-MOM has slow cycling, it is possible to infer that, because these areas have low vegetation cover and are considerably degraded, these low levels are justified. According to Mafra *et al.* (2015), the reduction of C-MOM in the managed areas in comparison with native vegetation area is associated with the breakdown of aggregates due to inadequate management over the years, exposing C to the action of microorganisms and external degradation agents, hindering the accumulation of TOC in the soil. However, this fraction is considered less sensitive to soil management in relation to POM, especially in the short term, due to being physically protected and considered more stable (Guimarães *et al.*, 2018).

The highest stocks of particulate organic matter (StockPOM) were found in the NF area in all layers evaluated, reaching 5.14 Mg ha^{-1} in the 0.00-0.05 m layer, differing ($p<0.05$) from the other areas (Table 4). This fact results from the absence of anthropic activities and the greater deposition of residues newly incorporated into the soil, as can be observed in the highest levels of C-POM in this area. Similar results were also observed by Rosset *et al.* (2019) comparing different management systems in relation to native Atlantic forest vegetation.

The lowest StockPOM were observed in the areas of PP, NTS and PNHR, with 2.17, 2.80 and 2.22 Mg ha^{-1} for the 0.00-0.05 m layer, 2.21, 2.31 and 1.68 Mg ha^{-1} for the 0.05-0.10 m layer and 1.85, 2.15 and 1.42 Mg ha^{-1} in the 0.10-0.20 m layer, respectively (Table 4). The values found in these managed areas in relation to the NF area corroborate the lowest levels of TOC (Table 3) and C-POM (Table 4), demonstrating that the forms of land use of these areas over the last few years have not been efficient in contributing to the increase in labile C stocks in the soil.

As for C-MOM contents, the NF and NTS areas had ($p<0.05$) the highest StockMOM in the most superficial layer, with 15.75 Mg ha^{-1} and 11.79 Mg ha^{-1}, respectively (Table 4). Bayer *et al.* (2004) reported that StockMOM is less altered by different forms of management. Carmo *et al.* (2012) observed that in deeper layers, this fraction is highly stable, undergoing little changes by the management system. If specific recovery practices are adopted in the PP area, such as reform of pasture with soil correction, in addition to forest density in the PNHR area, the entry of C into the soil can be reestablished and, consequently, promote the increase of stocks of labile fractions and subsequently recalcitrant, with consequent increases in the total StockC (Falcão *et al.*, 2020).

All managed areas presented CSI values lower than 1.00, except for the 0.10-0.20 m layer of the NTS area (Table 4). This fact indicates that these forms of management were not potentially efficient in stocking C in the soil. The CSI values observed in these areas followed the trend of the lowest TOC contents (Table 3). Among the managed areas, the NTS presented the highest ($p<0.05$) CSI (Table 4). Considering that prior to the implementation of the NTS, the area was managed under a conventional tillage system, the results of CSI infer that the land use in this area allowed the recovery of carbon stock, even if slowly. Similar results were obtained by Conceição *et al.* (2014), also in an area with alteration from CTS systems to NTS, and by Rosset *et al.* (2019) in NTS chronosequence, in areas previously cultivated with CTS. Zhang *et al.* (2020) observed that the adoption of management practices with a greater number of plant species can promote the accumulation of TOC in the soil more rapidly, resulting in a

greater amount of labile organic fractions in a short period after the adoption of this practice.

In general, the areas presented L values lower than 1.00, indicating the predominance of C in the fraction associated with minerals (MOM), which is desirable, because this fraction is more stable (Guimarães *et al.*, 2018). According to Santos *et al.* (2017), the system becomes more susceptible to C loss by the action of microorganisms when C-POM predominates, because in this fraction, C has lower stability and is exposed to the highest rate of decomposition.

The L values in the 0.00-0.05 m layer of the NF, PNHR and PP areas did not differ from each other ($p<0.05$), with values of 0.32, 0.30 and 0.31, respectively. It is also emphasized that in the 0.05-0.10 m layer the PP area had a value of 0.34, higher than the other areas ($p<0.05$) (Table 4). L is considered an excellent indicator of soil quality, being obtained through the ratio between POM and MOM fractions, and values closer to 1.00 suggest balance between these fractions (Benbi *et al.*, 2015). Similar results were obtained by Schiavo *et al.* (2011) in the state of Mato Grosso do Sul and Rosset *et al.* (2019) and Ozório *et al.* (2020) in the state of Paraná, both comparing managed and native areas. Except for the PP area, it was observed that for the other areas evaluated, the L of the SOM decreased according to the depth, especially in the area of NTS (Table 4). The same behavior was observed by Schiavo *et al.* (2011), Kunde *et al.* (2016) and Rosset *et al.* (2019).

In the 0.00-0.05 m layer, for the managed areas, the values of the lability index (LI) were close to the NF, and the NTS area showed a difference ($p<0.05$) in relation to the PP and PNHR areas. For the other layers, only the NTS area presented values lower than the NF (Table 4).

In none of the management systems evaluated, CMI values similar or higher ($p<0.05$) to those of the NF area were observed in all layers evaluated. However, evaluating only the managed areas, the highest values were observed in the NTS areas, with 64.21 in the 0.10-0.20 m layer, and PP, 65.51 in the 0.05-0.10 m layer. These results are probably due to the non-revolving of the soil in both the NTS and PP, and even if the PP area is considerably degraded, the presence of grasses is fundamental, as it favors a certain stabilization of C in subsurface by the action of the root system (Nanzer *et al.*, 2019; Santos *et al.*, 2019).

In general, presenting behavior similar to the levels of TOC (Table 3), C-POM and C-MOM (Table 4), it is noteworthy that the PNHR area presented lower CMI values ($p<0.05$) than those found in NTS and PP in the 0.05-0.10 m layer and NTS in the 0.10-0.20 m layer, ranging from 42.61 to 47.07 (Table 4). These results reflect the state of degradation in which the area is after being overexploited for decades, demonstrating that, in addition to the isolation done in 2017, it requires other recovery practices so that there is an increase in the quantity and improvement of the quality of the SOM, with consequent improvement of other edaphic attributes. Satisfactory results of increase in the C contents and physical fractions of SOM and CMI in an isolated area, with subsequent practice of forest density through planting of native tree species were found by Santos *et al.* (2021) in the municipality of Mundo Novo, MS.

3.3. Analysis of principal components and correlation between variables

A multivariate analysis was performed using the data of the attributes Sd, TOC, C-FA, C-HA, C-HUM, HA/FA, AE/HUM, StockC-FA, StockC-HA, StockC-HUM, C-POM, C-MOM, StockC-POM, StockC-MOM, CSI, L, LI and CMI, in which the edaphic variables in the 0-0.2 m layer explain 83.8% of the data variation for the first two axes (Figure 3). The areas of NF and NTS were in different positions in relation to the areas of PP and PNHR, in which the latter were more related to the variable AE/HUM. The NF area was related to all other attributes, except for C-FA, StockC-FA and Sd. It is important to highlight that the NTS area is closer to NF, that is, it has the closest one similarity to all the attributes evaluated (Figure 3).

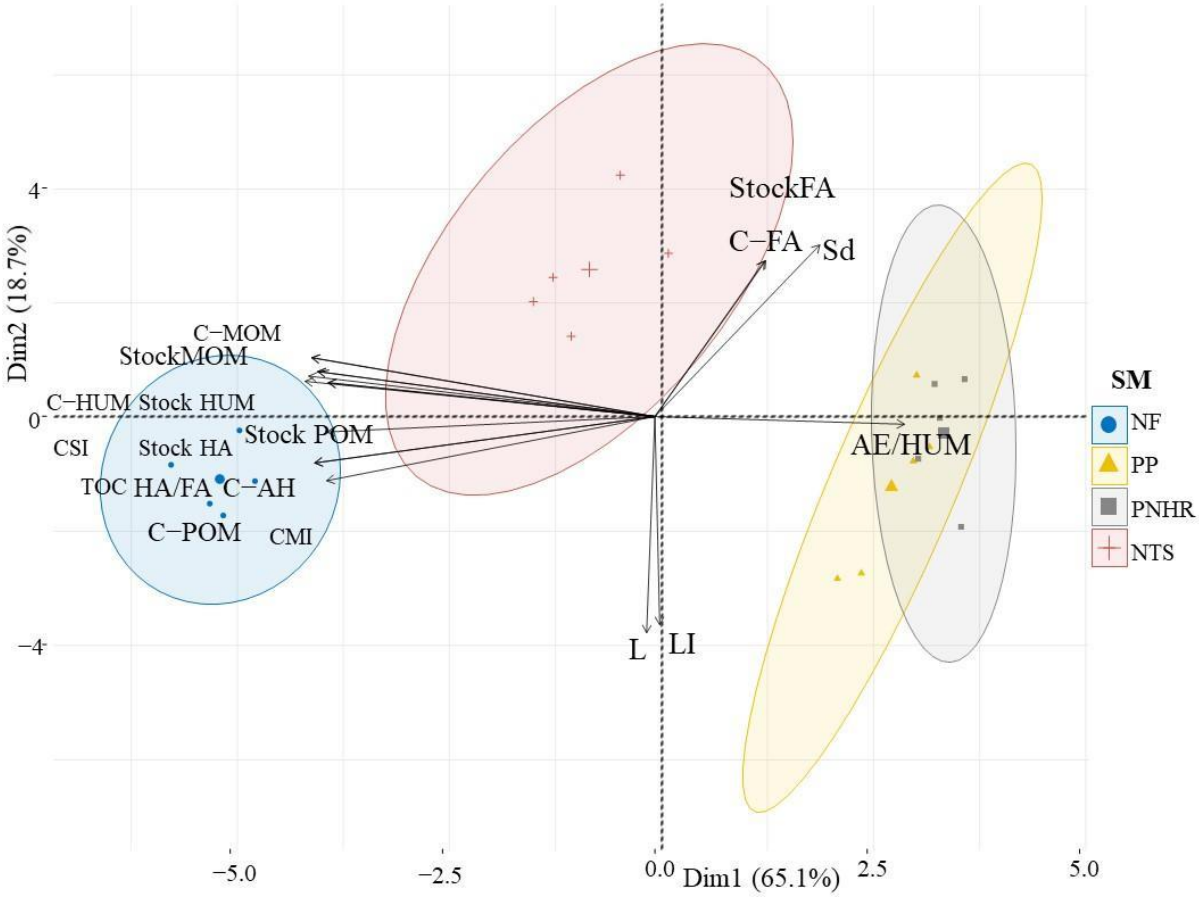

Figure 3. Principal Component Analysis - PCA for the different areas evaluated. PP: permanent pasture. NTS: no-tillage system. PNHR: Private Natural Heritage Reserve. NF: native forest. Carbon from fulvic acids (C-FA), humic acid (C-HA) and humin (C-HUM), HA/FA ratio, alkaline extract (AE)/HUM and carbon stock from fulvic acid fractions (StockFA), humic acid StockHA) and humin (StockHUM), carbon from particulate organic matter (C-POM) and mineral organic matter (C-MOM), carbon stock from POM (StockPOM) and MOM (StockMOM), carbon stock index (CSI), lability (L), lability index (LI) and carbon management index (CMI).

The areas of PP and PNHR, due to the arrangement of the groups, did not contribute effectively to the improvement of the edaphic quality within the parameters evaluated, and only the NTS area was closer to the NF. Rosset *et al.* (2014; 2016); Martins *et al.* (2020) and Troian *et al.* (2020) also observed the same behaviors found in this study, with the NF area of vegetation of the Atlantic Forest biome having better edaphic quality in relation to the other managed areas. Rosset *et al.* (2019) observed similarities between the areas of PP and NF. Unlike what was observed by Falcão *et al.* (2020), where the NF area of the Cerrado biome was similar to the areas of NTS and PP with six years of implementation.

In Pearson's correlation analysis presented in Figure 4, it is possible to highlight the positive and significant correlation ($p<0.05$) of the C-POM and C-MOM contents with the C-HA and C-HUM contents, and these four variables have a strong relationship with the TOC content. Such behavior is also observed in the stock values of these variables. These results show the importance of maintaining the TOC, to contribute to the different stages and composition of the SOM, and consequently in the improvement of soil quality, with greater structuring (Tisdal and Oades, 1982; Ferreira *et al.*, 2020), nutrient cycling (Santos *et al.*, 2019), mitigation of erosive processes that cause the loss of productive soil (Lal, 2018) and mainly reducing CO_2 emissions into the atmosphere.

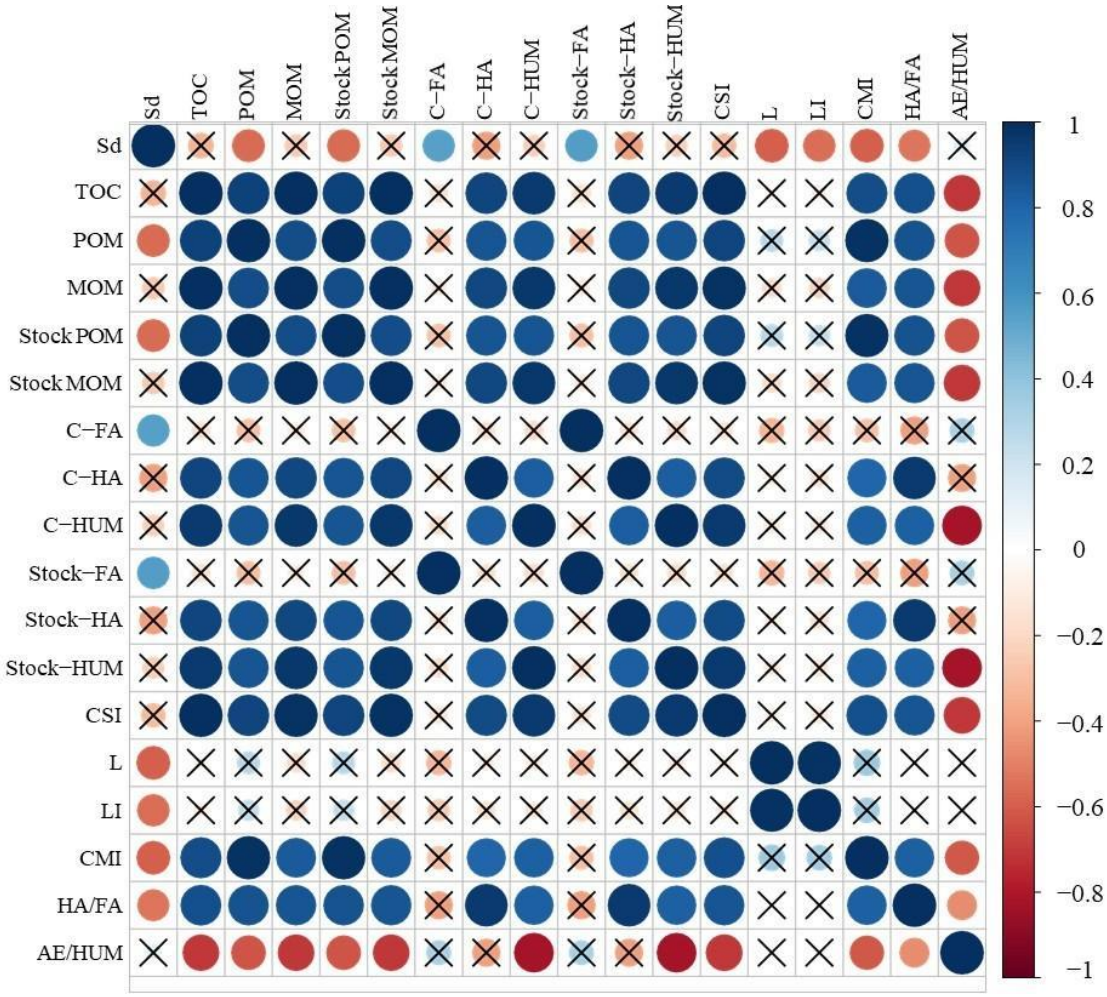

Figure 4. Correction matrix between variables using Pearson's correlation method. Carbon from fulvic acids (C-FA), humic acid (C-HA) and humin (C-HUM), HA/FA ratio, alkaline extract (AE)/HUM and carbon stock from fulvic acid fractions (Stock-FA), humic acid (Stock-HA) and humin (Stock-HUM), carbon from particulate organic matter (C-POM) and mineral organic matter (C-MOM), carbon stock from POM (Stock POM) and MOM (Stock MOM), carbon stock index (CSI), lability (L), lability index (LI) and carbon management index (CMI). Correlations identified with "X" do not present significant correction ($p<0.05$).

Figure 4 also shows a significant correlation ($p<0.05$) between CMI values and C-HA and C-HUM contents. This shows that even though fractionation techniques are different once the HS is changed, it changes the C in quality and quantity (CMI). Thus, we evidenced the complexity of the SOM, and sensitivity that it presents in identifying changes in the use and occupation of soil (Lal, 2018).

4. CONCLUSIONS

Based on our findings, the no-tillage system, even in the soybean/corn succession, contributes to carbon content and stocks, favoring the quantity and quality of organic matter. The no-tillage system also had characteristics closer to the reference area, compared to other available systems.

Among the managed areas, an area of direct planning system demonstrates the presence of fractions of greater stability and greater degree of humification of soil organic matter.

It is also concluded that degraded pastures and areas with intense exploitation accrue the presence of C in the soil, not offering environmental benefits in the mitigation of CO_2 emissions,

with significant losses of C in relation to areas of no-tillage system and native forest.

5. ACKNOWLEDGMENTS

The authors thank State University of Mato Grosso do Sul (UEMS); Foundation for the Support and Development of Teaching, Science and Technology of the State of Mato Grosso do Sul (Fundect) (Process UEMS n 25/2015) for the support to the graduation and post-graduation courses of UEMS; the PIBIC/UEMS for granting a scientific initiation scholarship to undergraduate students; Coordination for the Improvement of Higher Education Personnel (CAPES) for granting doctoral and master's scholarships.

6. REFERENCES

ANGHINONI, I. Fertilidade do solo e seu manejo no sistema plantio direto. *In*: NOVAIS, R. F.; ALVAREZ, V. H.; BARROS, N. F.; FONTES, R. L. F.; CANTARUTTI, R. B.; NEVES, J. C. L. **Fertilidade do solo**. Viçosa, SBCS, 2007, p. 873-928.

AZIZ, I.; MAHMOOD, T.; ISLAM, K. R. Effect of long term no-till and conventional tillage practices on soil quality. **Soil and Tillage Research**, v. 131, p. 28-35, 2013. https://doi.org/10.1016/j.still.2013.03.002

BALDOTTO, M. A.; BALDOTTO, L. E. B. Ácidos húmicos. **Revista Ceres**, v. 61, p. 856-881, 2014. https://doi.org/10.1590/0034-737x201461000011

BARROS, H. S.; FEARNSIDE, P. M. Soil carbon stock changes due to edge effects in central Amazon forest fragments. **Forest Ecology and Management**, v. 379, p. 30-36, 2016. https://doi.org/10.1016/j.foreco.2016.08.002

BAYER, C.; MARTIN-NETO, L.; MIELNICZUK, J.; PAVINATO, A. Armazenamento de carbono em frações lábeis da matéria orgânica de um Latossolo Vermelho sob plantio direto. **Pesquisa Agropecuária Brasileira**, v. 39, n. 7, p. 677-683, 2004. https://doi.org/10.1590/S0100-204X2004000700009

BENBI, D. K.; BRAR, K.; TOOR, A. S.; SINGH, P. Total and labile pools of soil organic carbon in cultivated and undisturbed soils in northern India. **Geoderma**, v. 237-238, n. 1, p. 149-158, 2015. https://doi.org/10.1016/j.geoderma.2014.09.002

BENITES, V. M.; MÁDARI, B.; MACHADO, P. L. O. A. **Extração e fracionamento quantitativo de substâncias húmicas do solo:** Um procedimento simplificado e de baixo custo. Rio de Janeiro, Embrapa Solos, 2003. 7p. (Comunicado Técnico, 16).

BIELUCZYK, W.; PICCOLO, M. C.; PEREIRA, M. G.; MORAES, M. T.; SOLTANGHEISI, A.; BERNARDI, C. C. A. *et al.* Integrated farming systems influence soil organic matter dynamics in southeastern Brazil. **Geoderma**, v. 371, 114368, 2020. https://doi.org/10.1016/j.geoderma.2020.114368

BLAIR, G. J.; LEFROY, R. D. B.; LISLE, L. Soil carbon fractions based on their degree of oxidation, and the development of a carbon management index for agricultural systems. **Australian Journal of Agricultural Research**, v. 46, n. 7, p. 1459-1466, 1995. https://doi.org/10.1071/AR9951459

BONGIORNO, G.; BÜNEMANN, E. K.; OGUEJIOFOR, C. U.; MEIER, J.; GORT, G.; COMANS, R. *et al.* Sensitivity of labile carbon fractions to tillage and organic matter management and their potential as comprehensive soil quality indicators across pedoclimatic conditions in Europe. **Ecological Indicators**, v. 99, p. 38-50, 2019. https://doi.org/10.1016/j.ecolind.2018.12.008

BORGES, S. C.; RIBEIRO, B. T.; WENDLING, B.; CABRAL, D. A. Agregação do solo, carbono orgânico e emissão de CO_2 em áreas sob diferentes usos no Cerrado, região do Triângulo Mineiro. **Revista Ambiente and Água**, v. 10, n. 3, p. 661-675, 2015. https://doi.org/10.4136/ambi-agua.1573

BRAVO, S.; GONZÁLEZ-CHANG, M.; DEC, D.; VALLE, S.; WENDROTH, O.; ZÚÑIGA, F.; DÖRNER, J. Using wavelet analyses to identify temporal coherence in soil physical properties in a volcanic ash-derived soil. **Agricultural and Forest Meteorology**, v. 285, p. 107909, 2020. https://doi.org/10.1016/j.agrformet.2020.107909

BRIEDIS, C.; SÁ, J. C. M.; LAL, R.; TIVET, F.; FRANCHINI, J. C.; FERREIRA, A. O. *et al.* How does no-till deliver carbon stabilization and saturation in highly weathered soils? **Catena**, v. 163, n. 4, p. 13-23, 2018. https://doi.org/10.1016/j.catena.2017.12.003

CAMBARDELLA, C. A.; ELLIOTT, E. T. Particulate soil organic-matter changes across a grassland cultivation sequence. **Soil Science Society of America Journal**, v. 56, n. 3, p. 777-783, 1992. https://doi.org/10.2136/sssaj1992.03615995005600030017x

CARMO, F. F.; FIGUEIREDO, C. C.; RAMOS, M. L. G.; VIVALDI, L. J.; ARAÚJO, L. G. Frações granulométricas da matéria orgânica em Latossolo sob plantio direto com gramíneas. **Bioscience Journal**, v. 28, n. 3, p. 420-431, 2012.

CLAESSEN, M. E. C. **Manual de métodos de análise de solo**. 2. ed. Rio de Janeiro: Embrapa, 1997, 212 p.

CONCEIÇÃO, P. C.; DIECKOW, J.; BAYER, C. Combined role of no-tillage and cropping systems in soil carbon stocks and stabilization. **Soil and Tillage Research**, v. 129, p. 40-47, 2013. https://doi.org/10.1016/j.still.2013.01.006

CONCEIÇÃO, P. C.; BAYER, C.; DIECKOW, J.; SANTOS, D. C. Fracionamento físico da matéria orgânica e índice de manejo de carbono de um Argissolo submetido a sistemas conservacionistas de manejo. **Ciência Rural**, v. 44, n. 5, p. 794-800, 2014. https://doi.org/10.1590/S0103-84782014005000004

CORRÊA, E. A.; MORAES, I. C.; PINTO, S. D. A. F. Qualidade física de solos arenosos submetidos a diferentes usos da terra. **Revista Brasileira de Geografia Física**, v. 9, n. 5, p. 1501-1512, 2016.

DOBBSS, L. B.; RUMJANECK, V. M. BALDOTTO, M. A.; VELLOSO, A. C. X; CANELLAS, L. P. Caracterização química e espectroscópica de Ácidos húmicos e fúlvicos isolados da camada superficial de Latossolos Brasileiros. **Revista Brasileira de Ciência do Solo**, v. 33. p. 51-63, 2009. https://doi.org/10.1590/S0100-06832009000100006

DINIZ, A. R.; GUARESCHI, R. F.; PEREIRA, M. G.; FERNANDES, D. A. C.; BALIEIRO, F. C.; SILVA, E. V. D. *et al.* Soil Carbon Fractions in Rubber Trees, Pasture, and Secondary Forest Areas. **Floresta e Ambiente**, v. 27, n. 2, p. 1-8, 2020. https://doi.org/10.1590/2179-8087.114917

DORAN, J. W.: PARKIN, T. B. Defining and assessing soil quality. *In*: DORAN, J. W.; COLEMAN, D. C.; BEZDICEK, D. F.; STEWART, B. A. (eds.). **Defining soil quality for a sustainable environment**. Madison: Soil Science Society of America, 1994. p. 3-22. https://doi.org/10.2136/sssaspecpub35.c1

FALCÃO, K. S.; NEVES, F. M.; OZÓRIO, J. M. B.; SILVA SOUZA, C. B.; FARIAS, P. G. S.; MENEZES, R. S. *et al.* Estoque de carbono e agregação do solo sob diferentes sistemas de uso no Cerrado. **Revista Brasileira de Ciências Ambientais**, v. 55, n. 2, p. 242-255, 2020. https://dx.doi.org/10.5327/Z2176-947820200695

FERREIRA, E. B.; CAVALCANTI, P. P.; NOGUEIRA, D. A**. ExpDes.pt**: Pacote Experimental Designs (Portuguese). R package Version 1.2.0. 2018. Available: https://CRAN.R-project.org/package=ExpDes.pt. Access: 15 jan. 2021.

FERREIRA, C. R.; SILVA NETO, E. C.; PEREIRA, M. G.; GUEDES, J. N.; ROSSET, J. S.; ANJOS, L. H. C. Dynamics of soil aggregation and organic carbon fractions over 23 years of no-till management. **Soil and Tillage Research**, v. 198, p. 1-9, 2020. https://doi.org/10.1016/j.still.2019.104533

GMACH, M. R.; DIAS, B. O.; SILVA, C. A.; NÓBREGA, J. C. A.; LUSTOSA FILHO, J. F.; SIQUEIRA NETO, M. Soil organic matter dynamics and land-use change on Oxisols in the Cerrado, Brazil. **Geoderma Regional**, v. 14, p. 1-8, 2018. https://doi.org/10.1016/j.geodrs.2018.e00178

GAZOLLA, P. R.; GUARESCHI, R. F.; PERIN, A., PEREIRA, M. G.; ROSSI, C. Q. Frações da matéria orgânica do solo sob pastagem, sistema plantio direto e integração lavoura-pecuária. **Semina: Ciências Agrárias**, v. 36, n. 2, p. 693-704, 2015. https://doi.org/10.5433/1679-0359.2015v36n2p693

GUIMARÃES, D. V.; GONZAGA, M. I. S.; SILVA, T. O.; DA SILVA, T. L.; DA SILVA DIAS, N. *et al.* Soil organic matter pools and carbon fractions in soil under different land uses. **Soil and Tillage Research**, v. 126, p. 177-182, 2013. https://doi.org/10.1016/j.still.2012.07.010

GUIMARÃES, D. V.; SILVA, M. L. N.; BEINIACH, A.; BISPO, D. F. A.; CONTINS, J. G. P.; CURI, N. Relationship between soil organic matter fractions and cover plants in Olive post planing. **Revista Brasileira de Fruticultura**, v. 40, n. 6, p. e-027, 2018. https://doi.org/10.1590/0100-29452018027

HAN, L.; SUN, K.; JIN, J.; XING, B. Some concepts of soil organic carbon characteristics and mineral interaction from a review of literature. **Soil Biology and Biochemistry**, v. 94, p. 107-121, 2016. https://doi.org/10.1016/j.soilbio.2015.11.023

ICMBio. **APA das Ilhas e Várzeas do Rio Paraná**. 2019. Available: http://www.icmbio.gov.br/portal/unidadesdeconservacao/biomas-brasileiros/mata-atlantica /unidades-de-conservacao-mata-atlantica/2176-apa-ilhas-e-varzeas-do-rio-parana. Access: 15 jan. 2021.

IUSS WORKING GROUP WRB. **World Reference Base for Soil Resources (WRB), sistema universal reconhecido pela International Union of Soil Science (IUSS) e FAO**. 2015. Available: http://www.fao.org/3/a-i3794e.pdf

KOVEN, C. D.; HUGELIUS, G.; LAWRENCE, D. M.; WIEDER, W. R. Higher climatological temperature sensitivity of soil carbon in cold than warm climates. **Nature Climate Change**, v. 7, n. 11, p. 817, 2017. https://doi.org/10.1038/nclimate3421

KUNDE, R. J.; LIMA, C. L. R.; SILVA, S. D. A.; PILLON, C. N. Frações físicas da matéria orgânica em Latossolo cultivado com cana-de-açúcar no Rio Grande do Sul. **Pesquisa Agropecuária Brasileira**, v. 51, n. 9, p. 1520-1528, 2016. https://doi.org/10.1590/S0100-204X2016000900051

LA SCALA, N. J.; LOPES, A.; SPOKAS, K.; BOLONHEZI, D.; ARCHER, D. W.; REICOSKY, D. C. Short-term temporal changes of soil carbon losses after tillage described by a first-order decay model. **Soil and Tillage Research**, v. 99, n. 1, p. 108-118, 2008. https://doi.org/10.1016/j.still.2008.01.006

LAL, R. Digging deeper: A holistic perspective of factors affecting soil organic carbon sequestration in agroecosystems. **Global Change Biology**, v. 24, p. 3285-3301, 2018. https://doi.org/10.1111/gcb.14054

LEHMANN, J.; KLEBER, M. The contentious nature of soil organic matter. **Nature**, v. 528, p. 60-68, 2015. https://doi.org/10.1038/nature16069

LOSS, A.; BASSO, A.; OLIVEIRA, B. S.; KOUCHER, L. P.; OLIVEIRA, R. A.; KURTZ, C. *et al.* Carbono orgânico total e agregação do solo em sistema de plantio direto agroecológico e convencional de cebola. **Revista Brasileira de Ciência do Solo**, v. 39, n. 4, p. 1212-1224, 2015. https://doi.org/10.1590/01000683rbcs20140718

MAFRA, M. S. H.; CASSOL, P. C.; ALBUQUERQUE, J. A.; GROSKOPF, M. A.; ANDRADE, A. P.; RAUBER, L. P. *et al.* Organic carbon contents and stocks in particle size fractions of a typic hapludox fertilized with pig slurry and soluble fertilizer. **Revista Brasileira de Ciência do Solo**, v. 39, n. 4, p. 1161-1171, 2015. https://doi.org/10.1590/01000683rbcs20140177

MAGALHÃES, S. S. A.; RAMOS, F. T.; WEBER, O. L. S. Carbon stocks of an Oxisol after thirty-eight years under different tillage systems. **Revista Brasileira de Engenharia Agrícola e Ambiental**, v. 20, n. 1, p. 85-91, 2016. https://doi.org/10.1590/1807-1929/agriambi.v20n1p85-91

MARQUES, J. D. O.; LUIZÃO, F. J.; TEIXEIRA, W. G.; SARRAZIN, M.; FERREIRA, S. J. F.; BELDINI, T. P. *et al.* Distribution of organic carbon in different soil fractions in ecosystems of central Amazonia. **Revista Brasileira de Ciência do Solo**, v. 39, n. 1, p. 232-242, 2015. https://doi.org/10.1590/01000683rbcs20150142

MARTINS, L. F. B. N.; TROIAN, D.; ROSSET, J. S.; SOUZA, C. B. S.; FARIAS, P. G. S.; OZÓRIO, J. M. B. *et al.* Soil carbon stock in different uses in the southern cone of Mato Grosso do Sul. **Revista de Agricultura Neotropical**, v. 7, n. 4, p. 86-94, 2020.

MATO GROSSO DO SUL. SEMADE. **Estudo da Dimensão Territorial do Estado de Mato Grosso do Sul**: Regiões de Planejamento. Campo Grande: Governo do Estado de Mato Grosso do Sul, 2015. 91 p.

MELO, G. B.; PEREIRA, M. G.; PERIN, A.; GUARESCHI, R. F.; SOARES, P. F. C. Estoques e frações da matéria orgânica do solo sob os sistemas plantio direto e convencional de repolho. **Pesquisa Agropecuária Brasileira**, v. 51, n. 9, p. 1511-1519, 2016. https://doi.org/10.1590/S0100-204X2016000900050

NANZER, M. C.; ENSINAS, S. C.; BARBOSA, G. F.; VECHETIN, P. G. B.; OLIVEIRA, T. P.; SILVA, J. R. M.; PAULINO, L. A. Estoque de carbono orgânico total e fracionamento granulométrico da matéria orgânica em sistemas de uso do solo no Cerrado. **Revista de Ciências Agroveterinárias**, v. 18, n. 1, p. 136-145, 2019. https://doi.org/10.5965/223811711812019136

OLK, D. C.; BLOOM, P. R.; MCKNIGHT, D. M.; CHEN, Y.; FARENHORST, A.; SENESI, N. *et al.* Environmental and Agricultural Relevance of Humic Fractions Extracted by Alkali from Soils and Natural Waters. **Journal of Environmental Quality**, v. 48, n. 2, p. 217-232, 2019. https://doi.org/10.2134/jeq2019.02.0041

OZÓRIO, J. M. B.; ROSSET, J. S.; SCHIAVO, J. A.; PANACHUKI, E.; SOUZA, C. B. S.; MENEZES, R. S. *et al.* Estoque de carbono e agregação do solo sob fragmentos florestais nos biomas Mata Atlântica e Cerrado. **Revista Brasileira de Ciências Ambientais**, v. 15, n. 53, p. 97-116, 2019. https://doi.org/10.5327/Z2176-947820190518

OZÓRIO, J. M. B.; ROSSET, J. S.; SCHIAVO, J. A.; SOUZA, C. B. S.; FARIAS, P. G. S.; OLIVEIRA, N. S. *et al.* Physical fractions of organic matter and mineralizable soil carbon in forest fragments of the Atlantic Forest. **Revista Ambiente e Água**, v. 15, n. 6, p. e2601, 2020. https://doi.org/10.4136/ambi-agua.2601

PEEL, M. C.; FINLAYSON, B. L.; MCMAHON, T. A. Updated world map of the Köppen-Geiger climate classification. **Hydrology and Earth System Sciences**, v. 11, p. 1633-1644, 2007. https://doi.org/10.5194/hess-11-1633-2007

PFLEGER, P.; CASSOL, P. C.; MAFRA, A. L. Substâncias húmicas em Cambissolo sob vegetação natural e plantios de *pinus* em diferentes idades. **Revista Ciência Florestal**, v. 27, n. 3, p. 807-817, 2017. https://doi.org/10.5902/1980509828631

PROJETO MAPBIOMAS. **Coleção 5.0 da Série Anual de Mapas de Cobertura e Uso de Solo do Brasil.** Available: https://mapbiomas.org/. Access: 12 Dec. 2021.

QGIS DEVELOPMENT TEAM. **QGIS Geographic Information System.** Open Source Geospatial Foundation Project, 2021. Available: https://www.qgis.org/en/site/. Access: 09 June 2021.

R CORE TEAM. **R: A language and environment for statistical computing**. Vienna, 2021. Available: https://www.R-project.org/. Access: 15 Jan. 2021.

REIS, V. R. R.; DEON, D. S.; MUNIZ, L. C.; SILVA, M. B.; REGO, C. A. R. M.; GARCIA, U. C. *et al.* Carbon stocks and soil organic matter quality under different land uses in the maranhense amazon. **Journal of Agricultural Science**, v. 10, n. 5, p. 329-337, 2018. https://doi.org/10.5539/jas.v10n5p329

ROSA, D. M.; NÓBREGA, L. H. P.; MAULI, M. M.; LIMA, G. P. D.; PACHECO, F. P. Substâncias húmicas do solo cultivado com plantas de cobertura em rotação com milho e soja. **Revista Ciência Agronômica**, v. 48, n. 2, p. 221-230, 2017. https://doi.org/10.5935/1806-6690.20170026

ROSSET, J. S; LANA, M. C.; PEREIRA, M. G.; SCHIAVO, J. A.; RAMPIM L.; SARTO, M. V. M. Carbon stock, chemical and physical properties of soils under management systems with different deployment times in western region of Paraná, Brazil. **Semina: Ciências Agrárias**, v. 35, n. 6, p. 3053-3072, 2014. https://doi.org/10.5433/1679-0359.2014v35n6p3053

ROSSET, J. S.; LANA, M. C.; PEREIRA, M. G.; SCHIAVO, J. A.; RAMPIM, L.; SARTO, M. V. M. Frações químicas e oxidáveis da matéria orgânica do solo sob diferentes sistemas de manejo, em Latossolo Vermelho. **Pesquisa Agropecuária Brasileira**, v. 51, n. 9, p. 1529-1538, 2016. https://doi.org/10.1590/S0100-204X2016000900052

ROSSET, J. S.; LANA, M. C.; PEREIRA, M. G.; SCHIAVO, J. A.; RAMPIM, L.; SARTO, M. V. M. Organic matter and soil aggregation in agricultural systems with different adoption times. **Semina: Ciências Agrárias**, v. 40, n. 6, p. 3443-3460, 2019. https://doi.org/10.5433/1679-0359.2019v40n6Supl3p3443

SANTOS, F. A. S.; PIERANGELI, M. A. P.; SILVA, F. L.; SERAFIM, M. E.; SOUSA, J. B.; OLIVEIRA, E. B. Dinâmica do carbono orgânico de solos sob pastagens em campos de murundus. **Scientia Agraria**, v. 18, n. 2, p. 43-53, 2017. http://dx.doi.org/10.5380/rsa.v18i2.50662

SANTOS, C. A.; REZENDE, C. D. P.; PINHEIRO, É. F. M.; PEREIRA, J. M.; ALVES, B. J.; URQUIAGA, S. *et al.* Changes in soil carbon stocks after land-use change from native vegetation to pastures in the Atlantic forest region of Brazil. **Geoderma**, v. 337, p. 394-401, 2019. https://doi.org/10.1016/j.geoderma.2018.09.045

SANTOS, H. G.; JACOMINE, P. K. T.; ANJOS, L. H. C.; OLIVEIRA, V. A.; LUMBRERAS, J. F.; COELHO, M. R. *et al.* **Sistema Brasileiro de Classificação de Solos**. 5. ed. Brasília: Embrapa, 2018.

SANTOS, T. M. D.; OZÓRIO, J. M. B.; ROSSET, J. S.; BISPO, L. S.; FARIA, E.; CASTILHO, S. C. P. Estoque de carbono e emissão de CO2 em áreas manejadas e nativa na Região Cone-Sul de Mato Grosso do Sul. **Revista em Agronegócio e Meio Ambiente**, v. 14, n. 2, e7666, 2021. https://doi.org/10.17765/2176-9168.2021v14n2e7666

SCHIAVO, J. A.; ROSSET, J. S.; PEREIRA, M. G.; SALTON, J. C. Índice de manejo de carbono e atributos químicos de Latossolo Vermelho sob diferentes sistemas de manejo. **Pesquisa Agropecuária Brasileira**, v. 46, n. 10, p. 1332-1338, 2011. https://doi.org/10.1590/S0100-204X2011001000029

SILVA, J. C. A.; SIGNOR, D.; BRITO, A. M. S. S.; CERRI, C. E. P.; CAMARGO, P. B.; PEREIRA, C. F. espectroscopia no infravermelho próximo e análise de componentes principais para investigação de solos submetidos a diferentes usos da Terra na Amazônia Oriental Brasileira. **Revista Virtual de Química**, v. 12, n. 1, p. 51-62, 2020. http://dx.doi.org/10.21577/1984-6835.20200006

SWIFT, R. S. Organic matter characterization. *In*: SPARKS, D. L. *et al.* (eds) **Methods of soil analysis**. Madison: Soil Science Society American, 1996. cap. 35, p.1011-1020.

TABIASOVÁ, E. The effect of organic matter on the structure of soils of different land uses. **Soil and Tillage Research**, v. 114, n. 2, p. 183-192, 2011. https://doi.org/10.1016/j.still.2011.05.003

TISDALL, J. M.; OADES, J. M. Organic matter and water-stable aggregates. **Journal of Soil Science**, v. 33, n. 2, p. 141-163, 1982. https://doi.org/10.1111/j.1365-2389.1982.tb01755.x

TROIAN, D.; ROSSET, J. S.; MARTINS, L. F. B. N.; OZÓRIO, J. M. B.; CASTILHO, S. C. P.; MARRA, L. M. Carbono orgânico e estoque de carbono do solo em diferentes sistemas de manejo. **Revista em Agronegócio e Meio Ambiente**, v. 13, n. 4, p. 1447-1469, 2020. https://doi.org/10.17765/2176-9168.2020v13n4p1447-1469

UNITED STATES. Natural Resources Conservation Service. **Keys to Soil Taxonomy.** 12th ed. Washington, DC: NRCS, Soil Survey Staff, 2014. 681p. 2014.

YEOMANS, A.; BREMNER, J. M. A rapid and precise method for routine determination of organic carbon in soil. **Communication Soil Science Plant Analysis**, v. 19, p. 1467-1476, 1988. https://doi.org/10.1080/00103628809368027

ZHANG, Q.; JIA, X.; WEI, X.; SHAO, M.; LI, T.; YU, Q. Total soil organic carbon increases but becomes more labile after afforestation in China's Loess Plateau. **Forest Ecology and Management**, v. 461, p. 117911, 2020. https://doi.org/10.1016/j.foreco.2020.117911

Ambiente & Água - An Interdisciplinary Journal of Applied Science
ISSN 1980-993X – doi:10.4136/1980-993X
www.ambi-agua.net
E-mail: ambi.agua@gmail.com

Aspects of a unique natural limnological phenomenon in the Brazilian Pantanal

ARTICLES doi:10.4136/ambi-agua.2870

Received: 21 Jun. 2022; Accepted: 20 Aug. 2022

Maria Helena da Silva Andrade[1*]; Ana Lúcia Brandimarte[2]; Débora Fernandes Calheiros[3]; Yzel Rondon Súarez[4]

[1]Faculdade de Engenharias, Arquitetura e Urbanismo e Geografia. Universidade Federal de Mato Grosso do Sul (UFMS), Cidade Universitária, Avenida Costa e Silva, s/n, CEP: 79070-900, Pioneiros, MS, Brazil.
[2]Instituto de Biociências. Departamento de Ecologia. Universidade de São Paulo (USP), Rua do Matão, Travessa 14, nº 101, CEP: 05508-090, São Paulo, SP, Brazil. E-mail: anabrand@ib.usp.br
[3]Embrapa Pantanal (EMBRAPA), Rua Cuiabá, n° 1640, CEP: 79331-100, Corumbá, MS, Brazil. E-mail: calheirosdebora@gmail.com
[4]Centro de Estudos em Recursos Naturais. Laboratório de Ecologia. Universidade Estadual de Mato Grosso do Sul (UEMS), Rodovia Dourados-Itahum, km 12, CEP: 79804-970, Dourados, MS, Brazil. E-mail: yzel@uems.br
[*]Corresponding author. E-mail: helena.andrade@ufms.br

ABSTRACT

This study compares physical and chemical parameters of water samples collected in a marginal lake (Castelo Bay) in the Paraguay River Basin in southern Pantanal during a significant natural phenomenon of hypoxia, locally called *decoada*, and shortly after it. Limnological parameters were analyzed from four sampling sites along the bay. Comparisons of the physical and chemical parameters between *decoada* and post-*decoada* periods were performed by Student's t-test, principal component analysis and multivariate permutational analysis of variance (permanova). During the period of the *decoada*, there was a significant reduction in mean values of water transparency and concentrations of dissolved oxygen, sodium and nitrite compared to the post-*decoada* period. On the other hand, water temperature and conductivity, and concentrations of orthophosphate, total nitrogen and total iron have all had higher values during the *decoada* period. An effect of connectivity between lake and river was found to generate a gradient of water characteristics at Castelo Bay. The limnological characteristics that differed the most between *decoada* and post-*decoada* periods are those associated with the reduction of dissolved oxygen that could cause natural death of fish and the increase in nutrients during the *decoada*, yet they vary on temporal and spatial scales.

Keywords: anoxia, dissolved oxygen, floodplain lakes.

Aspectos de um fenômeno limnológico natural único no Pantanal Brasileiro

RESUMO

Este estudo teve como objetivo comparar parâmetros físicos e químicos de amostras de água coletadas em um lago marginal (Baía do Castelo) na Bacia do Rio Paraguai no Pantanal Sul, durante um fenômeno natural significativo de hipóxia, localmente denominado decoada, e logo após. Parâmetros limnológicos foram analisados em quatro pontos de amostragem ao longo da baía. As comparações dos parâmetros físicos e químicos entre os períodos decoada e

pós-decoada foram realizadas pelo teste t de Student, análise de componentes principais e análise de variância permutacional multivariada (permanova). Durante o período da decoada, houve redução significativa nos valores médios de transparência da água e concentrações de oxigênio dissolvido, sódio e nitrito em relação ao período pós-decoada. Por outro lado, a temperatura e condutividade da água, e as concentrações de ortofosfato, nitrogênio total e ferro total apresentaram valores mais elevados durante o período de decoada. Um efeito de conectividade entre lago e rio foi encontrado para gerar um gradiente de características da água na Baía de Castelo. As características limnológicas que mais diferiram entre os períodos decoada e pós-decoada são aquelas associadas à redução do oxigênio dissolvido que pode causar a morte natural dos peixes e o aumento de nutrientes durante a decoada, porém variam em escalas temporais e espaciais.

Palavras-chave: anóxia, lagos de planícies alagadas, oxigênio dissolvido.

1. INTRODUCTION

The Pantanal is the largest wetland in the world, covering approximately 140,000 km^2 of the Upper Paraguay River Basin (Silva and Abdon, 1998). It is subjected to an annual flood pulse that causes the waters to "rise" and "fall", as annual floods and droughts, with extensive floodplain land-water interaction (Junk *et al.*, 1989; Calheiros *et al.*, 2012).

The changing water level of the floodplain profoundly affects the structure and functioning of this ecosystem, by favoring the occurrence of a natural phenomenon known locally as *decoada*. The term *decoada* is used to describe a change in the physical, chemical and biological aquatic environment that occurs as a result of rising water levels and their contact with the terrestrial environment during early flooding, which results in the decomposition of submerged vegetation biomass in lowland areas subject to flooding. At this stage of the summer hydrological cycle, temperatures are high, which contributes to the decomposition of the great mass of highly degradable plants, mostly grasses, submerged in the flooded fields.

In this context, *decoada* is a unique natural phenomenon; unique in the world in terms of coverage, duration and frequency, regardless of its magnitude (Calheiros *et al.*, 2000; Oliveira *et al.*, 2013). In the Brazilian Pantanal, *decoada* is perceptible through changes in various limnological parameters and its effects on the structure and dynamics of aquatic organisms (Oliveira and Calheiros, 2000; Oliveira *et al.*, 2010; 2011), such as significant fish kills (Calheiros *et al.*, 2000; Calheiros and Hamilton, 1998).

The change in water quality is characterized by the presence of a high amount of dissolved organic compounds from the decomposition of the submerged organic matter. During this period, there is an increase in electrical conductivity (approx. 40 to > 100 mS/cm^{-1}), alkalinity, dissolved carbon dioxide (6 mg.L^{-1} to > 100 mg.L^{-1}) and methane, and increased concentrations of nutrients such as nitrogen, phosphorus and carbon, as the result of decomposition. Ultimately there is a dramatic decrease in dissolved oxygen (from 8.0 to 0.0 mg.L^{-1}), as well as changes in pH (to about 5.0) and transparency (Hamilton *et al.*, 1995; 1997; Calheiros and Hamilton, 1998; Calheiros *et al.*, 2000; Bastviken *et al.*, 2010).

The first evidence of the formation of the water masses of a *decoada* occurs in February in some areas of the northern portion of the Pantanal, and move downriver as the flood pulse moves toward the southern portion of the Pantanal (Calheiros *et al.*, 2000; Hamilton *et al.*, 1997; Oliveira *et al.*, 2013).

Limnological studies of the *decoada* phenomenon and its relationship to fish kills in the Pantanal began in 1988 and have lasted for more than twenty years. From these studies, differences in limnological parameters between years without fish mortality and years with fish mortality have been observed.

The complexity and unpredictability of this phenomenon, both spatially and temporally, require ongoing analysis based on a lengthy time series of data collection. For these reasons, this study aimed to compare the physical and chemical parameters of water samples collected from an marginal lake of Paraguay River, called Castelo Bay, in the Paraguay River Basin of the southern portion of the Pantanal, during a significant *decoada* event and soon thereafter, with the goal of understanding how limnological parameters vary between *decoada* and post-*decoada* periods.

2. MATERIALS AND METHODS

2.1. Study Area

Castelo Bay is located in the Paraguay River floodplain of the Upper Paraguay River Basin (UPRB) in the southern portion of the Pantanal in western Brazil (18°35’28” S and 57°31’56.6” W) (Figure 1). The UPRB is formed of other sub-basins that drain into the Paraguay River. Each sub-basin drains different geological regions of varying rainfall regimes and have distinct hydrological and limnological characteristics. The climate is tropical seasonal, characterized by dry and rainy seasons. In the Southern Pantanal the flood peak of the Paraguay River occurs between May to July, a few months after the peak of the rainy season (November to March) due to the “floodplain effects” of delaying water mass displacements. The lowland vegetation around Castelo Bay is a mixture of flooded savannah, predominantly covered by grasses, and forests in the higher areas.

Analyzing a historical data set of hydrological level of the Paraguay River at Ladário Station, Soares *et al.* (2008), considered the 2007/2008 hydrological year as normal floods; however, rainfall was above mean values, and generated a significant *decoada* phenomenon in March 2008, which is evaluated in the present study.

2.2. Sampling

Limnological parameters were analyzed at four sampling sites along Castelo Bay (Figure 1), and distributed along a gradient of connectivity with the Paraguay River. The first sampling point was located near (approximately 2 km) the Paraguay River and the last point was located approximately 14.8 km from the Paraguay River in the extreme far portion of the lake. Castelo Bay was chosen for this study because it experiences *decoada* events every year (to a lesser or greater extent and magnitude) and because it is a large area, thereby allowing the evaluation of the role of flood dynamics in the *decoada* phenomenon.

Despite the existence of other studies about the *decoada* phenomenon in the Pantanal, none of them considered an *event* of such magnitude as the one in 2008, which demonstrated the full extent of the changes caused by the processes of decomposition. Results of the analysis of water samples collected in March 2008 (*decoada* period - D) and July 2008 (post-*decoada* period - PD) are presented, with those of the post-*decoada* period sampled after the "recovery" of the system.

The variables analyzed were temperature, hydrogen potential (pH), electrical conductivity, depth, water flow and water transparency, plus the concentration of dissolved oxygen, sulfate, orthophosphate, sodium, ammonia, nitrite, nitrate, total suspended solids, total nitrogen, total phosphorus, total iron and chlorophyll-*a* (Table 1).

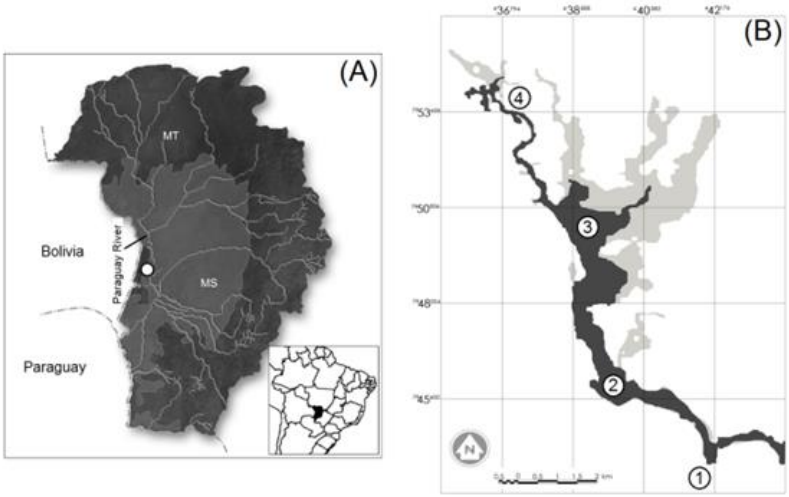

Figure 1. (A) Study area (white dot) located in the Upper Paraguay River Basin, Brazilian Pantanal. (B) Area occupied by Castelo Bay during dry (dark gray) and rainy (light gray) seasons in the Pantanal. Circled numbers indicate the sampling points (Brazil). Abbreviations: MT-Mato Grosso, MS-Mato Grosso do Sul.

Table 1. Evaluated limnological variables and the method of analysis used for characterizing the water during *decoada* and non-*decoada* periods in Castelo Bay, southern Pantanal.

Variables	**Methods**	**References**
Dissolved oxygen ($mg.L^{1}$)	Equipment electronic Hanna HI 9828	---
pH	Equipment electronic Hanna HI 9828	---
Total nitrogen ($mg.L^{-1}$)	Potassium Persulfate digestion/colorimetric flow injection (FIA)	Wetzel and Likens, 2001; Zagatto, 1981;
Total phosphorus ($\mu g.L^{-1}$)	Potassium Persulfate digestion/colorimetric flow injection (FIA)	Wetzel and Likens, 2001; Zagatto, 1981; Mackereth *et al.*, 1978
Alkalinity ($mg.L^{-1}$)	Titulometric	Wetzel and Likens, 2001; Gran,1952
Water temperature (°C)	Equipment electronic Hanna HI 9828	---
Total Suspended Solids (TSS) ($mg.L^{-1}$)	Gravimetric method (cellulose filters)	APHA*et al.*, 1998
Water transparency (m)	Secchi disk	APHA *et al.*, 1998
Electric Conductivity ($\mu.S.cm^{-1}$)	Equipment electronic Hanna HI 9828	---
Continue...		

Continued...		
Water flow	Flow meter model Marsh-McBirney 2000	---
Sulfate (μeq.L^{-1})	Turbidimetric method	APHA *et al.*, 1998; 2005
Orthophosphate (μM)	Colorimetric method	Wetzel and Likens, 2001; Mackereth *et al.*, 1978
Sodium (μeq.L^{-1})	Flame spectrophotometry	APHA *et al.*, 1998; 2005
Fe total (μeq.L^{-1})	Atomic absorption spectrometry	APHA *et al.*, 1998; 2005
Chlorophyll-a (mg.L^{-1})	Atomic absorption spectrometry	Wetzel and Likens, 2001
Nitrate, Nitrite, Ammonia	Colorimetric method	Zagatto, 1981; Krug *et al.* 1983; Wetzel and Likens, 2001

2.3. Data analysis

The first analysis performed was the Student's paired t-test to determine which limnological variables are statistically different between *decoada* and post-*decoada* periods.

The second analysis aimed to visualize, in multivariate space, differences in standard limnological variables between sampling sites along a connectivity gradient and between sampling periods, using principal components analysis (PCA). This procedure intended to remove the influence of the different scales of each limnological variable used. The principal components analysis was performed using the rda command in the vegan package.

Complementary to the PCA, we generated a matrix of Euclidean distances among sampling points — the same used in a principal components analysis — which was used to perform a multivariate nonparametric permutational analysis of variance (permanova) to compare differences in limnological variables during and after the *decoada* phenomenon using 9999 permutations to test statistical significance. The permanova analysis was performed using the function adonis in vegan package (Oksanen *et al.*, 2015). All statistical analyzes were performed in the R platform (R Core Team, 2013).

3. RESULTS

Of the eighteen limnological variables considered, only eight exhibited differences between the two analyzed periods (Table 2). During the *decoada* period – D, there was a significant decrease in the mean values of water transparency, dissolved oxygen and nitrite compared to the post-*decoada* period - PD. The variables which tended to have higher values during the *decoada* event were: water temperature, water conductivity, orthophosphate, total nitrogen, total phosphorus and total iron (Table 2). The pH, water flux, sulphate, sodium, nitrate, total suspended solids (TSS), and chlorophyll-*a* did not differ significantly between the periods.

The results of the principal components analysis showed a clear differentiation of *decoada* and post-*decoada* periods based on the limnological characteristics at Castelo Bay, with Axis 1 explaining 58.4% of the variation in the data. Complementary, an effect of connectivity was detected by a gradient in the position of sample sites along Axis 2, which explained 20.3% of the variation in the data.

Higher values of dissolved oxygen, water transparency, nitrite, nitrate and sodium were observed in the post-*decoada* period, but mainly in sampling sites further, and more isolated, from the Paraguay River. Some limnological variables were observed to be not associated with

any group, in particular chlorophyll-*a* and total suspended solids (Figure 2).

Table 2. Means and standard deviations of limnological variables of Castelo Bay during *decoada* and post-*decoada* periods in southern Pantanal. Paired student t-value and significance codes (ns=non-significant; *=significant to 5%; **=significant to 1% and ***=significant to 0.01%).

Variable	*Decoada*	Post-*Decoada*	t
Depth (m)	5.85±3.76	5.00±2.57	1.43ns
Water transparency (cm)	0.56±0.15	0.99±0.12	-5.73**
Water temperature	28.00±0.59	20.89±0.19	35.68***
Dissolved oxygen	0.40±19	7.79±0.13	-53.22***
pH	6.86±0.23	7.05±0.21	-1.39ns
Water conductivity	78.25±7.76	50.84±4.19	7.72**
Water Flux	0.05±0.04	0.01±0.01	2.21ns
Sulphate	6.41±1.78	4.90±0.79	1.58ns
Orthophosphate	8.18±0.67	1.87±0.51	13.66***
Na	1.70±0.05	1.82±0.10	-2.00ns
NH4	30.42±10.90	17.33±14.10	1.61ns
NO2	3.55±0.55	6.95±0.50	-7.67**
NO3	-1.19±1.39	3.61±3.20	-2.61ns
TSS	7.48±2.58	6.98±2.08	1.11ns
N total	674.10±56.14	569.30±42.30	4.13*
P total	36.70±6.37	29.30±2.50	1.93ns
Fe total	2.03±0.50	0.52±0.06	6.60**
Chlorophyll a	0.04±0.75	0.01±0.01	0.10ns

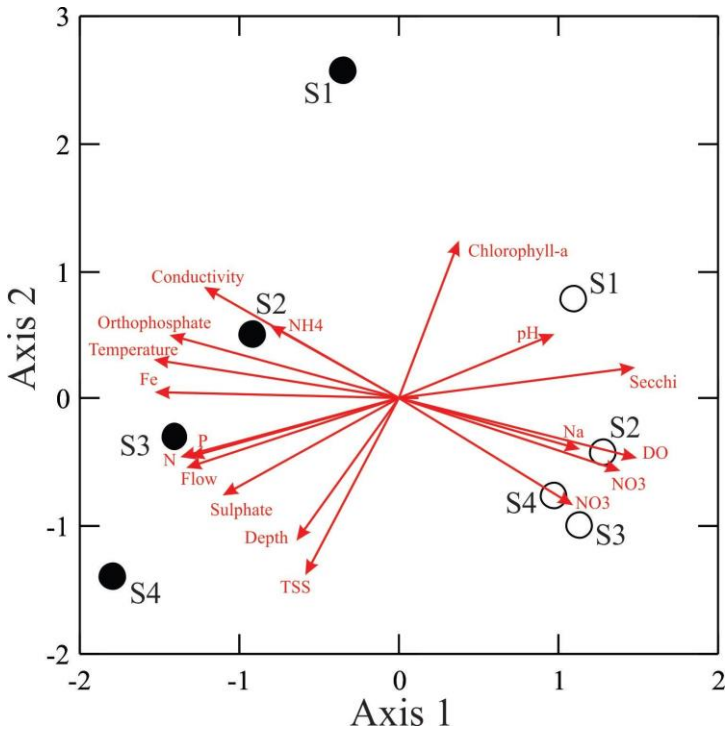

Figure 2. Scatterplot of the principal components analysis of four sampling sites during *decoada* (black circles) and post-*decoada* (white circles) in Castelo Bay in southern Pantanal, 2008.

Integrating all limnological variables, the permanova results also showed significant differences between *decoada* and post-*decoada* periods in Castelo Bay (F= 7.03; p= 0.03; r^2= 0.54), reinforcing the results of the PCA analysis.

4. DISCUSSION

The results indicate that there are significant differences between the two study periods with respect to some of the limnological variables, analyzed as a result of the *decoada* phenomenon. The rise in water level changes the limnological characteristics of water bodies as a result of interactions between the aquatic and terrestrial environments (Junk *et al.*, 1989; Hamilton *et al.*, 1997; Calheiros and Hamilton, 1998; Oliveira and Calheiros, 2000), due to leakage of water from the riverbeds and drainage channels that reach the floodplain. The *decoada* phenomenon at Castelo Bay can last more than one month and cause significant fish mortality (Calheiros and Hamilton, 1998; Oliveira and Calheiros, 2000; Oliveira *et al.*, 2013), thereby influencing fish density, diversity and species composition, as has been observed in another floodplain region (Bunch *et al.*, 2015)

The land-water interaction due to the annual flood pulse variation is responsible for the levels of dissolved oxygen, such that during flooding of the Pantanal, and especially in the months of February, March and April, the dissolved oxygen could be lower than 3.0 $mg.L^{-1}$. During *decoada* events, the concentrations of dissolved oxygen can fall from 8 $mg.L^{-1}$ to complete anoxia or 0.0 $mg.L^{-1}$. In the present study, we observed minimum dissolved oxygen levels between 0.15 and 0.55 $mg.L^{-1}$ during this period, compared to values considered "normal" (7.7 $mg.L^{-1}$). The decomposition of organic matter resulting from the death of submerged terrestrial vegetation, which had grown in the preceding dry season, and dead aquatic vegetation from the same period, directly affects the dissolved oxygen concentration because of the oxidation processes promoted by the decomposition of vegetation consuming the oxygen in the water column (Hamilton *et al.*, 1997; Calheiros and Hamilton, 1998). The low oxygen concentrations indicate high bacterial activity, originating from the drift of organic matter into the body of water (Motta and Uieda, 1995).

Temperature is another important factor in the process of *decoada*. Normally, at the time of flooding (December to April) high summer temperatures in the Pantanal help accelerate the decomposition, and are therefore indirectly responsible for the lower concentrations of dissolved oxygen during this period, as well as the natural decreasing of gases' dissolution into the aquatic environment. With the entry of cold fronts, the temperature can fall for a few days, slowing down decomposition processes and, consequently, improving the water quality (Oliveira and Calheiros, 2005).

In our study, during the *decoada* a lower dissolved oxygen content (DO = 0.15 $mg.L^{-1}$) was recorded than in 1994 when a major fish kill was observed (Calheiros and Hamilton, 1998). The observation of many fish breaking the surface to obtain swallow air, together with low levels of dissolved oxygen in the water and an increase in free carbon dioxide, strongly suggests that suffocation is the leading cause of fish death during a *decoada* on the flood plain (Calheiros and Hamilton, 1998).

Any environmental changes can be considered stressful when they are unpredictable and uncontrollable (Schulte, 2014). However, if *decoada* occurred every year at the Pantanal, yet the intensity remained variable, the life cycle of aquatic animals could adapt, and minimize its impact on their populations. For fish, *decoada* are known to cause respiratory distress culminating in mass mortality. Nevertheless, the intensity of hypoxia/anoxia can be explained by the exposed area (subject to grasses covering) and duration of the previous dry period and the velocity of next flooding (Bulhões *et al.*, 2020). Differences in hypoxia have been documented during the *decoada* phenomenon, with lower dissolved oxygen concentration in stagnant, vegetated waters (Calheiros and Hamilton, 1998; Hamilton, 2002). Nonetheless,

smaller fish species (eg. *Odontostilbe* spp., *Pyrhulina australis*, *Aphyocharax* spp., among others) can be encountered in these habitats, suggesting a higher tolerance to hypoxia. On the other hand, the exotic mollusc *Limnoperma fortunei*, which were broadly distributed in Castelo Bay in 2005, disappeared completely after the 2006 *decoada* (Oliveira *et al.*, 2011). Clearly a detailed evaluation of the effects of hypoxia on the distribution of the aquatic animals of the Pantanal is needed (Andrade *et al.*, 2015).

Seasonal hydrologic flood pulses play an important role in the functioning of the ecology and hydrology of floodplain wetlands by supplying sources of nutrients, including carbon and salts. These, in turn, are essential for the maintenance of the structure, composition and biomass dynamics of communities of aquatic organisms and, ultimately, the entire aquatic food chain (Junk *et al.*, 1989), resulting in the provision of ecosystem services such as fisheries (Calheiros and Oliveira, 2011; Calheiros *et al.*, 2012). Considering the many possible scenarios of global warming and possible hydrological alteration in the Pantanal, the dynamics of this ecosystem, like any other, can be altered, and the magnitude and duration of *decoadas* could be modified as well. On the other hand, the construction of hydroelectric power dams (HPD) in the rivers that form the Pantanal Wetland can alter water sediment and nutrient flows as well as the flooding area downstream (Oliveira *et al.*, 2020; Fantin-Cruz *et al.*, 2020). Many rivers are already blocked with 47 dams and 133 HPD are still predicted.

Therefore, a better understanding of this unique phenomenon is of fundamental importance for the development of conservation policies and the management of fisheries resources.

5. CONCLUSIONS

The results corroborate that the *decoada* is a unique limnological phenomenon, a synthesis of hydrological, geomorphological, biogeochemical and ecological interrelationships of the extensive seasonal and spatially flood-pulsed wetland of Pantanal. The extensive flooded area contributes as a self-source of nutrients and ions, and changes the respiratory gases' equilibrium, altering water quality and promoting the regulation of the structure and composition of aquatic organisms.

6. ACKNOWLEDGEMENTS

We thank the Empresa Brasileira de Pesquisa Agropecuária - Embrapa Pantanal for the logistic and staff support.

Y. R. Súarez was supported by productivity grants from CNPq.

7. REFERENCES

ANDRADE, M. H. S.; BRANDIMARTE, A. L.; CALHEIROS, D. F.; TAMBOSI, L. R. Spatial and limnological characterization of the Paraguay river floodplain area, Southern Pantanal, with emphasis on the 'decoada' phenomenon. **Geografia,** v. 40, p. 27-38, 2015.

APHA; AWWA; WEF. **Standard Methods for the Examination of Water and Wastewater**. 20. ed. Washington, 1998.

APHA; AWWA; WEF. **Standard Methods for the Examination of Water and Wastewater**. 21. ed. Washington, 2005.

BASTVIKEN, D.; SANTORO, A. L.; MAROTTA, H.; PINHO, L. Q.; CALHEIROS, D. F.; CRILL, P. *et al.* Methane emissions from Pantanal, South America, during the low water season: toward more comprehensive sampling. **Environmental Science and Technology,** v. 44, p. 5450-5455, 2010. https://doi.org/10.1021/es1005048

BULHOES, J. S.; MARTINS, C. L.; OLIVEIRA, M. D.; CALHEIROS, D. F.; CALIXTO, W. P. Indirect prediction system for variables that have gaps in their time series. **Chaos, Solitons & Fractals,** v. 131, 2020. https://doi.org/10.1016/j.chaos.2019.109509

BUNCH, A. J.; ALLEN, M. S.; GWINN, D. C. Influence of macrophyte-induced hypoxia on fish communities in lakes with altered hydrology. **Lake and Reservoir Management**, v. 31, p. 11-19, 2015. https://doi.org/10.1080/10402381.2014.964817

CALHEIROS, D. F.; OLIVEIRA, M. D. O rio Paraguai e sua planície de inundação: O Pantanal Mato-grossense. **Ciência & Ambiente**, v. 41, p. 113-130, 2011.

CALHEIROS, D. F.; HAMILTON, S. K. Limnological conditions associated with natural fish kills in the Pantanal Wetland of Brazil. **Internationale Vereinigung für Theoretische und Angewandte Limnologie: Verhandlungen,** v. 26, p. 2189–2193, 1998. https://doi.org/10.1080/03680770.1995.11901134

CALHEIROS, D. F.; SEILD, A. F.; FERREIRA, C. J. A. Participatory research methods in environmental science: local and scientific knowledge of a limnological phenomenon in the Pantanal wetland Brazil. **Journal of Applied Ecology,** v. 37, p. 684-696, 2000. https://doi.org/10.1046/j.1365-2664.2000.00524.x

CALHEIROS, D. F.; OLIVEIRA, M. D.; PADOVANI, C. R. Hydro-ecological Processes and Anthropogenic Impacts on the Ecosystem Services of the Pantanal Wetland. *In*: IORIS, A. A. R. (org.). **Tropical Wetland Management**: The South-American Pantanal and the International Experience. Farnham: Ashgate Publishing, 2012. p. 29-57.

FANTIN-CRUZ, I.; OLIVEIRA, M. D.; CAMPOS, J. A.; CAMPOS, M. M.; RIBEIRO, L. S.; MINGOTI, R. *et al.* Further Development of Small Hydropower Facilities will significantly reduce sediment transport to the Pantanal Wetland of Brazil. **Frontiers in Environmental Science,** v. 8, 2020. https://doi.org/10.3389/fenvs.2020.577748

GRAN, G. Determination of the equivalence point in potentiometric titrations, Part II. **Analyst**, v. 77, p. 661-671, 1952. https://doi.org/10.1039/AN9527700661

HAMILTON, S. K. Hydrological controls of ecological structure and function in the Pantanal wetland (Brazil). *In*: MCCLAIN, M. (ed.). **The ecohydrology of South American rivers and wetlands.** Wallingford: International Association of Hydrological Sciences, 2002. p. 133-158. (Special Publication, 6).

HAMILTON, S. K.; SIPPEL, S. J.; MELACK, J. M. Oxygen depletion and carbon dioxide and methane production in waters of the Pantanal wetland of Brazil. **Biogeochemistry**, v. 30, p. 115-141, 1995. https://doi.org/10.1007/BF00002727

HAMILTON, S. K.; SIPPEL, S. J.; CALHEIROS, D. F.; MELACK, J. M. An anoxic event and other biogeochemical effects of the Pantanal Wetland on the Paraguay River. **Limnology and Oceanography,** v. 42, p. 257-272, 1997. https://doi.org/10.4319/lo.1997.42.2.0257

JUNK, W. J.; BAYLEY, P. B.; SPARKS, R. E. The flood pulse concept in river-floodplain systems. **Canadian Journal of Fisheries and Aquatic**, v. 106, p. 110-127, 1989.

KRUG, F. J. *et al*. Zone trapping in flow injection analysis: Spectrophotometric determination of low levels of ammonium ion in natural waters. **Analytica Chimica Acta**, v. 151, p. 39-48, 1983. https://doi.org/10.1016/S0003-2670(00)80059-8

MACKERETH, F. J. H.; HERON. J.; TLLING, J. F. **Water analysis**: some revised methods for limnologist. Newby Bridge: Freshwater Ecological Association, 1978

MOTTA, R. L.; UIEDA, V. S. Food web structure in a tropical stream ecosystem. **Austral Ecology**, v. 30, p. 58-73, 2005. https://doi.org/10.1111/j.1442-9993.2005.01424.x

OKSANEN, J.; BLANCHET, F. G.; KINDT, R.; LEGENDRE, P.; O'HARA, R. B.; SIMPSON, G. L. *et al.* **Vegan**: community ecology package. Version 2.3-0. 2015. Available in: http://CRAN.R-project.org/package=vegan. Access: March 2022.

OLIVEIRA, M. D.; CALHEIROS, D. F. Flood pulse influence on a phytoplankton community in south Pantanal floodplain, Brazil. **Hydrobiologia**, v. 427, p. 101-112, 2000. https://doi.org/10.1023/A:1003951930525

OLIVEIRA, M. D.; CALHEIROS, D. F. Características e alterações limnológicas na bacia do rio Taquari. *In*: GALDINO, S.; VIEIRA, L. M.; PELLEGRIN, L. A. (eds.). **Impactos ambientais e socioeconômicos na bacia do rio Taquari - Pantanal.** Corumbá: Embrapa Pantanal, 2005. p. 199-208.

OLIVEIRA, M. D.; CALHEIROS, D. F.; PADOVANI, C. Mapeamento e Descrição das Áreas de Ocorrência dos Eventos de Decoada no Pantanal. **Boletim de Pesquisa e Desenvolvimento,** v. 121, p. 1-21, 2013.

OLIVEIRA, M.; CALHEIROS, D. F.; JACOBI C. M.; HAMILTON, S. K. Abiotic factors controlling the establishment and abundance of the invasive golden mussel *Limnoperna fortunei*. **Biological Invasions,** v. 13, p. 717-729, 2011. https://doi.org/10.1007/s10530-010-9862-0

OLIVEIRA, M. D.; HAMILTON, S. K.; CALHEIROS, D. F.; JACOBI, C. M. Oxygen depletion events control the invasive golden mussel (*Limnoperna fortunei*) in a tropical floodplain. **Wetlands,** v. 30, p. 705-716, 2010. https://doi.org/10.1007/s13157-010-0081-3

OLIVEIRA, M. D.; FANTIN-CRUZ, I.; CAMPOS, J. A.; CAMPOS, M. M.; MINGOTI, R.; SOUZA, M. L. *et al.* Further development of Small Hydropower Facilities may alter nutrient transport to the Pantanal Wetland of Brazil. **Frontiers of the Environmental Science,** v. 8, 2020. https://doi.org/10.3389/fenvs.2020.577793

R CORE TEAM. **R**: A language and environment for statistical computing. Vienna, 2013.

SCHULTE, P. M. What is environmental stress? Insights from fish living in a variable environment. **The Journal of Experimental Biology**, v. 217, p. 23-34, 2014. https://doi.org/10.1242/jeb.089722

SILVA, J. S. V.; ABDON, M. M. Delimitação do Pantanal Brasileiro e suas sub-regiões. **Pesquisa Agropecuária Brasileira**, v. 33, p. 1703-1711, 1988.

SOARES, M. T. S.; SORIANO, B. M. A.; SANTOS, S. A.; ABREU, U. G. P.; BERGIER, I.; PELLEGRIN, L. A. **Monitoramento do comportamento do rio Paraguai no Pantanal Sul-Mato-Grossense 2007/2008**. Corumbá: Embrapa Pantanal, 2008. (Comunicado Técnico, 72).

WETZEL, R. A.; LIKENS, G. E. **Limnological analyses**. New York: Springer. 2001. 391 p.

ZAGATTO, E. A. G. **Manual de análises de plantas e águas empregando sistemas de injeção em fluxo**. Piracicaba: Universidade de São Paulo/CENA, 1981. 45 p.

Ambiente & Água - An Interdisciplinary Journal of Applied Science
ISSN 1980-993X – doi:10.4136/1980-993X
www.ambi-agua.net
E-mail: ambi.agua@gmail.com

Macronutrient cycling in hydroponic lettuce cultivation

ARTICLES doi:10.4136/ambi-agua.2849

Received: 20 Apr. 2022; Accepted: 12 Aug. 2022

Priscila Helena da Silva Macedo[1]; Emily Mariano da Cruz Lopes[2]; Mariano Vieira dos Santos de Souza Lopes[2]; Fernando César Sala[3]; Claudinei Fonseca Souza[2*]

[1]Departamento de Recursos Naturais e Proteção Ambiental. Programa de Pós-Graduação em Agricultura e Ambiente. Universidade Federal de São Carlos (UFSCar), Rodovia Anhanguera, km 174, Zona Rural, CEP: 13604-900, Araras, SP, Brazil. E-mail: priscila.silva@ufscar.br
[2]Departamento de Recursos Naturais e Proteção Ambiental. Universidade Federal de São Carlos (UFSCar), Rodovia Anhanguera, km 174, Zona Rural, CEP: 13604-900, Araras, SP, Brazil.
E-mail: emilymclopes21@gmail.com, mariano@estudante.ufscar.br
[3]Departamento de Biotecnologia e de Produção Vegetal e Animal. Universidade Federal de São Carlos (UFSCar), Rodovia Anhanguera, km 174, Zona Rural, CEP: 13604-900, Araras, SP, Brazil.
E-mail: fcsala@ufscar.br
[*]Corresponding author. E-mail: cfsouza@ufscar.br

ABSTRACT

In order to address issues of limited resources and contamination by fertilizers, nutrient solutions may be reused in hydroponics as an alternative to their disposal in the environment. This work evaluated the feasibility of nutrient replacement for the nutrient solutions reused during lettuce hydroponic cultivation. The experiment was carried out in an agricultural greenhouse in an NFT hydroponic system using the “Milena” lettuce cultivar. The experiment was divided into two stages: 1) monitoring and data collection and proposition of nutrient replacement management; and 2) validation of the proposed replacement management. Monitoring the consumption of the crop's nutritional solution in the first stage served as the basis for the proposed nutritional replacement management. Management was validated in the second stage through the evaluation of fresh and dry mass, crop nutritional status, and the amount of the fertilizer applied in the treatments: T1 - nutrient replacement with nutrient solution reuse; and T2 - nutrient replacement without nutrient solution reuse. The fresh and dry mass data and the amount of nutrients absorbed by the plants were submitted to the t-test at 5% probability, showing no significant difference between the treatments, making it possible to conclude that the nutrient solution reuse provided nutrient replacement during the lettuce crop cultivation.

Keywords: hydroponic system, *Lactuca sativa* L., macronutrient rational use.

Ciclagem de macronutrientes no cultivo de alface hidropônica

RESUMO

O reúso de soluções nutritivas em hidroponia se torna alternativa ao descarte de água e nutrientes no ambiente, já que a escassez desses recursos e a contaminação do solo por fertilizantes são problemas, tanto econômicos quanto ambientais. Este trabalho avaliou a viabilidade da reposição de nutrientes para o reúso das soluções nutritivas descarte durante o

desenvolvimento da cultura da alface em hidroponia. O experimento foi realizado em estufa agrícola, em sistema hidropônico NFT utilizando a cultivar de alface Milena. O experimento foi dividido em duas etapas, sendo a primeira: monitoramento e coleta de dados e proposição de manejo da reposição de nutrientes e a segunda: validação do manejo de reposição proposto. O monitoramento do consumo da solução nutricional da cultura, na primeira etapa, serviu como base para o manejo de reposição nutricional proposto. O manejo foi validado na segunda etapa através da avaliação das massas fresca e seca, o estado nutricional da cultura e a quantidade de fertilizantes aplicados nos tratamentos, T1 - reposição de nutrientes com reaproveitamento da solução nutritiva e T2 - reposição de nutrientes sem reaproveitamento da solução nutritiva. Os dados de massa fresca e seca e a quantidade de nutrientes absorvidos pelas plantas foram submetidos ao teste estatístico T ao nível de 5% de significância, mostrando não haver diferença significativa entre os tratamentos, sendo possível concluir que a reposição de nutrientes proporcionou o reúso da solução nutritiva durante o desenvolvimento da cultura da alface.

Palavras-chave: hidroponia, *Lactuca sativa* L., uso racional de macronutrientes.

1. INTRODUCTION

In recent decades, population growth and agriculture modernization have led to increased consumption of resources. One of these is water, the consumption of which has brought environmental problems such as contamination and scarcity. In this sense, to meet growing food demand with minimal impact on the environment, agriculture must be managed rationally.

Water scarcity and soil contamination are problems felt worldwide, leading the productive sectors to more rigorous management of water resources, such as considering water reuse, controlling losses and waste, and reducing consumption and residue production (Barros *et al.*, 2015). In this scenario, the protected cultivation of vegetables, which has been developed on a large scale under the hydroponic system, represents an alternative for producers looking for cultivation technologies that guarantee their production with less environmental impact.

The number of establishments that produce lettuce in Brazil is 108,603 units (approximately 80,000 hectares), which have a total of 908,186 tons per year (IBGE, 2017). It is estimated that the hydroponic cultivation of leafy vegetables in Brazil is approximately 2,000 hectares, with a growth trend for the coming decades (Lima *et al.*, 2018). The adoption of new cultivation technologies has been increasing in recent years, such as the cultivation of lettuce in a hydroponic system of the NFT (Nutrient Film Technique) under protected cultivation (Sala, 2019).

The NFT (Nutrient Film Technique) system is a hydroponic cultivation technique that makes nutrients available to plants through a thin film of nutrient solution adequate to meet the requirements of each plant species (Bezerra Neto and Paes, 2011). It has shown significant growth in the last decades because of its advantages over soil cultivation, such as the potential for efficient use of water and nutrients (Santos *et al.*, 2013), less exposure to climate factors and phytosanitary problems, higher yield, and added value to the product, precocity, and better plant quality (Bezerra Neto, 2016). In addition to the efficient use of water, as it reduces losses by evaporation, NFT hydroponics can also reduce the environmental risks associated with salt accumulation in the environment (Alves *et al.*, 2011).

However, some producers who use NFT hydroponics have discarded nutrient solutions after partial nutrient consumption by plants or due to disease occurrence (Badgery-Parker, 2002). Such disposal is often done after a period of use since producers still do not have a fast and cheap method to quantify nutrient contents in the solution to provide an appropriate nutritional balance by replacing missing nutrients. Thus, the disposal and non-reuse of nutrient solutions from hydroponic systems have been environmental and economic concerns but little

discussed in the literature. Nutrient replacement can be done in NTF cultivations by nutrient solution reuse for several crop cycles without impacting productivity (Backes *et al.*, 2003). Therefore, nutrient solution disposal can be reduced and/or eliminated by periodic adjustments in its composition throughout plant growth and development cycles (Gimenez *et al.*, 2008).

Furthermore, in 2020, Brazil imported more than 80% of the fertilizers used in agriculture (SAE, 2020). For this reason, nutrient solution reuse becomes a good alternative as it enables savings of these inputs. Another advantage of such a practice is mitigating environmental impacts by not releasing salts into the environment. In Brazil, lettuce is the main species and represents 80% of the vegetables grown under the NFT hydroponic system (Furlani, 1999; Sala and Costa, 2012). Moreover, this vegetable is among the five most marketed in Brazilian supply centers (CONAB, 2020).

Since producers need practical information for the rational use of nutrients and water, this study evaluated the feasibility of nutrient replacement with nutrient solution reuse during the lettuce development in hydroponics.

2. MATERIAL AND METHODS

The study was carried out in the Department of Natural Resources and Environmental Protection (DRNPA) of the Center for Agricultural Sciences (CCA), Federal University of São Carlos (UFSCar), Campus of Araras, São Paulo State, Brazil. The area lies at the UTM coordinate: 7531348 N; 254144 E; datum WGS 84, and Zone 23K. According to Köppen's classification, the local climate is classified as *Cwa*, which is characterized by two well-defined seasons, one dry with mild temperatures (April to September) and another rainy with higher temperatures (October to March). Annual temperature and rainfall averages are 21°C and 1400 mm, respectively (Valadares *et al.*, 2008).

The experiment was carried out in an arched-roof greenhouse (commercially known as Poly House). It measured 6.4 x 20.0 x 3.5 m (width x length x height) and was enveloped with a transparent UV-treated polyethylene sheet and white shade screen on the sides. The crisp lettuce cultivar Milena was used under NFT hydroponic cultivation.

The experimental area consisted of eight benches containing four polypropylene channels (75 mm wide x 3.0 m long). The channels were spaced at 0.30 m, the plants at 0.25 m, and the benches at 0.70 m to facilitate handling. Each bench had 44 plants, 11 per channel, with a useful plot covering the 18 central plants (Figure 1). The experiments were carried out in a completely randomized block design, with three replications in the first stage and one in the second.

The hydroponic solutions were supplied by two 500-L reservoirs, a pumping system, cultivation benches, a system for returning the nutrient solution to the reservoir by gravity, and an aerator. Nutrient solutions were supplied to each channel at an average flow rate of 1.5 L min^{-1} (Martinez and Silva Filho, 2004). In addition, the pump timer was set to 15 minutes for every half-hour during the daytime and 15 minutes for every hour during the nighttime, providing an intermittent nutrient solution flow to the plants (Cuba *et al.*, 2015).

The experiment was divided into two stages: 1) monitoring and data collection and proposition of nutrient replacement management; and 2) validation of the proposed replacement management. Monitoring the consumption of the crop's nutritional solution in the first stage served as the basis for the proposed nutritional replacement management.

2.1. Nutrient solutions

Nutrient solutions for Stages 1 and 2 were prepared according to the lettuce crops recommendations adapted from Furlani *et al.* (1999), Table 1.

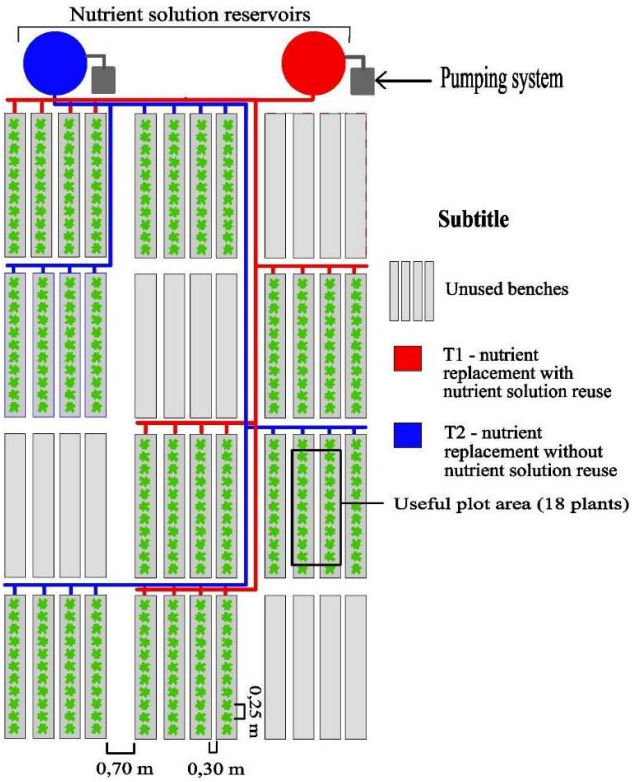

Figure 1. Schematic of the hydroponic system structure and treatment distribution.

Table 1. Lettuce nutrient recommendation used, which results in a nutrient solution with a pH - 6.3 and an electrical conductivity - 1.6 dS m^{-1}.

Fertilizer	Concentration (g 1000 L^{-1})
Calcium nitrate	500
Potassium nitrate	500
Magnesium sulfate	350
Monoammonium Phosphate	100
Conmicros Standard	20

Nutrient solution pH and electrical conductivity (EC) were monitored daily to maintain a suitable environment for lettuce growth (Martinez, 2002).

2.2. Stage 1 – Nutrient solution monitoring and crop data collection

The nutrient solution was prepared and made available on the same day plants were transplanted to the hydroponic channels (0 days after transplanting – DAT) and discarded at 7 DAT. Moreover, solution preparation, disposal, and collection were performed weekly until 28 DAT (the end of the lettuce cycle). The macronutrients present in the nutrient solution were analyzed weekly. The nitrogen (N), phosphorus (P), potassium (K), calcium (Ca), and magnesium (Mg) contents were determined to use these results in the following experiment stage. Solution samples were collected in triplicates, and the contents of N were determined by TOC-LCPN development; P by the vanadomolybdophosphoric acid method with a wave reading of 440 nm in length; K in a Digimed flame spectrophotometer (Model DM-62); Ca in an atomic absorption spectrophotometer and Mg in an Iris-HI801 model spectrophotometer - HANNA Instruments.

Plants were also sampled weekly to characterize nutrient contents and build a lettuce shoot absorption curve. Leaves were dried in a forced-air circulation oven at 70°C until reaching a constant weight (Silva, 2009), with macronutrients (N, P, K, Ca, and Mg) being quantified (Carmo *et al.*, 2000).

Lettuce shoot fresh (FM) and dry (DM) masses were determined using the same plants sampled weekly for leaf analysis. These plants were weighed on an analytical scale right after being collected from benches (FM) and after drying (DM). At 28 DAT, yield per square meter was obtained, and the useful plot area and border comprised 1.8 m^2 each.

The experimental design consisted of entirely randomized blocks, with 44 plants per bench and 176 plants per reservoir, totaling 528 plants in three replications.

Statistical analyzes were performed using the EXCEL software. The results of absorbed nutrient content from the nutrient solution (three replicates) were t-tested at 5% significance, and no significant differences were found between treatments.

2.3. Stage 2 – Nutrient replacement proposal validation

In Stage 2, two treatments were carried out in the same structure as in Stage 1, T1 - nutrient replacement with nutrient solution reuse and T2 - nutrient replacement without nutrient solution reuse.

Macronutrient consumption data were validated, and fertilizer replacement in T1 was based on the difference between nutrient contents in the initial and discarded nutritional solutions, thus obtaining the amount of nutrients absorbed by plants. The values were obtained in nutrient concentration (mg L^{-1}) and transformed into amounts of salts (calcium nitrate, potassium nitrate, magnesium sulfate, mono-ammonium phosphate, potassium sulfate, urea, and ConMicros). The entire solution volume was considered to adjust nutrients, considering the amount remaining in the reservoir and evapotranspiration. Mean micronutrient consumptions were calculated to be used as a basis for replacement. The nutrient solution in T2 was according to the procedure performed in Stage 1. Nutrient solution pH and electrical conductivity (EC) were monitored daily.

The experimental design consisted of completely randomized blocks. For leaf fresh and dry mass measurements, the useful area of each bench was divided into two subplots for plant sampling (9 subsamples), totaling 72 samples per treatment at the end of the crop cycle (30 DAT).

T1 and T2 were compared for plant-absorbed nutrient contents and plant fresh and dry weights. In addition, data were subjected to analysis of variance to verify the differences for the studied variables.

Water consumption was measured weekly based on reservoirs' water balance, so the Water Use Efficiency (WUE) (estimated in kg m^{-3}) was obtained by dividing the production (kg) by the water consumed volume (m^{-3}) of each treatment applied during the lettuce crop cycle.

3. RESULTS AND DISCUSSION

3.1. Stage – 1

As expected, nutrient solution pH varied throughout the experiment since solutions have no buffering capacity (Backes *et al.*, 2004). However, the values were maintained from 5.45 to 6.75 for the best plant growth (Castellane and Araújo, 1995).

Average electrical conductivity (EC) was within the recommended range for hydroponic lettuce cultivation, from 1.5 to 1.8 dS m^{-1}. These values corroborate the recommendation of Castellane and Araújo (1995), who reported a range from 1.5 to 2.5 dS m^{-1}, a reference for EC monitoring. EC remained virtually constant between 0 and 7 days after transplanting (DAT), and nutrient solution absorption was low compared to other plant growth stages. Such low absorption is due to the reduced size of lettuce plants at the beginning of the cycle. Yet, from 7

to 21 DAT, EC increased by 9.2% due to higher plant water demands and the absence of water replacement in the reservoir between nutrient solution changes, thus concentrating the nutrients. In the last week of evaluation (21 and 28 DAT), EC showed an inverse behavior, decreasing by 4.0% from the optimal value. This reduction is due to plants' increased demand for water and nutrients at the end of the cycle.

3.1.1. Nutrient solution chemical analysis

Nitrogen exports were constant throughout the crop cycle, and this nutrient was consumed (159.47 mg L^{-1}) at 28 DAT. As to Heinen *et al.* (1991), differences between nutrient solution N reductions and plant-absorbed N contents are significant, which can be explained by N denitrification and/or immobilization. Up to 21 DAT, nutrient solution P concentrations decreased, while its consumption by plants increased (6.75 mg L^{-1} between 0 and 7 DAT; 19.58 mg L^{-1} between 7 and 14 DAT; and 38.78 mg L^{-1} between 14 and 21 DAT); however, its concentrations remained practically constant from 21 to 28 DAT (34.88 mg L^{-1}). Potassium was the most exported nutrient from the nutrient solution, with the highest expression between 21 and 28 DAT (224.36 mg L^{-1}), followed by 14 to 21 DAT (187.13 mg L^{-1}). However, Ca was less exported between 7 and 14 DAT (15.35 mg L^{-1}), with a marked increase between 14 and 21 DAT (39.79 mg L^{-1}) and 21 and 28 DAT (84.48 mg L^{-1}). Up to 21 DAT, Mg exports remained constant, which were 4.84 mg L^{-1} between 0 and 7 DAT, 7.40 mg L^{-1} between 7 and 14 DAT, and 8.60 mg L^{-1} between 14 and 21 DAT, but increased from 21 to 28 DAT (26.48 mg L^{-1}) (Figure 2).

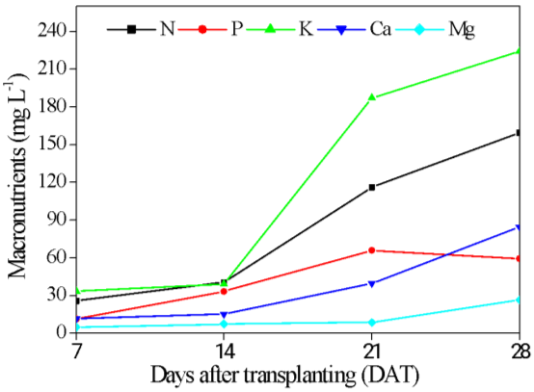

Figure 2. Averages of macronutrient contents from nutrient solution at 7, 14, 21, and 28 days after transplanting (DAT).

3.1.2. Nutrient absorption curve and agronomic evaluation of lettuce cv. Milena

Average leaf analysis results (Figure 3) were compared to the optimal ranges for macronutrients by Raij *et al.* (1997). All of them were within their respective suggested content, and no visual symptoms of nutrient deficiency or toxicity were observed in plants.

Leaf analysis showed that K was the nutrient most absorbed by plants, followed by N, Ca, P, and Mg. This result corroborates the findings on lettuce plants of Fernandes *et al.* (2002) on the cultivars Regina, Babá de Verão (butterhead), and Grandes Lagos (iceberg), and those of Gondim *et al.* (2010) on the cultivar Brasil 303 (butterhead), both in experiments with the hydroponic system in autumn. Our findings also agree with Benini *et al.* (2005) on the cultivar Verônica (loose-leaf) under hydroponic and conventional approaches in the autumn/winter.

Fresh shoot mass accumulation was slow until 14 DAT, representing 1.4% of the total accumulated from 0 to 7 DAT and 6% from 7 to 14 DAT. Then, fresh mass accumulation increased from 14 to 21 DAT, reaching 22.4% of the total. The highest expansion was 69.6%, achieved in the last week (21 to 28 DAT). At harvest time (28 DAT), plants had an average of

226.2 g total fresh weight. These values are higher than Vaz, Junqueira (1998), and Benini *et al.* (2005) on cv. Verônica (207.8 g, 183.4 g, and 124.5 g, respectively). When researching the performance of lettuce seedlings cv. Vanda in trays with different cell volumes, Lima *et al.* (2018) reported an average of 246 g plant^{-1} at 29 DAT.

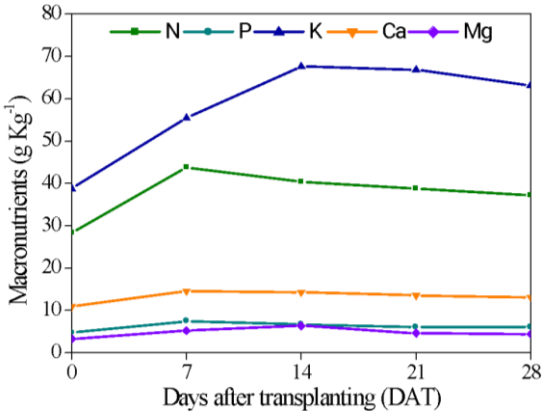

Figure 3. Macronutrient concentrations in dry shoot matter of lettuce cv. Milena at 0, 7, 14, 21, and 28 days after transplanting (DAT).

At 28 DAT, total water consumption averaged 4.1 L (Figure 4), around 144.5 mL plant^{-1} day^{-1}. According to Furlani *et al.* (2009), water absorption by hydroponic lettuce is, on average, between 75 and 100 mL plant^{-1} day^{-1}. High consumption may be related to production system failures, such as water loss due to leakages and evaporation from uncapped holes after plant sampling.

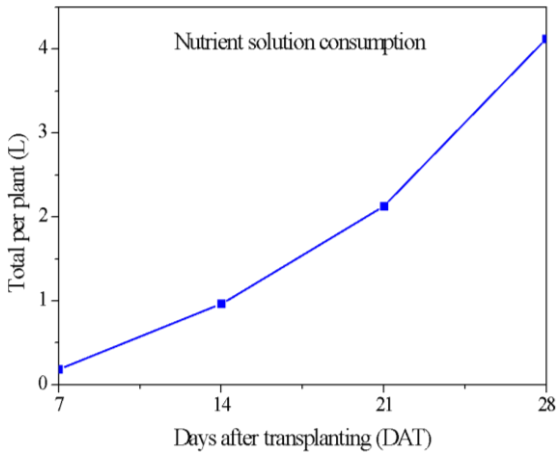

Figure 4. Nutrient solution consumption throughout the cycle of the lettuce cv. Milena.

The yield of the lettuce cv. Milena reached, on average, 2.75 kg m^{-2}, similar to that found by Lima *et al.* (2018) (2.51 kg m^{-2}).

Shoot dry mass (SDM) accumulation was, on average, 13.04 g plant^{-1} at 28 DAT, which is similar to that obtained by Lima *et al.* (2018) of 12.42 g plant^{-1}.

3.2. Stage 2

Nutrient solution pH ranged from 5.8 to 6.7 in T1 and 6.0 to 6.7 in T2. To reduce pH, phosphoric acid was added to the solution, as Martinez (2006) recommended.

Average electrical conductivity (EC) ranged from 1.69 to 2.33 dS m^{-1} in T1 and from 1.60 to 2.00 dS m^{-1} in T2. These values were within the range from 1.5 to 2.5 dS m^{-1} recommended

by Castellane and Araújo (1995).

Table 2 describes the amounts of salts used in T1 and T2. Since the nutrient solution of T1 was not discarded, the parts of salts used could be reduced compared to T2 without damaging fresh mass production. In the third week of cultivation, besides the salts already used, potassium sulfate and urea were used to avoid adding some nutrients in excess.

Table 2. Total contents of fertilizers used during the crop cycle in T1 and T2 are expressed in salts and individual nutrients for a total volume of 512.5 L for T1 and 1400 L for T2.

Fertilizer	The total amount of salts		The total amount of nutrients	
	T1 (g)	T2 (g)	T1 (g)	T2 (g)
Calcium nitrate	407.7	700	N – 142.45	N – 240.5
Potassium nitrate	423.5	700	P – 49.46	P – 216
Magnesium sulfate	249.4	490	K – 190.57	K – 315
Monoammonium phosphate (MAP)	91.6	140	Ca – 77.46	Ca – 133
ConMicros Standard	15.2	28	Mg – 22.45	Mg – 45
Potassium sulfate	18.9	–		
Urea	8.3	–		

During Stage 2, plants of both treatments showed no visual symptoms of nutrient deficiency. Therefore, the leaf analysis results of T1 and T2 were compared to the optimal ranges of macronutrients recommended by Raij *et al.* (1997), which are: N = 30–50 g kg^{-1}, P = 4–7 g kg^{-1}, K = 50–80 g kg^{-1}, Ca = 15–25 g kg^{-1}, and Mg = 4–6 g kg^{-1}. The results for T1 were 45 g N kg^{-1}, 8.32 g P kg^{-1}, 69.25 g K kg^{-1}, 7.70 g Ca kg^{-1}, and 2.78 g Mg kg^{-1}, while those of T2 were 46.50 g N kg^{-1}, 9.23 g P kg^{-1}, 56.12 g K kg^{-1}, 7.06 g Ca kg^{-1}, and 2.61 g Mg kg^{-1}.

The order of nutrient absorption found in the leaf analysis was K > N > P > Ca > Mg. Grangeiro *et al.* (2006) found a similar result in field cultivation.

The contents of N and K were within the range considered adequate for lettuce (Raij *et al.*, 1997). Otherwise, P content was above the optimal range in both T1 and T2; however, plants showed no visual toxicity symptoms. According to Malavolta (2006), excess P toxicity is not commonly seen in plants; yet, it can cause micronutrient deficiencies (e.g., copper, iron, manganese, and zinc), leading to reduced biomass. Such excess may be related to the addition of phosphoric acid to decrease nutrient solution pH, thus increasing P contents and hence luxury consumption by plants.

Both treatments showed Ca and Mg contents below the optimal range for lettuce growth. It may be related to high K contents in nutrient solutions. Potassium excess decreases Ca and Mg contents in the medium (Rosolem, 2005) since these ions compete for the same absorption sites. Despite the low levels, no deficiency symptoms of these nutrients were observed. This may have occurred because the cultivar Milena has a high tolerance to lack of Ca and is slow-growing (late cultivar), thus masking the symptoms.

At 30 DAT, total shoot fresh mass accumulation reached 156.7 g plant^{-1} in T1 and 156.3 g plant^{-1} in T2. These values are close to those of Vaz and Junqueira (1998) and Benini *et al.* (2005). They obtained 183.4 g and 124.5 g of fresh biomass per plant for the cultivar Verônica, respectively. On the other hand, Ceccherini *et al.* (2020) studied a different number of tray cells for lettuce production under conventional and hydroponic systems for summer cultivation. They obtained a fresh mass of about 280 g plant^{-1}. In our study, the low mass yields achieved in both treatments may be related to the K effect on Ca and Mg absorption, which was below the range recommended (Raij *et al.*, 1997). In addition, high K contents in nutrient solutions may impair plant growth or production (Rosolem, 2005).

Total water consumption per plant for T1 and T2 at 30 DAT was, on average, 2.0 L (Figure

5), about 66 mL per plant^{-1} day^{-1}. Milder temperatures and high relative humidity decrease water consumption by plants.

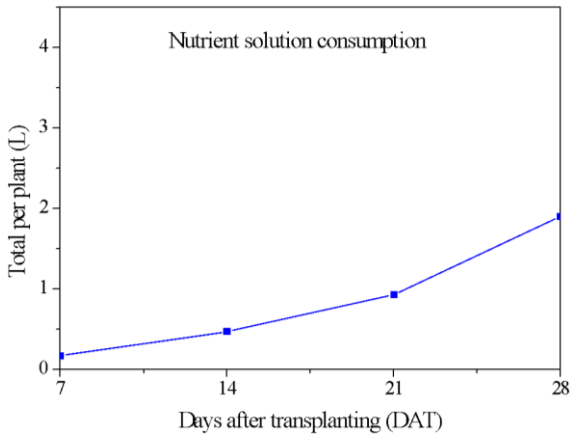

Figure 5. Nutrient solution consumption throughout the cycle of the lettuce cv. Milena.

At 30 DAT, the total shoot dry mass accumulated reached 6.53 g plant^{-1} for T1 and 6.43 g plant^{-1} for T2, with no difference between these treatments ($p \leq 0.05$) and a *p*-value of 0.3185976. The total water volume used in Stage 2 was 512.5 L for T1 and 1400 L for T2.

The WUE for T1 and T2 were, respectively, 53.81 kg m^{-3} and 19.65 kg m^{-3}. These results show that T1 increased the WUE with the solution reuse during the crop cycle. However, the fresh mass production was equal, T1 – 27.580 kg and T2 – 27.508 kg.

4. CONCLUSION

Under this study, we concluded that nutrient solution reuse provided replacement of nutrients during the lettuce crop cultivation.

5. REFERENCES

ALVES, M. S.; SOARES, T. M.; SILVA, L. T.; FERNANDES, J. P.; OLIVEIRA, M. L. A.; PAZ, V. P. S. Estratégias de uso de água salobra na produção de alface em hidroponia NFT. **Revista Brasileira de Engenharia Agrícola e Ambiental**, v. 15, n. 5, p. 491-498, 2011. https://doi.org/10.1590/S1415-43662011000500009

BACKES, F. A. A. L.; SANTOS, O. S. S.; PILAU, F. G.; BONNECARRÈRE, R. A. G.; MEDEIROS, S. L. P.; FAGAN, E. B. Reposição de nutrientes em solução nutritiva para o cultivo hidropônico de alface. **Ciência Rural**, v. 34, n. 5, p. 1407-1414, 2004. https://doi.org/10.1590/S0103-84782004000500013

BACKES, F. A. A. L.; SANTOS, O.; SCHMIDT, D.; NOGUEIRA FILHO, H.; MANFRON, P. A.; CASAROLI, D. Reposição de nutrientes durante três cultivos de alface em hidroponia. **Horticultura Brasileira**, v. 21, n. 4, p. 590-596, 2003. https://doi.org/10.1590/S0102-05362003000400002

BADGERY-PARKER, J. Managing waste water from intensive horticulture: a wetland system. **Agnote**, v. 381, n. 2, p. 1–4, 2002.

BARROS, H. M. M.; VERIATO, M. K. L.; SOUZA, L. P.; CHICÓ, L. R.; BAROSI, K. X. L. Reúso de água na agricultura. **Revista Verde de Agroecologia e Desenvolvimento Sustentável**, v. 10, n. 5, p. 11-16, 2015. https://doi.org/10.18378/rvads.v10i5.3868

BENINI, E. R. Y.; TAKAHASHI, H. W.; NEVES, C. S. V. J. Concentração e acúmulo de macronutrientes em alface cultivada em sistemas hidropônico e convencional. **Semina: Ciências Agrárias**, v. 26, n. 3, p. 273-282, 2005. http://dx.doi.org/10.5433/1679-0359.2005v26n3p273

BEZERRA NETO, E.; PAES, L. B. As técnicas de hidroponia. **Anais da Academia Pernambucana de Ciência Agronômica**, v. 8, p. 107-137, 2011.

BEZERRA NETO, E. Hidroponia. **Cadernos do Semiárido: riquezas & oportunidades**, v. 6, n. 6, 2016.

CARMO, C. A. F. S; ARAÚJO, W. S. A.; BERNARDI, A. C. C.; SALDANHA, M. F. C. **Métodos de análise de tecidos vegetais utilizados na embrapa solos**. Curricular técnica 6. Rio de Janeiro: EMBRAPA, 2000. 41 p.

CASTELLANE, P. D.; ARAÚJO. J. A. C. **Cultivo sem solo: hidroponia**. Jaboticabal: FUNEP, 1995. 43 p.

CECCHERINI, G. J.; LIMA, T. J. L. D.; SALA, F. C. Different tray cell volumes for lettuce grown in conventional and hydroponic system. **Ciência Rural**, v. 50, n. 1, e20190491, 2020. https://doi.org/10.1590/0103-8478cr20190491

CONAB. Alface. **Boletim hortigranjeiro**, v. 6, n. 3, p.15-18, 2020.

CUBA, R. S.; CARMO, J. R.; SOUZA, C. F.; BASTOS, R. G. Potencial de efluente de esgoto doméstico tratado como fonte de água e nutrientes no cultivo hidropônico de alface. **Revista Ambiente & Água**, v. 10, n. 3, p. 574 - 586, 2015. https://doi.org/10.4136/ ambi-agua.1575

FERNANDES, A. A.; MARTINEZ, H. E. P., PEREIRA, P. R. G.; FONSECA, M. C. M. Produtividade, acúmulo de nitrato e estado nutricional de cultivares de alface, em hidroponia, em função de fontes de nutrientes. **Horticultura brasileira**, v. 20, n. 2, p. 195-200, 2002.

FURLANI, P. R. Hydroponic vegetable production in Brazil. **Acta Horticulturae**, v. 2, n. 481, p. 777-778, 1999. https://doi.org/10.17660/ActaHortic.1999.481.98

FURLANI, P. R.; BOLONHEZI, D.; SILVEIRA, L. C. P.; FAQUIN, V. Nutrição mineral de hortaliças, preparo e manejo de soluções nutritivas. **Informe Agropecuário**, v. 20, n. 200/201, p. 90-98, 1999.

FURLANI, P. R.; SILVEIRA, L. C. P.; BOLONHEZI, D.; FAQUIN, V. **Cultivo Hidropônico de Plantas: Parte 1 - Conjunto hidráulico**. 2009. Available: www.infobibos.com/Artigos/2009_1/hidroponiap1. Access: April 2022.

GIMENEZ, G.; ANDRIOLO, J.; GODOI, R. Cultivo sem solo do morangueiro. **Ciência Rural**, v. 38, n. 1, p. 273-279, 2008. https://doi.org/10.1590/S0103-84782008000100048

GONDIM, A. R. O.; FLORES, M. E. P.; MARTINEZ, H. E. P.; FONTES, P. C. R.; PEREIRA, P. R. G. Condutividade elétrica na produção e nutrição de alface em sistema de cultivo hidropônico NFT. **Bioscience Journal**, v. 26, n. 6, p. 894-904, 2010.

GRANGEIRO, L. C; COSTA, K. R; MEDEIROS, M. A.; SALVIANO, A. M.; NEGREIROS, M. Z.; BEZERRA NETO, F. *et al.* Acúmulo de nutrientes por três cultivares de alface cultivadas em condições do Semi-Árido. **Horticultura Brasileira,** v. 24, n. 2, p. 190-194, 2006.

HEINEN, M.; JAGER, A.; NIERS, H. Uptake of nutrients by lettuce on NFT with controlled composition of the nutrient solution. **Netherlands Journal of Agricultural Science**, v. 39, p. 197-212, 1991.

IBGE. **Censo Agropecuário.** 2017. Available: https://www.ibge.gov.br/explica/producao-agropecuaria/alface/br. Access: 27 jul. 2022.

LIMA, T. J.; GAZAFFI, R.; CECCHERINI, G. J.; MARCHI, L.; MARTINEZ, M.; FERREIRA, C. G. *et al.* Volume of cells on trays influences hydroponic lettuce production. **Horticultura Brasileira**, v. 36, n. 3, p. 408-413. 2018. http://dx.doi.org/10.1590/S0102-053620180320

MALAVOLTA, E. **Manual de nutrição de plantas**. São Paulo: Editora Agronômica Ceres, 2006. 638 p.

MARTINEZ, E. P. **O uso do cultivo hidropônico de plantas em pesquisa**. Viçosa: Editora UFV, 2002. 76 p.

MARTINEZ, H. E. P. **Manual prático de hidroponia**. Viçosa: Editora UFV, 2006. 271p.

MARTINEZ, H. E. P.; SILVA FILHO, J. B. **Introdução ao cultivo hidropônico de plantas**. Viçosa: Editora UFV, 2004. 111 p.

RAIJ, B.; CANTARELLA, H.; QUAGGIO, J. A.; FURLANI, A. M. C. **Recomendações de Adubação e Calagem para o Estado de São Paulo**. Campinas: IAC/FUNDAG, 1997. 285 p.

ROSOLEM, C. A. Interação do potássio com outros íons. *In*: YAMADA, T.; ROBERTS, T. L. **Potássio na agricultura brasileira**. Piracicaba: Potafós, 2005. p. 239-260.

SALA, F. C.; COSTA, C. P. Retrospectiva e tendência da alfacicultura brasileira. **Horticultura Brasileira**, v. 30, n. 2, p. 187-194, 2012. https://doi.org/10.1590/S0102-05362012000200002

SALA, F. C. A. Cultura. *In*: NICK, C.; BORÉM, A. (eds.). **Alface**: do plantio à colheita. Viçosa: Editora UFV, 2019. 232 p.

SANTOS, J. D.; SILVA, A. L. L.; LUZ COSTA, J.; SCHEIDT, G. N.; NOVAK, A. C.; SYDNEY, E. B. *et al.* Development of a vinasse nutritive solution for hydroponics. **Journal of environmental management**, v. 114, p. 8-12, 2013. https://doi.org/10.1016/j.jenvman.2012.10.045

SAE. **Produção Nacional de Fertilizantes**. 2020. 26 p. Available in: https://www.gov.br/planalto/pt-br/assuntos/assuntos-estrategicos/documentos/estudos-estrategicos/sae_publicacao_fertilizantes_v10.pdf. Access in September 2021.

SILVA, F. C. **Manual de análises químicas de solos, plantas e fertilizantes**. Brasília: Embrapa Informação Tecnológica, 2009. 627 p.

VALADARES, G. S.; AVANCINI, C. S. A.; TÖSTO, S. G. **Uso e Cobertura das Terras do Município de Araras.** Campinas: EMBRAPA, 2008. 12 p. Available in: https://www.embrapa.br/busca-de-publicacoes/-/publicacao/31424/uso-e-cobertura-das-terras-do-municipio-de-araras. Access in April 2022

VAZ, R. M. R.; JUNQUEIRA, A. M. R. Desempenho de três cultivares de alface sob cultivo hidropônico. **Horticultura Brasileira**, v. 16, n. 2, p. 178-189, 1998. https://doi.org/10.1590/S0102-05361998160000200018

Ambiente & Água - An Interdisciplinary Journal of Applied Science
ISSN 1980-993X – doi:10.4136/1980-993X
www.ambi-agua.net
E-mail: ambi.agua@gmail.com

Ibuprofen biosorption by chemically activated *Saccharomyces cerevisiae*

ARTICLES doi:10.4136/ambi-agua.2862

Received: 07 Jun. 2022; Accepted: 02 Aug. 2022

Bruna Assis Paim dos Santos[1]; Evandro Luiz Dall'Oglio[2]; Adriano Buzutti de Siqueira[2]; Danila Soares Caixeta[1,3]; Viviane Cristina Padilha Lopes[1]; Leonardo Gomes de Vasconcelos[2]; Eduardo Beraldo de Morais[1,3*]

[1]Faculdade de Arquitetura, Engenharias e Tecnologias. Departamento de Engenharia Sanitária e Ambiental. Universidade Federal de Mato Grosso (UFMT), Campus Universitário de Cuiabá, Avenida Fernando Corrêa da Costa, n° 2367, CEP: 78060-900, Cuiabá, MT, Brazil. E-mail: bruna.santos_assis@hotmail.com, danilacaixeta@gmail.com, vivianelops@gmail.com
[2]Instituto de Ciências Exatas e da Terra. Departamento de Química. Fundação Universidade Federal de Mato Grosso (FUFMT), Campus Universitário de Cuiabá, Avenida Fernando Corrêa da Costa, n° 2367, CEP: 78060-900, Cuiabá, MT, Brazil. E-mail: dalloglio.evandro@gmail.com, buzutti7@hotmail.com, vasconceloslg@gmail.com
[3]Faculdade de Arquitetura, Engenharia e Tecnologia. Departamento de Engenharia Sanitária e Ambiental. Universidade Federal de Mato Grosso (UFMT), Campus Universitário de Cuiabá, Avenida Fernando Corrêa da Costa, n° 2367, CEP: 78060-900, Cuiabá, MT, Brazil. E-mail: danilacaixeta@gmail.com
[*]Corresponding author. E-mail: beraldo_morais@yahoo.com.br

ABSTRACT

Saccharomyces cerevisiae biomass was activated chemically, and its ibuprofen (IBP) biosorption capabilities were assessed regarding IBP removal from an aqueous solution. The effects of pH (2-10), contact time (0-90 min), IBP concentration (5-35 mg L^{-1}), and temperature (20, 30, 40°C) were evaluated in batch studies. Higher removal rates of IBP were found at pH 2.0. The pseudo-second-order kinetic model best described the experimental data. Both the Langmuir and Freundlich isotherm models described the equilibrium data satisfactorily. The maximum biosorption capacity for IBP onto chemically activated *Saccharomyces cerevisiae* biomass (CA-YB) was estimated at 13.39 mg g^{-1} at 40°C. The activation energy calculated by the Dubinin-Radushkevich isotherm model was 9.129 kJ mol^{-1}, indicating that a chemical process mediated the biosorption of IBP onto CA-YB. According to thermodynamic studies, IBP biosorption is spontaneous and endothermic. FTIR analysis revealed that the carboxyl, hydroxyl, phosphoryl, and amino groups were involved in the biosorption process of IBP. These findings indicated that CA-YB could be an alternative biosorbent for IBP removal from aqueous media.

Keywords: isotherms, kinetic, microbial biomass, pharmaceutical drugs, thermodynamic study.

Biossorção de ibuprofeno por *Saccharomyces cerevisiae* ativada quimicamente

RESUMO

Biomassa de *Saccharomyces cerevisiae* foi ativada quimicamente e sua capacidade de

biossorção foi explorada para a remoção do ibuprofeno (IBP) da solução aquosa. Os efeitos do pH (2-10), tempo de contato (0-90 min), concentração de IBP (5-35 mg L^{-1}) e temperatura (20, 30, 40°C) foram avaliados em estudos de bateladas. Em pH 2,0 foram encontradas as maiores taxas de remoção de IBP. O modelo cinético de pseudo-segunda ordem foi o mais adequado para descrever os dados experimentais. Ambos os modelos de isoterma de Langmuir e Freundlich descreveram os dados de equilíbrio de forma satisfatória. A capacidade máxima de biossorção para IBP pela biomassa de *Saccharomyces cerevisiae* quimicamente ativada (CA-YB) foi estimada em 13,39 mg g^{-1} a 40°C. A energia de ativação calculada pelo modelo de isoterma de Dubinin-Radushkevich foi de 9,129 kJ mol^{-1}, indicando que um processo químico mediou a biossorção de IBP por CA-YB. De acordo com os estudos termodinâmicos, a biossorção do IBP é espontânea e endotérmica. A análise de FTIR revelou que os grupos carboxila, hidroxila, fosforila e amino estavam envolvidos no processo de biossorção do IBP. Essas descobertas indicaram que CA-YB pode ser um biossorvente alternativo para a remoção de IBP do meio aquoso.

Palavras-chave: biomassa microbiana, cinética, estudo termodinâmico, fármacos, isotermas.

1. INTRODUCTION

Widespread use of anti-inflammatory drugs is the main reason they are commonly detected in sewage wastewaters, surface and ground waters, and even drinking waters (Yamkelani *et al.*, 2019). During medical care, these drugs are excreted as unchanged or metabolites by animals and humans, and their concentrations in aquatic media are usually in the range of ng L^{-1} or µg L^{-1}. Despite the low concentration, there is still cause for concern, as these pollutants are persistent, bioaccumulative, and endocrine disruptor (Oba *et al.*, 2021).

Ibuprofen [2-(4-isobutylphenyl) propanoic acid] is a non-steroidal anti-inflammatory widely used worldwide (Santaeufemia *et al.*, 2018). It is usually prescribed to relieve aches, pains, and fever. The concentration of ibuprofen (IBP) in the aquatic environment was found to range from 4198.4 to 10864.0 ng L^{-1} in sewage wastewater, 5.7 to 223.6 ng L^{-1} in drinking water, and 5 to 62 ng L^{-1} in surface water (Aristizabal-Ciro *et al.*, 2017). These concentrations pose a potential hazard to organisms. Immunosuppression, nephrotoxicity, and endocrine disruption are some deleterious effects on fishes and mussels (Oba *et al.*, 2021).

Many technologies have been applied to remove IBP from water and wastewater, such as electrochemical and photocatalytic degradation (Li *et al.*, 2016), heterogeneous electro-Fenton process (Liu *et al.*, 2018), ozonation (Saeid *et al.*, 2018), and adsorption (Santaeufemia *et al.*, 2018). However, most of these technologies are expensive, require high-tech operations and skilled personnel, and can generate toxic by-products (secondary pollution) or incomplete removal. Among these technologies, adsorption has become a well-established technology to remove different pollutants, including pharmaceutical drugs. The easy availability, low cost or zero cost of some adsorbents, simplicity of design and operation, and ability to treat wastewater with a low or high concentration of pollutants make the adsorption a techno-economically viable solution for eliminating pollutants from aqueous media (Castro *et al.*, 2017).

Recently, the adsorption of IBP onto biological adsorbents has been studied in detail. Pinewood biochar (Essandoh *et al.*, 2015), *Aegle marmelos* shell biochar (Chakraborty *et al.*, 2018a), and activated sugarcane bagasse (Chakraborty *et al.*, 2018b) are some examples. Microbial biomasses have also been used to efficiently remove pollutants from water (Castro *et al.*, 2017). Their pollutant-adsorptive capacity is due to the chemical characteristics of their cell walls, which possess many polysaccharides and some proteins, among other components. These biomacromolecules have several functional groups, such as carboxyl, amino, thiol, phosphate, and sulfhydryl, responsible for the adsorption phenomena (Ramanaiah *et al.*, 2007).

The yeast *Saccharomyces cerevisiae* is an inexpensive and readily available biomass source used in pollutant adsorption. It can be easily cultivated on a large scale or obtained as a by-product of the food and beverage industries. *Saccharomyces cerevisiae* biomass has been used as a biosorbent to remove heavy metals and textile dyes (Castro *et al.*, 2017). However, this yeast is little-explored with regard to its ability to remove anti-inflammatory drugs. In this study, we investigated the adsorption of IBP by chemically activated *Saccharomyces cerevisiae* biomass under different experimental conditions.

2. MATERIAL AND METHODS

2.1. Chemicals

Ibuprofen sodium salt (IBP) (linear formula: $C_{13}H_{17}O_2Na$; molecular weight: 228.26 g/mol) was obtained from Sigma Aldrich – Brazil (>98% purity, pKa = 4.91). Hexane, methanol, HCl, and NaOH were of analytical grade.

2.2. Preparation and characterization of biosorbent

Saccharomyces cerevisiae was purchased from a local market as Baker's yeast. Yeast biomass (YB) was sieved through a 149 μm standard sieve and activated by extraction with hexane for 6 h and subsequently with methanol for 6 h. The extraction occurred in a Soxhlet extractor. Following the process, the chemically activated yeast biomass (CA-YB) was rinsed with distilled water and dried in an oven at 60°C for 48 h. The CA-YB was kept in a desiccator until use.

2.3. Biosorbent characterization

The functional groups on the surface of CA-YB were investigated using the Fourier transform infrared spectroscopy (FTIR) analyses. The samples of CA-YB were prepared using the KBr disk method, and the transmission FTIR spectra were recorded in the 4000 and 400 cm^{-1} (Shimadzu IRAffinity-1 spectrophotometer). The thermal stability of CA-YB was evaluated with thermogravimetric analysis (TGA) and differential thermal analysis (DTA) using a thermogravimetric analyzer (Shimadzu DTG-60H). The analysis was conducted in an air atmosphere at a heating speed of 20°C /min from ambient temperature (26°C) up to 1000°C. The point of zero charge (pH_{PZC}) of CA-YB was determined using the method described by Dahri *et al.* (2014). 20 mL of KNO_3 solutions (0.1 M) was added to the Erlenmeyer flasks, and the pH values were adjusted in the range of 2.1–10.3 by adding 0.1 M of NaOH/HCl. Then, 0.03 g of CA-YB was added to the Erlenmeyer flasks and the flasks were shaken at 150 rpm for 24 h, at 24°C. Next, the final pH of KNO_3 solutions was measured, and the pH_{pzc} was determined by plotting ΔpH (final pH – initial pH) versus initial pH.

2.4. Batch biosorption experiments

All biosorption experiments were performed with 100 mL Erlenmeyer flasks containing 30 mL of IBP aqueous solution. The flasks were agitated on a shaking incubator at 150 rpm. The influence of various parameters on the biosorption efficiency was evaluated: pH (2, 4, 6, 8, and 10, adjusted by the addition of 0.1 M NaOH or 0.1 M HCl solutions), initial IBP concentration (5.0-35.0 mg L^{-1}), contact time (0-90 min), and temperature (20, 30, and 40°C). Aliquots were withdrawn from the flasks at predetermined time intervals and filtered (filter membrane Ø 0.45 μm) to remove biosorbent particles. The residual IBP concentration in the solution was analyzed by using a UV/Vis spectrophotometer (Hach DR6000) at λ_{max} = 221 nm. All biosorption experiments were conducted in triplicate. The IBP removal percentage, R (%), and the amount of IBP adsorbed per unit of biosorbent, q_e (mg g^{-1}) were determined according to Equations 1 and 2:

$$R(\%) = \frac{C_i - C_e}{C_i} \times 100 \quad (1)$$

$$q_e = \frac{(C_i - C_e)}{b} \quad (2)$$

Where C_i and C_e are the initial and the equilibrium IBP concentrations (mg L^{-1}), and b is the biosorbent concentration in solution (g L^{-1}).

2.5. Kinetic and isotherms models

The kinetic and isotherms models (Chakraborty *et al.*, 2018b; Santaeufemia *et al.*, 2018) used in this study are listed in Table 1. The usability of these models in fitting to data was evaluated by the coefficient of determination (R^2) and the root mean square error (*RMSE*) (Equation 3):

$$RMSE = \sqrt{\frac{1}{n}\sum\left(q_{exp} - q_{cal}\right)^2} \quad (3)$$

Where q_{exp} and q_{cal} are the experimental and calculated values, and n is the number of samples.

Table 1. Kinetic and isotherm models.

Model	Equation	Parameters
	Kinetic models	
Pseudo-first-order	$\log(q_e - q_t) = \log q_e - \frac{K_1}{2.303}t$	q_e (mg g^{-1}): biosorption capacity at equilibrium q_t (mg g^{-1}): biosorption capacity at time t K_1 (min^{-1}): pseudo-first-order rate constant
Pseudo-second-order	$\frac{t}{q_t} = \frac{1}{K_2 q_e^2} + \frac{1}{q_e}t$	K_2 (g mg^{-1} min^{-1}): pseudo-second-order rate constant
Isotherm models		
Langmuir	$\frac{1}{q_e} = \frac{1}{q_m} + \left(\frac{1}{q_m K_L}\right)\frac{1}{C_e}$	q_e (mg g^{-1}): biosorption capacity at equilibrium q_m (mg g^{-1}): maximum biosorption capacity C_e (mg L^{-1}): equilibrium adsorbate concentration in solution K_L (L mg^{-1}): Langmuir constant
Freundlich	$\ln q_e = \ln K_f + \frac{1}{n}\ln C_e$	K_f ((mg g^{-1}) (mg L^{-1})$^{-1/n}$): Freundlich constant n: heterogeneity factor
Dubinin-Radushkevich	$ln\ q_e = ln\ q_m - \beta\varepsilon^2$	ε: Polanyi potential β (mol^2 kJ^{-2}): biosorption energy constant
	$\varepsilon = RT\ ln\left(1 + \frac{1}{C_e}\right)$	R: universal gas constant (8.314 J mol^{-1} K^{-1})

2.6. Adsorption thermodynamics

The thermodynamics parameters of IBP biosorption onto CA-YB, *i.e.*, Gibbs free energy change (ΔG), entropy (ΔS), and enthalpy (ΔH), were calculated by using the Equations 4, 5 and 6:

$$\Delta G = -RT\, lnK_D \quad (4)$$

$$\Delta G = \Delta H - T\Delta S \quad (5)$$

$$lnK_D = \frac{\Delta S}{R} - \frac{\Delta H}{R} x \frac{1}{T} \quad (6)$$

Where K_D (qe/Ce) refers to the distribution coefficient, R is the universal gas constant (8.314 J K^{-1} mol^{-1}), and T (K) is the absolute temperature.

3. RESULTS AND DISCUSSION

3.1. FTIR, TGA-DTA analysis, and pH_{pzc}

FTIR spectroscopy identifies the functional groups on the adsorbents surfaces and the possible interactions between them and the adsorbate. FTIR spectra (Figure 1a) show a diversity of organic compounds on the surface of the pristine cell. The broadband observed in the region 3800-3000 cm^{-1} could be assigned to O–H stretching in carbohydrates and N–H stretching of proteins, and amide II of chitin. The peak at 2931 cm^{-1} can be attributed to the CH_2 group of lipids. The peak at 1651 cm^{-1} was assigned to the C=O stretching vibration or N–H bending vibration to the amide I from protein. Bonds of amide II and III (N–H or C–N vibration) also from proteins are observed at peaks 1543 and 1242 cm^{-1}, respectively. The band at 1404 cm^{-1} was due to the symmetric stretching of –COOH, and the peak at 1049 cm^{-1} was C–O stretching vibration of polysaccharides skeleton. The characteristic peak at 578 cm^{-1} corresponds to O–P–O bending vibration of phosphate groups (Chen *et al.*, 2020; Rossi *et al.*, 2020; Wang *et al.*, 2017; Zhang *et al.*, 2019). After the chemical activation of *S. cerevisiae* biomass, the peaks at 3309 (O–H/N–H), 1543 (N–H/C–N), 1049 (C–O), and 578 (O–P–O) cm^{-1} shifted to 3286, 1535, 1056, and 570 cm^{-1}, respectively. After IBP adsorption, some of the bands have shifted from 3286 to 3278 cm^{-1} (O–H/ N–H), 1651 to 1658 cm^{-1} (amide I), 1242 to 1234 cm^{-1} (amide III), 1056 to 1049 (C–O), and 570 o 555 cm^{-1} (O–P–O). These results indicate that the carboxyl, hydroxyl, phosphoryl, and amino groups were involved in the biosorption process of IBP.

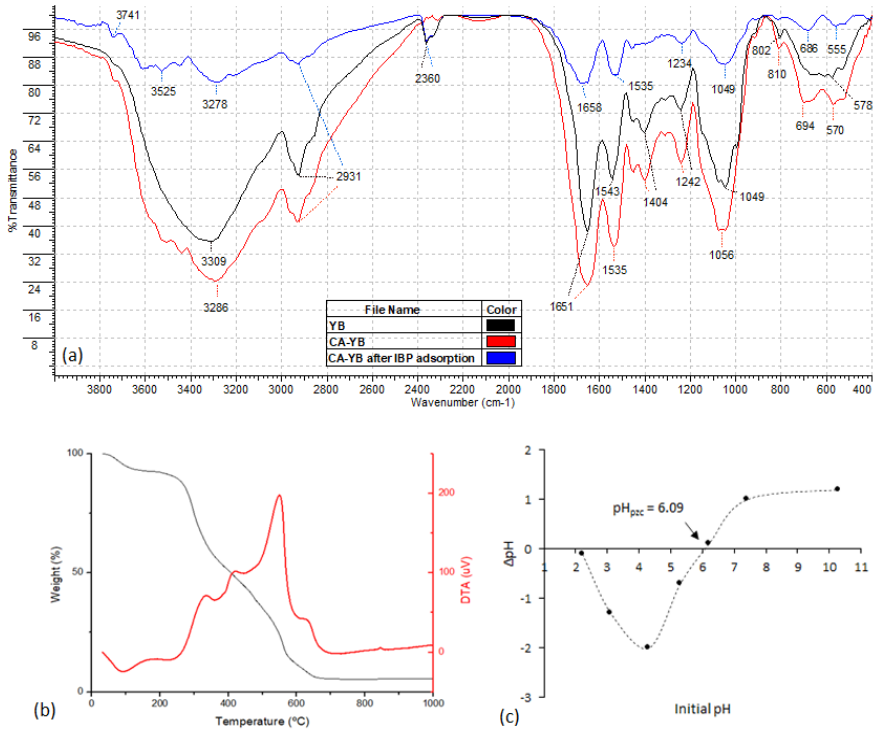

Figure 1. Characterization of CA-YB: FTIR spectra (a), TGA/DTA curve (b), and point of zero charge (pH_{PZC}) (c).

The thermogravimetric diagrams from TGA/DTA are displayed in Figure 1b. The TGA curve from CA-YB decomposition revealed some mass loss steps, which have been accompanied by endothermic and exothermic peaks in the DTA curve. The mass loss observed from room temperature to approximately 130°C is endothermic and corresponds to surface water evaporation. From 130 to 280°C represents the removal region of bound moisture and light volatile compounds (Padmavathy *et al.*, 2003). The maximum mass loss was achieved in the next two exothermic steps, i.e., between 270 and 420°C and 420 and 670°C, indicating that the yeast compounds degraded in these ranges (Rossi *et al.*, 2020). At a temperature above 670°C, no other thermal effects and mass loss were observed.

The point of zero charge (pH_{pzc}) is the pH value where the net charge on the adsorbent surface is zero. The adsorbent surface will be negatively charged when the pH_{pzc} < pH of the solution and positively charged when the pH_{pzc} > pH of the solution. The plot of ΔpH versus initial pH showed that the pH_{pzc} for CA-YB was 6.09 (Figure 1c).

3.2. Effect of pH

The effect of different initial pH on the removal of IBP by CA-YB is shown in Figure 2. The results indicated that the adsorption of IBP decreased from 4.0 to 0.3 mg g^{-1} when the pH increased from 2 to 10. The removal of IBP by pristine YB was also studied, but the removal was practically negligible (data not shown). The pKa value of ibuprofen is 4.9 (Chakraborty *et al.*, 2018a), and can be used to explain the effect of pH on the IBP biosorption. When the pH value is above 4.9, the anionic form of IBP is the predominant species, while below this value, its molecular form is predominant (Chakraborty *et al.* 2018b). With an increase in the pH, the CA-YB surface becomes less positive, and the anionic form of IBP increases, decreasing the adsorption. At pH 2, the increased IBP removal suggests a minor electrostatic repulsion between the CA-YB surface with IBP.

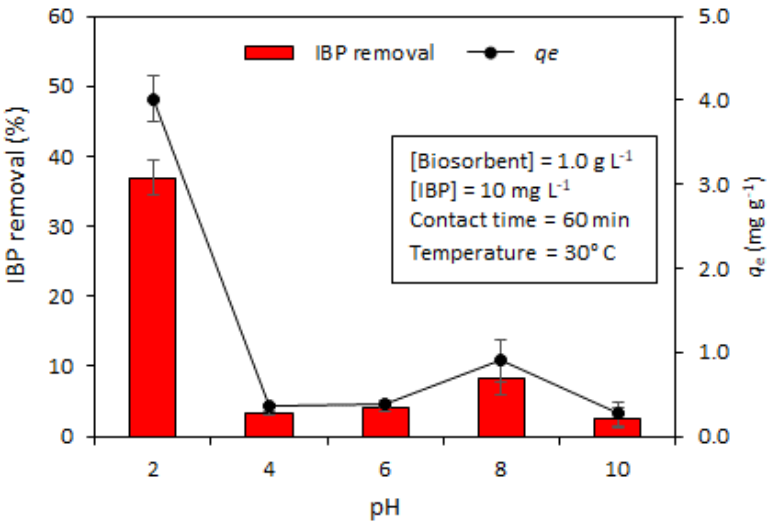

Figure 2. Effect of pH on the biosorption of IBP onto CA-YB.

3.3. Effect of contact time and temperature

Figure 3a shows the IBP biosorption by CA-YB at different contact times and temperatures. Rapid adsorption of IBP occurred during the first 10 min and was practically negligible after this time, which is advantageous considering the practical application. This rapid adsorption is attributed to the abundant availability of free active sites on the biosorbent surface at the beginning of the biosorption process, which became less efficient when these functional groups were occupied. Also, it can be seen that the biosorption capacity of CA-YB increased from 5.37 to 7.29 mg g^{-1} when the temperature was increased from 20 to 40°C,

indicating that an endothermic process controls the biosorption of IBP onto CA-YB. Since the highest removal efficiency (72,9%) was observed at 40°C, this temperature was used in subsequent experiments.

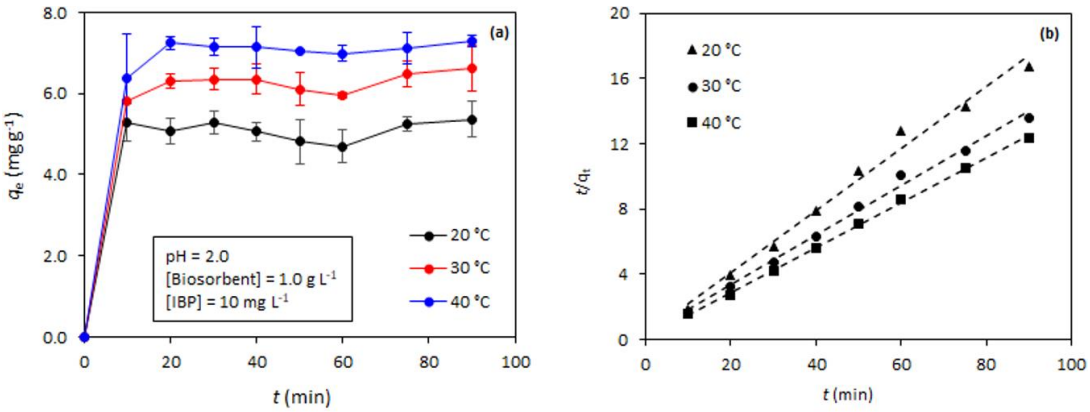

Figure 3. Effect of contact time (a) and plot for pseudo-second-order model (b) for IBP biosorption onto CA-YB, at different temperatures.

3.4. Kinetic studies

Kinetics studies are essential for the modeling and design of the adsorption process. In this study, kinetic experiments of IBP removal were conducted at constant initial IBP concentration (10.0 mg L^{-1}), 1.0 g L^{-1} of biosorbent, and temperatures of 20, 30, and 40°C. The experimental data of IBP adsorption were fitted with two well-established kinetic models, pseudo-first-order model and pseudo-second-order model (Table 1).

The kinetic parameters (R^2 and *RMSE*) calculated from two kinetic models are summarized in Table 2. Extremely high R^2 values (R^2 = 0.989-0.99, Figure 3b) for the pseudo-second-order model for all tested temperatures and values of calculated q_e in agreement with the experimental q_e values indicated that this model was the optimum kinetic model to represent IBP biosorption on CA-YB.

Table 2. Pseudo-first-order and pseudo-second-order kinetic parameters for the biosorption of IBP onto CA-YB, at different temperatures.

Model	Temperature (°C)		
	20	30	40
$q_{experimental}$	5.37	6.61	7.29
Pseudo-first-order			
q_1 (mg g^{-1})	7.43	1.354	4.74
k_1 (min^{-1})	0.013	0.016	0.002
R^2	0.121	0.313	0.002
RMSE	0.379	0.257	0.436
Pseudo-second-order			
q_2 (mg g^{-1})	5.25	6.60	7.26
k_2 (g mg^{-1} min^{-1})	0.128	0.069	0.142
R^2	0.989	0.994	0.999
RMSE	0.600	0.346	0.133

3.5. Equilibrium isotherms

This study conducted equilibrium experiments using solutions with different initial IBP concentrations (5.0-35.0 mg L^{-1}), 1.0 g L^{-1} of biosorbent at 40°C. The biosorption of IBP onto

CA-YB was evaluated by Langmuir, Freundlich, and Dubinin-Radushkevich (D-R) isotherms models. Figure 4 shows the linearized plots for the isotherm models, and the calculated parameters are presented in Table 3.

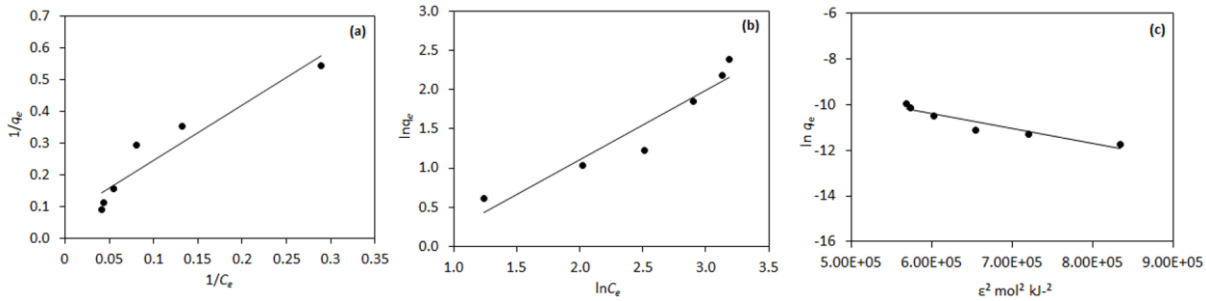

Figure 4. Plots for the isotherm models: (a) Langmuir, (b) Freundlich, and (c) D-R.

Table 3. Isotherm parameters for the biosorption of IBP onto CA-YB.

Model	Parameter
Langmuir	
q_{max} (mg g^{-1})	13.39
K_L (L mg^{-1})	0.043
R^2	0.903
RMSE	0.049
Freundlich	
K_F (mg g^{-1}) (mg L^{-1})$^{-1/n}$	1.940
n	1.133
R^2	0.911
RMSE	0.190
D-R	
q_m (mmol g^{-1})	1,392
β (mol^2 J^{-2})	6.00 x 10^{-8}
E (kJ mol^{-1})	9.129
R^2	0.896
RMSE	0.334

Langmuir and Freundlich models described the equilibrium data quite well, with R^2 higher than 0.9 and low *RMSE*. The Freundlich model, however, provided a better R^2 value, with n > 1.0, indicating that the biosorption process is favorable (Khadir *et al.*, 2020). The maximum biosorption capacity predicted by the Langmuir model was 13.39 mg g^{-1}. Table 4 compared the maximum adsorption capacities of CA-YB and other adsorbents. It was observed that the IBP adsorption capability using the CA-YB was comparable to those obtained for other adsorbents.

The D-R isotherm model was used to determine the nature of the biosorption process as physical or chemical. From the activity coefficient β, the mean free energy of biosorption (E, kJ mol^{-1}) was estimated using the Equation 7:

$$E = \frac{1}{\sqrt{2\beta}} \tag{7}$$

The biosorption process is controlled by a chemical mechanism when E value falls in the range from 8-16 kJ mol^{-1}, or the biosorption process proceeds through a physical mechanism if E < 8 kJ mol^{-1}. The E value of 9.129 kJ mol^{-1} (Table 3) indicated that the biosorption of IBP onto CA-YB follows a chemical process.

Table 4. Maximum biosorption capacity of IBP onto CA-YB and other adsorbents.

Adsorbent	q_{max} (mg g-^{1})
Graphene oxide nanoplatelets (Banerjee *et al.*, 2016)	3.72
Pine wood biochar (Essandoh *et al.*, 2015)	10.74
Physically activated *Cocos nucifera* shell biochar (Chakraborty *et al.*, 2019)	9.43
Chemically activated *Cocos nucifera* shell biochar (Chakraborty *et al.*, 2019)	11.38
Chemically activated date seed biochar (Chakraborty *et al.*, 2020)	11.23
Steam activated date seed biochar (Chakraborty *et al.*, 2020)	13.17
Cellulosic Sisal modified by polypyrrole-polyaniline nanoparticles (Khadir *et al.*, 2020)	19.45
Chemically activated *Saccharomyces cerevisiae* biomass (Present study)	13.39

3.6. Thermodynamics studies

Values of ΔS and ΔH were calculated by plotting $\ln K_D$ vs $1/T$ (Figure 5). Thermodynamic parameters calculated at different temperatures (20, 30, and 40°C) are summarized in Table 5. The negative values of ΔG indicate that the IBP biosorption onto CA-YB is thermodynamically spontaneous and feasible. The positive ΔH value of 33.07 KJ mol^{-1} suggests an endothermic biosorption process facilitated by increasing temperature. The ΔS was also found to be positive (113.71 J mol^{-1} K^{-1}), revealing the affinity of the CA-YB for IBP and showing that the randomness at the solid/solution interface increases during the biosorption of the drug.

Table 5. Thermodynamic parameters estimated for IBP biosorption onto CA-YB.

T (°C)	K_D	ΔG (KJ mol^{-1})	ΔH (KJ mol^{-1})	ΔS (J mol^{-1} K^{-1})
20	1.05	-0.263	33.07	113.71
30	1.98	-1.400		
40	2.48	-2.537		

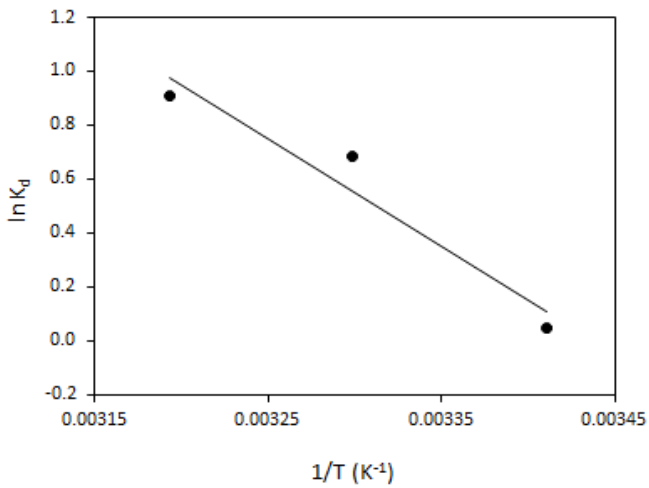

Figure 5. Plot of $\ln K_D$ versus $1/T$ for estimation of thermodynamic parameters.

4. CONCLUSIONS

In this study, chemically activated *Saccharomyces cerevisiae* was used for IBP removal from aqueous solution. The highest biosorption rate was found at pH 2. The pseudo-second-order model explained the kinetic data, and both Langmuir and Freundlich isotherm models described the equilibrium data well. The maximum biosorption capacity was estimated at 13.39

mg g^{-1} at 40°C. The biosorption of IBP onto CA-YB was chemical, endothermic, and spontaneous. FTIR analyses indicated that the carboxyl, hydroxyl, phosphoryl, and amino groups mediated the biosorption process of IBP. These findings proved that CA-YB could be used in IBP biosorption from aqueous media.

5. ACKNOWLEDGMENT

This study was financed in part by the Coordenação de Aperfeiçoamento de Pessoal de Nível Superior – Brasil (CAPES) – Finance Code 001

6. REFERENCES

ARISTIZABAL-CIRO, C.; BOTERO-COY, A. M.; LÓPEZ, F. J.; PEÑUELA, G. A. Monitoring pharmaceuticals and personal care products in reservoir water used for drinking water supply. **Environmental Science and Pollution Research,** n. 52, p. 7335–7347, 2017. https://doi.org/10.1007/s11356-016-8253-1

BANERJEE, P.; DAS, P.; ZAMAN, A.; DAS, P. Application of graphene oxide nanoplatelets for adsorption of Ibuprofen from aqueous solutions: Evaluation of process kinetics and thermodynamics. **Process Safety and Environmental Protection**, v. 101, p. 45–53, 2016. https://dx.doi.org/10.1016/j.psep.2016.01.021

CASTRO, K. C.; COSSOLIN, A. S.; REIS, H. C. O.; MORAIS, E. B. Biosorption of anionic textile dyes from aqueous solution by yeast slurry from brewery. **Brazilian Archives of Biology and Technology**, v. 60, p. 1-13, 2017. http://dx.doi.org/10.1590/1678-4324-2017160101

CHAKRABORTY, P.; BANERJEE S.; KUMAR, S.; SADHUKHAN, S.; HALDER, G. Elucidation of ibuprofen uptake capability of raw and steam activated biochar of *Aegle marmelos* shell: Isotherm, kinetics, thermodynamics and cost estimation. **Process Safety and Environmental Protection**, v. 118, p. 10–23, 2018a. https://doi.org/10.1016/j.psep.2018.06.015

CHAKRABORTY, P.; SHOW, S.; BANERJEE, S.; HALDER, G. Mechanistic insight into sorptive elimination of ibuprofen employing bi-directional activated biochar from sugarcane bagasse: Performance evaluation and cost estimation. **Journal of Environmental Chemical Engineering**, v. 6, n. 4, p. 5287–5300, 2018b. https://doi.org/10.1016/j.jece.2018.08.017

CHAKRABORTY, P.; SHOW, S.; RAHMAN, W. U.; HALDER, G. Linearity and non-linearity analysis of isotherms and kinetics for ibuprofen remotion using superheated steam and acid modified biochar. **Process Safety and Environmental Protection**, v. 126, p. 193–204, 2019. https://doi.org/10.1016/j.psep.2019.04.011

CHAKRABORTY, P.; SINGH, S. D.; GORAI, I.; SINGH, D.; RAHMANA, W. U.; HALDER, G. Explication of physically and chemically treated date stone biochar for sorptive remotion of ibuprofen from aqueous solution. **Journal of Water Process Engineering**, v. 33, p. 1-11, 2020. https://dx.doi.org/10.1016/j.jwpe.2019.101022

CHEN, C.; HU, J.; WANG, J. Biosorption of uranium by immobilized *Saccharomyces cerevisiae*. **Journal of Environmental Radioactivity**, v. 213, p. 1-10, 2020. https://doi.org/10.1016/j.jenvrad.2020.106158

DAHRI, M. K.; KOOH, M. R. R.; LIM, L. B. L. Water remediation using low cost adsorbent walnut shell for removal of malachite green: Equilibrium, kinetics, thermodynamic and regeneration studies. **Journal of Environmental Chemical Engineering**, v. 2, n. 3, p. 1434–1444, 2014. https://doi.org/10.1016/j.jece.2014.07.008

ESSANDOH, M.; KUNWAR, B.; PITTMAN, C. U.; MOHAN, D.; MLSNA, T. Sorptive removal of salicylic acid and ibuprofen from aqueous solutions using pine wood fast pyrolysis biochar. **Chemical Engineering Journal**, v. 265, p. 219–227, 2015. https://doi.org/10.1016/j.cej.2014.12.006

KHADIR, A.; MOTAMEDI, M.; NEGARESTANI, M.; SILLANPÄÄ, M.; SASANI, M. Preparation of a nano bio-composite based on cellulosic biomass and conducting polymeric nanoparticles for ibuprofen removal: Kinetics, isotherms, and energy site distribution. **International Journal of Biological Macromolecules**, v. 162, p. 663–677, 2020. https://doi.org/10.1016/j.ijbiomac.2020.06.095

LI, F.; KANG, Y.; CHEN, M.; LIU, G.; LV, W.; YAO, K.; CHEN, P.; HUANG, H. Photocatalytic degradation and removal mechanism of ibuprofen via monoclinic $BiVO_4$ under simulated solar light. **Chemosphere**, v. 150, p. 139–144, 2016. https://doi.org/10.1016/j.chemosphere.2016.02.045

LIU, D.; ZHANG, H.; WEI, Y.; LIU, B.; LIN, Y.; LI, G. *et al.* Enhanced degradation of ibuprofen by heterogeneous electro-Fenton at circumneutral pH. **Chemosphere**, v. 209, p. 998–1006, 2018. https://doi.org/10.1016/j.chemosphere.2018.06.164

OBA, S. N.; IGHALO, J. O.; ANIAGOR, C. O.; IGWEGBE, C. A. Removal of ibuprofen from aqueous media by adsorption: A comprehensive review. **Science of The Total Environment**, v. 780, p. 1-23, 2021. https://doi.org/10.1016/j.scitotenv.2021.146608

PADMAVATHY, V.; VASUDEVAN, P.; DHINGRA, S. C. Thermal and spectroscopic studies on sorption of nickel (II) ion on protonated baker's yeast. **Chemosphere**, v. 52, p. 1807–1817, 2003. https://doi.org/10.1016/S0045-6535(03)00222-4

RAMANAIAH, S. V.; VENKATA MOHAN, S.; SARMA, P. N. Adsorptive removal of fluoride from aqueous phase using waste fungus (*Pleurotus ostreatus* 1804) biosorbent: Kinetics evaluation. **Ecological Engineering**, v. 31, n. 1, p. 47–56, 2007. https://doi.org/10.1016/j.ecoleng.2007.05.006

ROSSI, A.; RIGUETO, C. V. T.; DETTMER, A.; COLLA, L. M.; PICCIN, J. S. Synthesis, characterization, and application of Saccharomyces cerevisiae/alginate composites beads for adsorption of heavy metals. **Journal of Environmental Chemical Engineering**, v. 8, n. 4, p. 1-7, 2020. https://doi.org/10.1016/j.jece.2020.104009

SAEID, S.; TOLVANEM, P.; KUMAR, N.; ERÄNEN, K.; PELTONEN, J.; PEURLA, M. *et al.* Advanced oxidation process for the removal of ibuprofen from aqueous solution: A non-catalytic and catalytic ozonation study in a semi-batch reactor. **Applied Catalysis B: Environmental**, v. 230, p. 77–90, 2018. https://doi.org/10.1016/j.apcatb.2018.02.021

SANTAEUFEMIA, S.; TORRES, E.; ABALDE, J. Biosorption of ibuprofen from aqueous solution using living and dead biomass of the microalga *Phaeodactylum tricornutum*. **Journal of Applied Phycology**, v. 30, n. 1, p. 471–482, 2018. https://doi.org/10.1007/s10811-017-1273-5

WANG, T.; ZHENG, X.; WANG, X.; LU, X.; SHEN, Y. Different biosorption mechanisms of Uranium (VI) by live and heat-killed *Saccharomyces cerevisiae* under environmentally relevant conditions. **Journal of Environmental Radioactivity**, v. 167, p. 92–99, 2017. https://doi.org/10.1016/j.jenvrad.2016.11.018

YAMKELANI, N.; NCUBE, N.; MAHLAMBI, P. N.; CHIMUKA, L.; MADIKIZELA, L. M. Adsorbents and removal strategies of non-steroidal anti-inflammatory drugs from contaminated water bodies. **Journal of Environmental Chemical Engineering**, v. 7, n. 3, p. 1-14, 2019. https://doi.org/10.1016/j.jece.2019.103142

ZHANG, J.; CHEN, X.; ZHOU, J.; LUO, X. Uranium biosorption mechanism model of protonated *Saccharomyces cerevisiae*. **Journal of Hazardous Materials**, v. 385, p. 1-10, 2019. https://doi.org/10.1016/j.jhazmat.2019.121588

Ambiente & Água - An Interdisciplinary Journal of Applied Science
ISSN 1980-993X – doi:10.4136/1980-993X
www.ambi-agua.net
E-mail: ambi.agua@gmail.com

Optimization of effluent treatment from healthcare waste incineration by electrocoagulation with iron electrodes

ARTICLES doi:10.4136/ambi-agua.2834

Received: 04 Feb. 2022; Accepted: 20 Jul. 2022

Mariana Aguiar dos Santos[1*]; Flávia Mariani Barros[1]; Sérgio de Sousa Castro[1]; Fábio Orssatto[2]

[1]Departamento de Ciências Exatas e Naturais. Universidade Estadual do Sudoeste da Bahia (UESB), BR 415, s/n, CEP: 45700-000, Itapetinga, BA, Brazil. E-mail: fbarros@uesb.edu.br, scastro@uesb.edu.br
[2]Departamento Acadêmico de Ciências Ambientais e Biológicas. Programa de Pós-Graduação em Tecnologias Ambientais. Universidade Tecnológica Federal do Paraná - Campus Medianeira (UTFPR-MD), Avenida Brasil, n° 4232, CEP: 85884-000, Medianeira, PR, Brazil. E-mail: orssatto@utfpr.edu.br
[*]Corresponding author. E-mail: marianaeng.amb@outlook.com

ABSTRACT

This study evaluated the efficiency of electrocoagulation in removing chemical oxygen demand (COD), turbidity, and apparent color from the incineration effluent generated in a gas cleaning system (GCS). Modeling and optimization of the variables electric current (I), hydraulic retention time (HRT), and electrode distance (ED) were also performed in a batch reactor using iron electrodes. A 2^3 rotatable central composite design CCRD was used, with a total of 19 trials, with electric currents ranging from 1A and 5A, a retention time of the effluent in the reactor from 15 to 40 minutes, and electrode distance of 1 and 3 centimeters. An algorithm with the desirability function was created to optimize simultaneously the parameters studied. The treatment of GCS by electrocoagulation was satisfactory in removing turbidity, apparent color, and COD, with maximum removal efficiencies above 70% for all parameters, using HRT of 27.5 minutes, ED of 2 centimeters, and electric current of 1 A. The statistical analysis showed a good fit of the model, with a coefficient of determination of $R^2 > 0.9$. The optimum operating condition was observed at 1A electric current, 27 minutes HRT, and 2 centimeters of electrode distance, with removals of 82.07, 86.86, and 70.82% of COD, turbidity, and apparent color, respectively. The simulated trials showed that lower electrolysis times can be used without impairing the treatment efficiency. Therefore, electrocoagulation may be a potential tool in the treatment of GCS.

Keywords: coagulation, electrolysis, gas scrubber, incineration.

Otimização do tratamento de efluentes da incineração de resíduos de saúde por eletrocoagulação com eletrodos de ferro

RESUMO

Este estudo teve como objetivo avaliar a eficiência da eletrocoagulação na remoção da demanda química de oxigênio (DQO), turbidez e cor aparente do efluente de incineração gerado em um sistema de limpeza de gases (SLG). A modelagem e otimização das variáveis corrente elétrica (I), tempo de retenção hidráulica (TRH) e distância do eletrodo (DE) também foram realizadas em um reator em batelada utilizando eletrodos de ferro. Foi utilizado um

delineamento composto central rotacional (DCCR) na 2^3 com um total de 19 ensaios, com correntes elétricas variando de 1A e 5A, tempo de retenção do efluente no reator de 15 a 40 minutos e distância dos eletrodos de 1 e 3 centímetros. Um algoritmo com função de conveniência foi criado para otimizar simultaneamente os parâmetros estudados. O tratamento da GCS por eletrocoagulação foi satisfatório na remoção de turbidez, cor aparente e DQO, com eficiência máxima de remoção acima de 70% para todos os parâmetros, utilizando TRH de 27,5 minutos, ED de 2 centímetros e corrente elétrica de 1 A. A análise estatística apresentou um bom ajuste do modelo com coeficiente de determinação de R2 > 0,9. A condição ótima de operação foi observada em corrente elétrica de 1A, 27 minutos de TRH e 2 centímetros de distância do eletrodo, com remoções de 82,07, 86,86 e 70,82% de DQO, turbidez e cor aparente, respectivamente. Os ensaios simulados mostraram que tempos de eletrólise mais baixos podem ser utilizados, sem prejudicar a eficiência do tratamento. Portanto, a eletrocoagulação pode ser uma ferramenta potencial no tratamento de SLG.

Palavras-chave: coagulação, eletrólise, incineração, purificador de gás.

1. INTRODUCTION

Incineration is the most used method to treat healthcare waste (HCW), as it provides a significant reduction in the volume of waste and inactivation of pathogenic microorganisms. However, the emissions from HCW incineration often contain dioxins, polycyclic aromatic hydrocarbons, numerous volatile organic compounds, heavy metals, sulfur dioxide, nitrogen dioxide, particulate matter, and others, thus requiring atmospheric emission control (Thind *et al.*, 2021).

Emission control applications include the use of scrubber systems, in which pollutants are removed from the gas stream through the contact between the gas stream and a solvent, water, alkaline, or acidic solutions (Mendes, 2016). The effluents generated in the gas scrubbers of incineration plants (GCS) have a high polluting potential, with low pH and high concentration of dissolved and suspended solids. The fly ash contains contaminants like polychlorinated biphenyls, and trace metals such as, arsenic, beryllium, cadmium, chromium, lead, mercury and nickel, which can subsequently condense to form metallic particles, acid gasses, some salts, and chlorinated organic compounds (Silva and Lange, 2008; Bhargava, 2016; Thind *et al.*,2021).

In the state of Bahia, there is no specific legislation for effluent discharge, thus CONAMA Resolution 430/2011 is adopted, which has established that the pH of effluents for discharge must be between 5 and 6, among other parameters. Therefore, the removal of pollutants from the effluents generated in the incinerator scrubbers is essential to mitigate possible impacts to the environment from their release into water resources.

Electrocoagulation (EC) is considered a promising technique for the treatment of effluents generated during washing and separation of pollutants from HCW incineration. Studies have shown its efficiency in the removal of contaminants, such as textile dyes (Papadopoulos *et al.* 2019), organic matter (Modenes *et al.*, 2017; Piovesan, 2017), and nitrogen and phosphorus (Orssatto, 2017).

As reported by Moussa *et al.* (2017), EC is an emerging technology for wastewater treatment since it combines the benefits of coagulation, flocculation, flotation, and electrochemistry.

The EC process consists of the deposition of coagulants in situ, by electrolytic oxidation reactions of conducting and semiconducting metals, triggered by the application of electric current (Chen, 2004; Vepsäläinen and Sillanpää, 2020), and iron stands out as the most used metal for this purpose (Módenes *et al.*, 2017; Papadopoulos et al., 2019). In EC (Figure 1), ions from electrolytic oxidation of anode and cathode (iron) destabilize and neutralize the repulsive

forces that keep the particles suspended in water, favoring aggregation of the destabilized phase, contributing to easy physical removal of pollutants (Chen, 2004; Moussa *et al.*, 2017). The main function of the sacrificial anode is the generation of polymeric hydroxides while the cathode allows a reduction of metal ions (Chen, 2004). The formation of bubbles during the process can also assist in the flotation of pollutants to the aqueous surface (Hakizimana *et al.*, 2017). At acidic pH, iron is predominantly found as Fe^{3+} ions that can react with anions present in the effluent (SO_4^{2-}, F^-, Cl^-, organic matter, among others) (Vepsäläinen and Sillanpää, 2020). It can occur in bivalent or trivalent form depending on the oxidation state, and when subjected to hydrolysis, different metal species can coexist in solution (Moussa *et al.*, 2017). According to Chen (2004), the dissolution of coagulants by the application of electric current with iron electrodes is three times "higher when compared to aluminum electrodes.

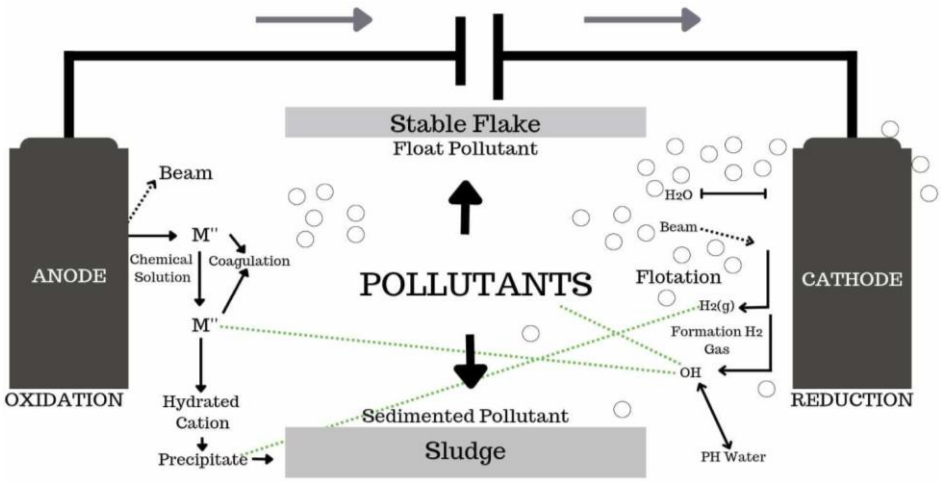

Figure 1. Schematic diagram of the electrocoagulation treatment.

The efficiency of electrocoagulation in the effluent treatment depends on several factors, including the concentration of pollutants and the operating conditions in the reactor, such as electrode area, hydraulic retention time, voltage, current density, types of electrodes, and the amount and spacing between them (Hakizimana *et al.*, 2017; Vepsäläinen and Sillanpää, 2020). Therefore, optimizing the factors involved in the process allows for problem-solving through the use of specific techniques under simulated conditions, enabling flexibility and application (Algeri *et al.*, 2017).

The importance of the waste treatment sector is noteworthy, given the increase in particle generation, mainly due to the COVID-19 pandemic, which has increased the demand for the health services around the world (OWS, 2020). There are no guidelines about the treatment of effluents from HCW incineration in fixed combustion chambers using water spray scrubbing systems.

Given the above, this study investigated the efficiency of electrocoagulation in removing COD, turbidity, and apparent color from HCW by modeling and optimization of the parameters, using a batch reactor and iron electrodes.

2. MATERIAL AND METHODS

2.1. Gas scrubber effluent from HCW incineration

The effluent from a gas scrubbing cleaning system was used in the study, from a dual-chamber incinerator, with a capacity of 50kg h^{-1}, located in a company that treats HCW from Groups A, B, and E. The company has an installed capacity of 385 tons of waste per year and generates 72 m^3day^{-1} of effluent. The system works in a closed circuit, with the reuse of the effluent generated, which is stored in three 5,000 L tanks.

The effluent was collected at the scrubber outlet after waste incineration (Groups A, B, and

E), and characterized for COD (closed reflux Method-5220 C), turbidity (nephelometric Method-2130 B), apparent color (Method 2120), pH (electrometric Method-4500 H+ B), iron concentration (flame atomic absorption spectrometry -FAAS), and electrical conductivity (Method 2510 A) (APHA *et al.*, 1995).

2.2. Experimental unit

The EC treatment consisted of a batch reactor composed of a rectangular glass box with capacity of 2 L. For each trial, 1.5 L of effluent was used, and the pH was corrected to 2.8 with sodium hydroxide (NaOH) solution. The system was kept under constant stirring (100 rpm).

The iron electrode was made from carbon steel plates A36. Electrodes consisting of four iron plates (7.0 cm width, 13.0 cm height, 1 mm thickness, 56 cm2) were arranged in parallel, and placed on a nylon technyl bar.

2.3. Experimental design and statistical analysis

A rotatable central composite design (RCCD) was used, with three independent variables (I, HRT, and ED). A 2^3 complete factorial design was performed, including 6 axial points and 5 repetitions in the central point, totaling 19 trials, according to Table 1.

Table 1. Number of trials and combination of the actual (I, HRT, and ED) and coded independent variables.

		Coded levels			Actual Levels –Independent Variables		
N.	Trials	x1	x2	x3	I (A)	HRT (min)	ED (cm)
1	1	-1	-1	-1	1.809	20	1.5*
2	2	-1	-1	1	1.809	20	2.5*
3	3	-1	1	1	1.809	35	2.5*
4	4	1	-1	-1	4.19	20	1.5*
5	5	1	1	-1	4.19	35	1.5*
6	6	1	1	1	4.19	35	2.5*
7	7	-1	1	-1	1.809	35	1.5*
8	8	1	-1	1	4.19	20	2.5*
9	9	-1.68	0	0	1	27.5	2
10	10	1.68	0	0	5	27.5	2
11	11	0	-1.68	0	3	15	2
12	12	0	1.68	0	3	40	2
13	13	0	0	-1.68	3	27.5	1
14	14	0	0	1.68	3	27.5	3
15	15	0	0	0	3	27.5	2
16	15	0	0	0	3	27.5	2
17	15	0	0	0	3	27.5	2
18	15	0	0	0	3	27.5	2
19	15	0	0	0	3	27.5	2

* Values rounded from 1.4 cm to 1.5 cm and from 2.6 cm to 2.5 cm due to difficulties in setting up the design.

The electric currents varied from 1A (5.9 mA cm^{-2}) to 5A (29.7mA cm^{-2}), the retention time of the effluent in the reactor varied from 15 to 40 minutes, and the distance between the electrodes ranged from 1 to 3 centimeters. The operation conditions were determined in preliminary tests.

The results of COD, turbidity, and apparent color removal were used to determine the effluent purification efficiency.

From the RCCD data, statistical models were generated using the software Statistical Analysis System (SAS) 9.4 to evaluate the relationship between the response variables (removal

efficiency of COD, turbidity, and color) and the other independent variables. Analysis of variance (ANOVA) was performed to validate the models at a 95% confidence interval for F Test, and p-values indicated the significance of the models at a 95% confidence interval for the t-Test.

Response surface graphs were used to determine the optimal operating parameters, and the adjustment of the parameters of the quadratic models was done by regression analysis. Equation 1 shows the general model used.

$$Removal\ of\ COD, or\ turbidity, or\ color = \hat{\beta}_0 + \hat{\beta}_1 I + \hat{\beta}_2 HRT + \hat{\beta}_3 DE + \hat{\beta}_{12} I\,.HRT + \hat{\beta}_{13} I.ED + \hat{\beta}_{23} HRT.ED + \hat{\beta}_{11} I^2 + \hat{\beta}_{22} HRT^2 + \hat{\beta}_{33} ED^2 \quad (1)$$

Where $\hat{\beta}_0, \hat{\beta}_1, \hat{\beta}_2, \hat{\beta}_3, \hat{\beta}_{12}, \hat{\beta}_{13}, \hat{\beta}_{23}, \hat{\beta}_{11}, \hat{\beta}_{22}, \hat{\beta}_{33}$ are the parameters estimated for the model; the coefficient $\hat{\beta}$ 0 is the constant term; (I) is the electrical current; (HRT) is the hydraulic retention time; and (ED) is the electrode distance.

The desirability function approach defined by Derringer and Suich (1980) was used to simultaneously optimize the parameters, which provides direct search optimization algorithms in Scilab for the variables studied.

3 RESULTS AND DISCUSSION

3.1. Characterization of the effluent

A high iron concentration (259.97 mg L^{-1}) and high electrical conductivity (1396.65 ms cm^{-1}), was observed in the effluent, which contributes to an effective electrocoagulation, since it leads to a decrease in the ohmic resistance of the effluent (Tahreen *et al.*, 2020).

The effluent exhibited 319 mg O_2L^{-1}, 360 NTU, and 170 mg Pt L^{-1} for COD, turbidity, and apparent color, respectively, indicating a large amount of suspended and dissolved solids, giving it a dark appearance. There are few studies in the literature on the physicochemical properties of the effluent generated in scrubber systems after incineration of health service waste, without pH neutralization. Silva and Santos (2019) characterized the effluents from the gas cleaning system after incineration of hazardous solid waste, in a moving bed type plant, subjected to acidic or alkaline washing, through six monitoring trials. The authors reported turbidity up to 97 NTU, color changes from 10 to 208 mg Pt L^{-1}, total suspended solids between 65 and 3080 mg L^{-1}, and neutral pH of the effluent, due to the capture of the acid gases by the sodium hydroxide during the alkaline washing. They also reported that the COD of the ash washing water varied between 370 and 3004 mgO_2 L^{-1}, which indicates a relevant amount of organic matter present in that type of effluent.

The effluent of this study presented a high acidity, and pH 1.85. This result may be due to the formation of oxides during the combustion of solid waste, which forms strong acids when interacting with the water used in the atmosphere control system (Sampaio, 2014).

3.2. Pollutant Removal Efficiency

The different efficiencies of turbidity, COD, and apparent color removal after 19 trials are presented in Figure 2. All parameters reached more than 70% removal in at least one trial.

The turbidity removal efficiency varied between 71.39% and 89.77% indicating a great removal of suspended solids for all assays. The higher turbidity removal was observed for Trial 9, with 27.5 minutes of HRT, electrode distance of 2 cm, and 1ª of electric current or 5.9 mA.cm-² of current density. In turn, the lower efficiency was observed for Trial 6, with 35 minutes of HRT, 2.5 cm electrode distance, and 4.19 A or 29.7 mA.cm-² of current density.

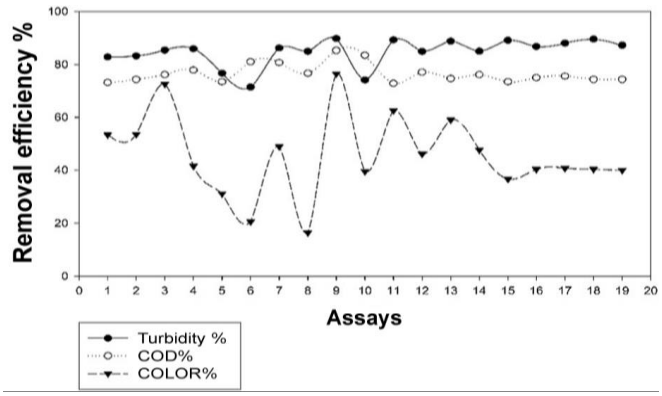

Figure 2. Removal efficiency for turbidity, COD, and apparent color.

For COD, removal efficiency ranged from 72.78% to 85.32%, proving the effectiveness of the treatment in the removal of organic compounds. A higher COD removal efficiency was observed for Trial 9, while Trial 11 presented the lower removal efficiency.

Concerning the apparent color, as also observed for turbidity and COD, Trial 9 exhibited the higher removal efficiency, with 76.47%, while Trial 8 presented the lower removal efficiency, with 16.47%. These results show that electrocoagulation is efficient in the removal of dissolved solids as a function of the processing conditions. The low color removal (47.06%) may be due to a large amount of Fe present in the samples resulting from anodic dissolution (Moussa *et al.* 2017), since pH values below 5 during electrocoagulation lead to a predominance of trivalent Fe and Fe $(OH)_3$ (Vepsäläinen and Sillanpää, 2020). Furthermore, the wastewater under study was subjected to no filtration procedure. After 24 h, iron decantation and a significant improvement of the effluent clarity were observed.

The use of EC for pollutant removal using iron electrodes in this study was also performed by other authors. Módenes *et al.* (2017) reported removal efficiencies of 92, 99.63, and 99.16% for COD, color, and turbidity, respectively, in the treatment of poultry slaughterhouse effluent, while Piovesan (2017) studied landfill leachate treatment and found 86.58, 70.09, and 55.69% removal of turbidity, color, and COD, respectively, using 2 cm of ED.

3.3. Modeling of the GCS electrocoagulation

The adjusted models that describe the behavior of the response variables at a 95% confidence interval ($p < 0.05$) are presented in Equations 2, 3, and 4.

$$Turbidity\ Removal = 57.1832 + 15.63602x_1 + 0.75156\,x_2 + 3.88284\,x_3 - 0.34162\,x_1.x_2 - 1.95622\,x_1.x_3 - 0.9157x_1^2 \quad (2)$$

$$COD\ removal = 80.99837 - 12.15065x_1 + 0.54821\,x_2 + 0.0546x_3 - 0.1625\,x_1.x_2 + 2.70046\,x_1^2 \quad (3)$$

$$Apparent\ color\ removal = 155.22376 - 5.57645\,x_1 - 2.65721x_2 - 57.56173x_3 - 13.51197x_1.x_3 + 1.43413x_2.x_3 + 3.24454\,x_1^2 + 13.59540\,x_3^2 \quad (4)$$

The model validation was performed by analysis of variance (ANOVA). The results (Table 2) showed reasonable regressions for turbidity, COD, and color, once they presented satisfactory fit to the model, with determination coefficients (R^2) higher than 90%, and adjusted R^2 higher than 84%, with a confidence interval of 95% ($p<0.05$) in the F test, indicating no significant difference between the experimental and predicted values. The discrepancies may

be due to the presence of noisy data.

Table 2. ANOVA for turbidity, COD, and apparent color removal

Parameter	DF	SS	R^2	Adjusted -R^2	RMSE	CV	F tab.	F value	p-value
Turbidity	7	445.47060	0.9432	0.9034	1.63824	1.93973	3.135	23.71	<.0001
COD	6	173.48380	0.9020	0.8433	1.37263	1.80409	3.217	15.35	0.0002
Color	8	3786.966	0.9763	0.9526	3.38837	7.51635	3.438	41.23	<.0001

The response surface of the model (Figure 3) showed wide optimal ranges of electric current, hydraulic retention time, and electrode distance for high turbidity removals. For the electric current, the range with the best removal varied from 1 A (5.9 mA cm^{-2}) to 3.2 A (19.04 mA cm^{-2}), which was limited by increasing ED and HRT. The variables ED and HRT showed high turbidity removal for all conditions tested, with a small improvement for the conditions of 2.5 to 3 cm and 35 to 40 min, respectively.

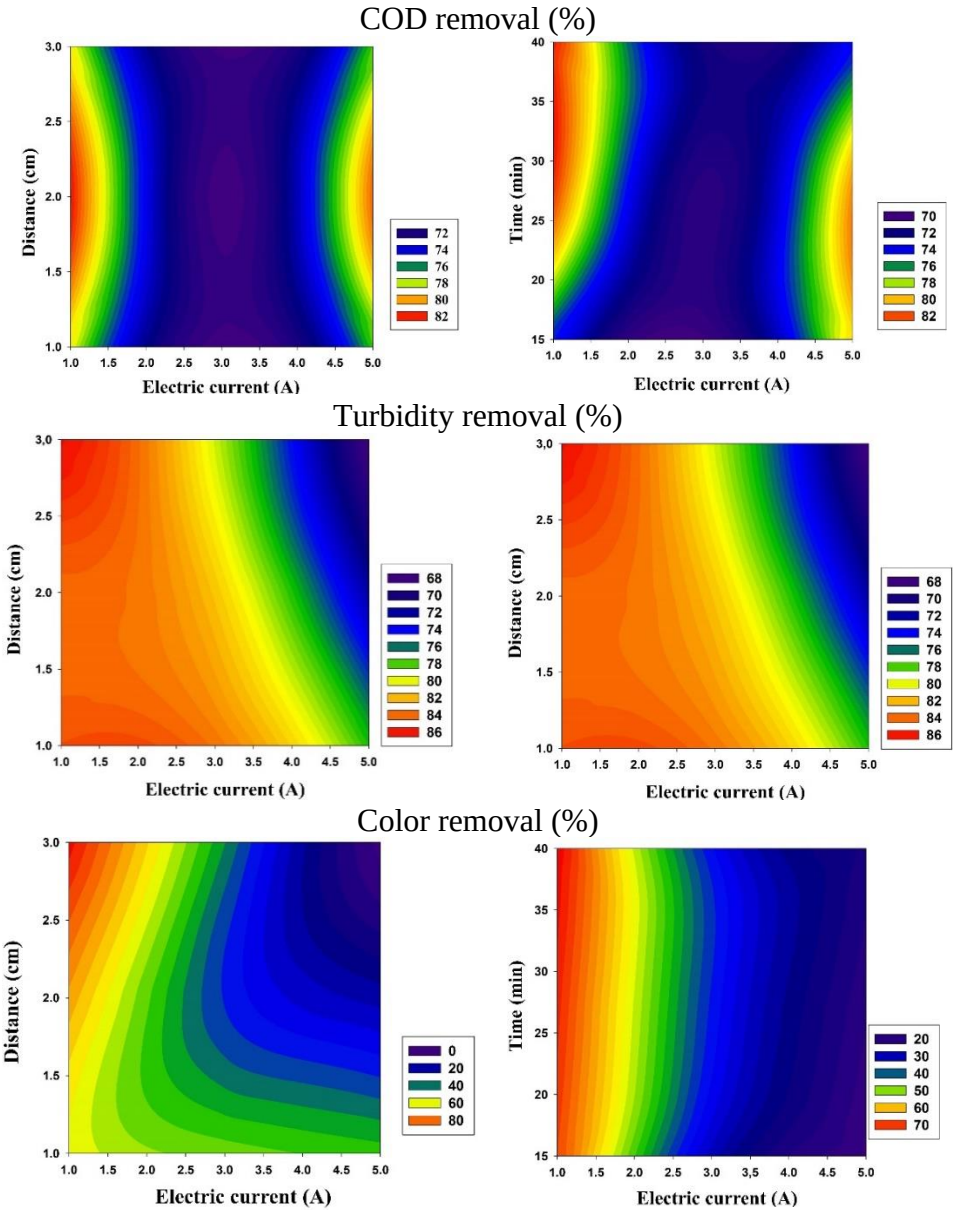

Figure 3. Response surfaces for percent removal of COD, turbidity, and apparent color as a function of electric current, electrode distance, and hydraulic retention time.

According to the response surface in Figure 3, the optimum COD removal was represented by a minimum point in the center and two optimal points for each independent variable, which was near 1A (5.9 mA cm^{-2}) and 5 A (29.7 mA cm^{-2}). For a lower current value, which is a desirable condition due to the lower operation costs, the optimal ED ranged from 1.3 -2.5 cm and HRT from 24 to 40 min.

The response surfaces for color removal efficiency showed a tendency towards a lower optimal range for the electric current, from 1 to 1.5 A, for all HRT conditions, as observed for COD, and an optimal range for ED from 1.7 - 3.0 cm.

The tendency of increasing the turbidity and color removals in Figure 3 is due to the higher efficiency of the electrocoagulation from the beginning of the process, with the application of a lower electric current. This behavior indicates that higher concentrations of iron hydroxide species are not necessary to clarify the effluent, once the crude effluent has high Fe concentration, which when submitted to hydrolysis in the system contributes to the formation of coagulants, which is a pH-dependent event (Moussa *et al.*, 2017; Vepsäläinen and Sillanpää, 2020).

However, the COD removal (Figure 3) demanded a longer hydraulic retention time, which was also observed by Combatt *et al.* (2017), who studied the elimination of COD from slaughterhouse effluent using an iron electrode and similar pH and current density conditions, and reported a removal efficiency of 88.8% for an HRT of 60 minutes.

Moreno-Casillas *et al.* (2007) investigated the electrocoagulation for COD removal and concluded that the removal efficiency and its variability depends on several factors, including the formation of agglomerates, which generally occurs at pH above 7.5 for Fe electrodes, the reactivity of organic compounds with Fe oxides, the solubility of the compounds formed, the final pH (especially for acidic compounds), and the pH increment with a consequent increase in the acidity. Probably, in this study, higher COD removals were not observed due to the low pH of GCS, which was lower than 6 for all trials.

3.4. Global optimization of the GCS electrocoagulation

The global optimization of GCS by electrocoagulation is necessary since wide and different regions of maximum efficiency were found for the three response variables. The Scilab algorithm using the desirability function allowed determining the global desirability D= 1(Figure 4) of the system, which was maximized when all responses reached the maximum removal. The optimal point of the modeled system was reached with an electric current of 1A (5.9 mA cm^{-2}), 27 minutes of HRT, and 2cm of ED, for simultaneous removal of 82.07, 86.86, and 70.82% of COD, turbidity, and apparent color, respectively.

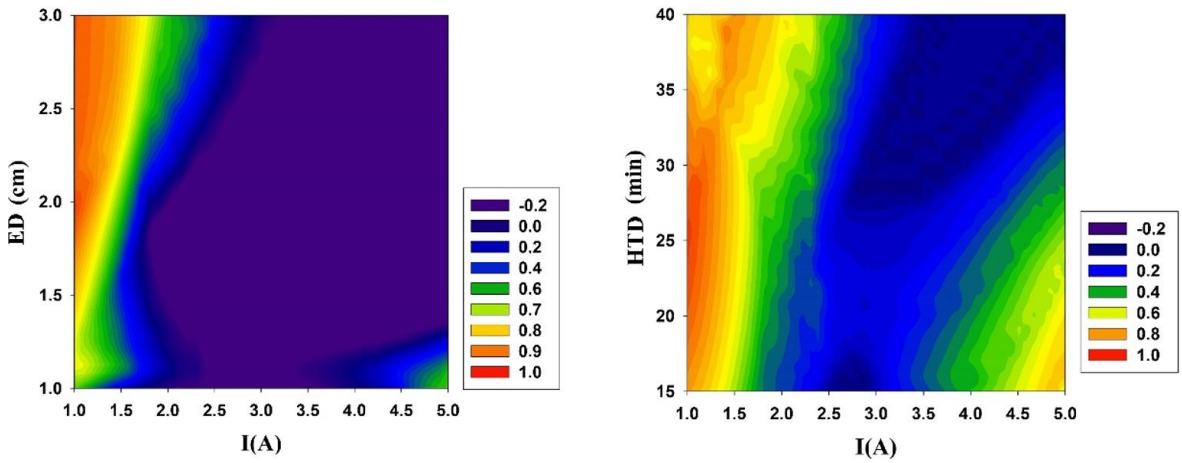

Figure 4. Response surface plots for overall desirability of GCS electrocoagulation using iron electrodes, for the variables ED (cm), I(A), and HRT (min).

The response surface plots for the global desirability function (Figure 4) confirmed the optimal point, showing that the factors ED and HRT can vary in a wide range without affecting the global desirability, i.e., a good removal efficiency can be reached unlike the electric current (I) that exhibited a narrow optimal range, causing a sharp drop in the global desirability even with small variations, which impairs the effluent treatment.

The optimum point observed for the current of 1A (5.9 $mA.cm^{-2}$) evidenced that this variable is a key operational parameter for the performance of the EC treatment of GCS. The antagonistic effect of this parameter for pollutant removal is due to the high iron concentration in the effluent. In contrast, some authors reported higher treatment efficiency with increasing the electric current, once it directly affects the dissociation of metal ions through anode oxidation and hydrogen formation at the cathode (Papadopoulos *et al.*, 2019; Vepsäläinen and Sillanpää, 2020). Therefore, increasing the EC in the treatment of effluents with high iron concentration may not improve treatment efficiency.

In contrast, Módenes *et al.* (2017) reported high removal efficiency of pollutants in wastewater by electrolytic processes at low current or current density, with maximum removals of 92.00, 99.63, and 99.16% for COD, color, and turbidity, respectively, with an electrolysis time of 50 min and current intensity of 2 A.

An electrode distance of 2 cm is effective to prevent the passivating effect of the iron electrode and the increase in resistivity. As shown in Figure 4, at a lower current, ED lower than 1.5 cm led to a reduction in desirability index. According to Feng *et al.* (2021), lower distances can hinder the rapid movement of the bubbles and agglomerates generated in the plate electrolysis, and accelerate plate passivation, increasing resistivity, leading to reduced current efficiency and ion production rate.

Despite the wide optimal range of ED from 1.5 cm (Figure 4), the increase in the spacing between the electrodes may not be an effective approach, once the passivating effect of the anode is potentiated with the increase of the distance between electrodes, leads to the formation of metal hydroxide film on the electrode surface, inhibits the oxidation of the anode, and decreases the amount of coagulant in situ, which leads to a lower efficiency in the removal of pollutants (Ghosh *et al.*, 2005). In addition, the decrease in ohmic potential leads to maximum pollutant removal efficiency. This decrease in potential is proportional to the distance between electrodes, so its reduction is required to decrease energy costs (Chen, 2004) and electrolysis time, and increase the efficiency of the process, because there is an increase in mass transfer during the CE due to turbulence generated by the large formation of gas bubbles in this condition (Martínez-Villafañe *et al.*, 2009).

The electrolysis time can also directly affect the coagulant production *in situ*. According to Chen (2004), the COD removal in electrocoagulation occurs by oxidation of organic matter at the anode at higher detention times, allowing all electrochemical reactions to occur. The increase in the concentration of ions and their hydroxide agglomerates is proportional to the electrolysis time.

4. CONCLUSION

The crude effluent from GCS presented high concentrations of COD, iron, as well as very acidic pH and high turbidity and apparent color, therefore requiring treatment before release into water bodies.

The high removal of turbidity, COD, and apparent color of this study showed that electrocoagulation was effective for the treatment of gas scrubber effluents.

Statistical analysis showed that mathematical models can be used to simulate the effects of the parameters electric current intensity, hydraulic retention time, and electrode distance on turbidity, COD, and color removal. All models presented a good fit to the data, with a coefficient of determination $R^2 > 0.9$ at a 95% confidence interval.

The optimum point was reached with an electrical current of 1A, a hydraulic retention time of 27 minutes, and electrode distance of 2 centimeters, with removals of 82.07, 86.86, and 70.82% of COD, turbidity, and apparent color, respectively. The simulated conditions showed that lower electrolysis times can be used without impairing the treatment efficiency.

5. REFERENCES

ALGERI, A.; LUCHESE, A. V.; MORINI, P. M.; SEHN, E. Aplicação da técnica de eletrocoagulação para a remoção da corante têxtil. **Revista de Estudos ambientais,** v. 19, p. 31-39, 2017. http://dx.doi.org/10.7867/1983-1501.2017v19n2p31-39

APHA; AWWA; WEF. **Standard Methods for the Examination of Water and Wastewater**. 19. ed. Washington, 1995.

BHARGAVA, A. Wet Scrubbers-Design of Spray Tower to Control Air Pollutants. **International Journal of Environmental Planning and Development**, p. 68-73, 2016.

CHEN, G. Electrochemical technologies in wastewater treatment. **Separation and Purification Technology**, v. 38, p. 11–41, 2004. https://doi.org/10.1016/j.seppur.2003.10.006

COMBATT, M. P. M.; MENDONCA, R. C. S.; VALENTE, G. F. S.; SILVA, C. M. Validação do processo de eletrocoagulação e avaliação da eletrodissolução de eletrodos no tratamento de efluentes de abatedouros de aves. **Química Nova**, v. 40, n. 4, p. 447-453, 2017. https://doi.org/10.21577/0100-4042.20170008

DERRINGER, G.; SUICH, R. Simultaneous optimization of several response variables. **Journal of Quality Technology,** v. 12, n. 4, p. 214–219, 1980. https://doi.org/10.1080/00224065.1980.11980968

FENG, Q.; ZHANG, K.; LIU, X.; GUAN, W.; CHEN, X.; SONG, L. *et al.* An improved kinetic model for dephosphorization of laundry wastewater by electrocoagulation. **Journal Water Process Engineering**, v. 39, 2021. https://doi.org/10.1016/j.jwpe.2020.101750

GHOSH, D.; SOLANKI, H.; PURKAIT, M. K. Removal of Fe (II) from tap water by electrocoagulation technique. **Journal of Hazardous Materials,** v. 155, p. 135–143, 2005. https://doi.org/10.1016/j.jhazmat.2007.11.042

HAKIZIMANA, J. N.; GOURICH, B.; CHAFI, M.; STIRIBA, Y.; VIAL, C.; DROGUI, P. *et al.* Electrocoagulation process in water treatment: A review of electrocoagulation modeling approaches. **Desalination,** v. 404, p. 1-21, 2017. https://doi.org/10.1016/j.desal.2016.10.011

MARTÍNEZ-VILLAFAÑE, J. F.; MONTEIRO-OCAMPO, C.; GARCÍA-LARA, A. M. Energy and electrode consumption analysis of electrocoagulation for the removal of arsenic from underground water. **Journal of Hazardous Materials**, v. 172, p. 1617–1622, 2009. https://doi.org/10.1016/j.jhazmat.2009.08.044

MENDES, A. I. R. **Otimização do Consumo de Água num Equipamento de Tratamento de Gases**. 2016. Dissertação (Mestrado em Ciências e Tecnologia do Ambiente) - Departamento de Geociências, Ambiente e Ordenamento do Território - Faculdade de Ciências da Universidade do Porto, Porto, 2016.

MÓDENES, A. N.; ESPINOZA-QUIÑONES, F. R.; YASSUE, P.H.; PORTO, T. M.; THEODORO, P. S. Aplicação da técnica de eletrocoagulação no tratamento de efluentes de abatedouro de aves. **Engenharia Sanitária e Ambiental**, v. 22, n. 3, p. 571-578, 2017. https://doi.org/10.1590/S1413-4152201775999

MORENO-CASILLAS, H. A.; DAVID, L. C.; GOMES, J. A.G.; MORKOVSKY, P.; PARGA, J. R.; PETERSON, E. Electrocoagulation mechanism for COD removal**. Separation and Purification Technology**, v. 56, p. 204–211, 2007. https://doi.org/10.1016/j.seppur.2007.01.031

MOUSSA, D. T.; EL-NAAS, M. H.; MUSTAFA NASSER, M.; AL-MARRI, M. J. A comprehensive review of electrocoagulation for water treatment: Potentials and challenges. **Journal of Environmental Management,** v. 186, p. 24-41, 2017. https://doi.org/10.1016/j.jenvman.2016.10.032

ORSSATTO, F**. Otimização do tratamento de efluente de matadouro e frigorífico de suínos pela eletrofloculação e combinação eletrofloculação/coagulação orgânica**. 2017. 102f. Tese (Doutorado em Engenharia Agrícola) – Centro de Ciências Exatas e Tecnológicas - Universidade Estadual do Oeste do Paraná, Cascavel, 2017.

OWS. **Maintaining essential health services: operational guidance for the COVID-19 context: interim guidance, 1 June 2020**. 2020 June 01. Available: https://apps.who.int/iris/handle/10665/332240 Access: Ago. 2022.

PAPADOPOULOS, K. P.; ARGYRIOU, R.; ECONOMOU, C. N.; CHARALAMPOUS, N.; DAILIANIS, S.; TATOULIS, T. *et al.* Treatment of printing ink wastewater using electrocoagulation**. Journal of Environmental Management**, v. 237, p. 442-448, 2019. https://doi.org/10.1016/j.jenvman.2019.02.080

PIOVESAN, M. **Tratamento de efluentes industriais utilizando eletrofloculação com eletrodos de alumínio e ferro**. 2017. 90f. Dissertação (Mestrado) - Universidade do Estado de Santa Catarina, Centro de Ciências Agro veterinárias, Programa de Pós-Graduação em Ciências Ambientais, Lages, 2017.

SAMPAIO, R. P**. Estudo de caso dos possíveis efeitos deletérios causados pelo combustível derivado de resíduo (CDR) em caldeiras voltadas a produção de energia elétrica queimando principalmente bagaço de cana**. 2014. 162p. Dissertação (Mestrado) – Escola de Engenharia de São Carlos, Universidade de São Paulo–EESC/USP, São Carlos, 2014.

SILVA, R. B. L.; SANTOS, G. O. Caracterização físico-química preliminar dos efluentes da incineração de resíduos perigosos de Fortaleza-CE. **Conexões Ciência e Tecnologia,** v. 13, n. 3, p. 61 - 71, 2019. https://doi.org/10.21439/conexoes.v13i3.1285

SILVA, M. L.; LANGE, L. C. Caracterização das cinzas de incineração de resíduos industriais e de serviços de saúde**. Química Nova**, v. 31, n. 2, p. 199-203, 2008. https://doi.org/10.1590/S0100-40422008000200002

TAHREEN, A.; JAMI, M. S.; ALI, F. Role of electrocoagulation in wastewater treatment: A developmental review. **Journal of Water Process Engineering,** v. 37, n. 101440, 2020. https://doi.org/10.1016/j.jwpe.2020.101440

THIND, P. S.; SAREEN, A.; SINGH, D. D.; SINGH, S.; JOHNA, S. Compromising situation of India's bio-medical waste incineration units during pandemic outbreak of COVID-19: Associated environmental-health impacts and mitigation measures. **Environmental Pollution**, v. 276, 116621, 2021. https://doi.org/10.1016/j.envpol.2021.116621

VEPSÄLÄINEN, M.; SILLANPÄÄ, M. Chapter 1 - Electrocoagulation in the treatment of industrial waters and wastewaters. **Advanced Water Treatment -Electrochemical Methods**, p. 1-78, 2020. https://doi.org/10.1016/B978-0-12-819227-6.00001-2